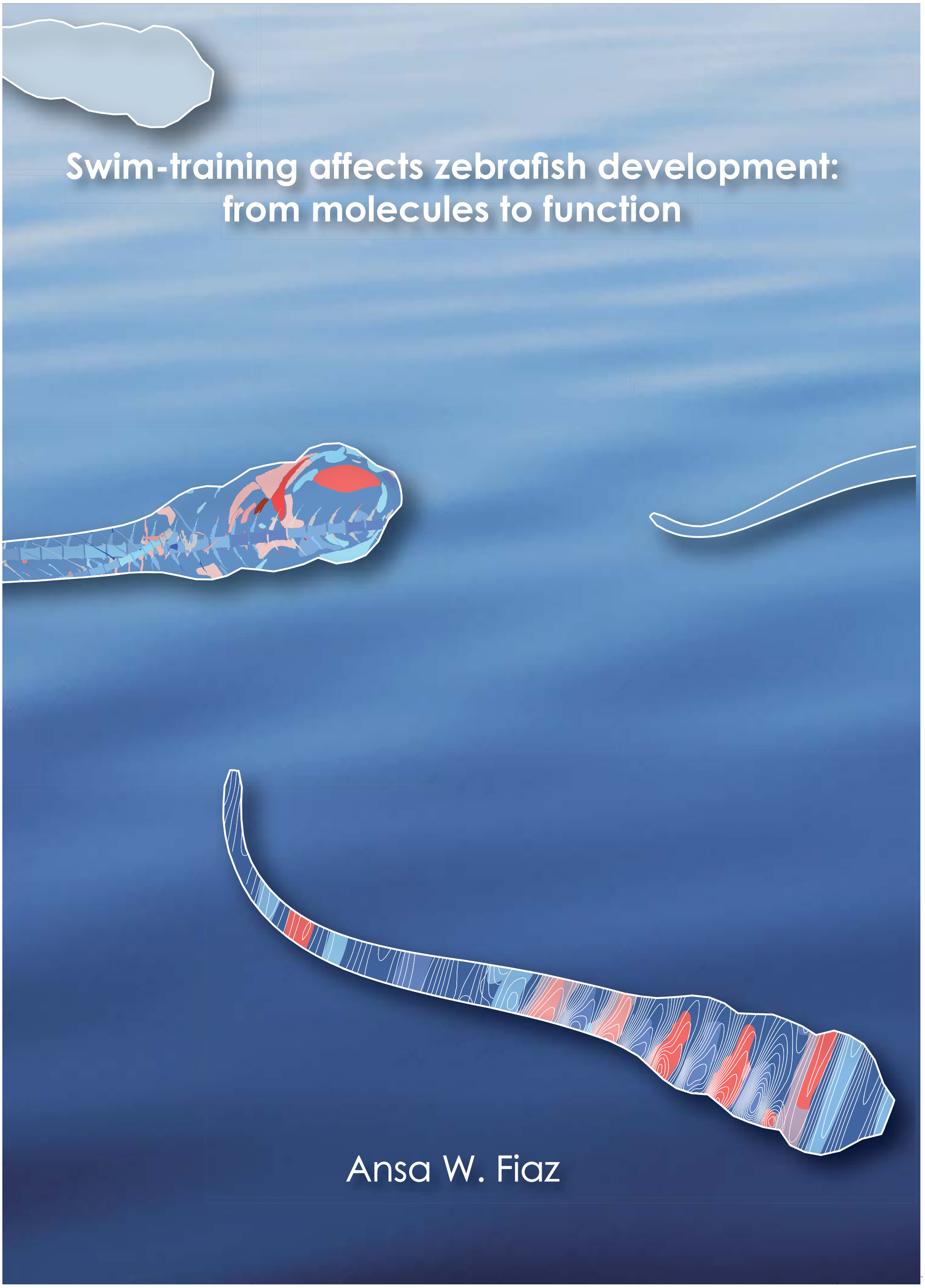

Swim-training affects zebrafish development: from molecules to function

Ansa W. Fiaz

Swim-training affects zebrafish development: from molecules to function

Ansa W. Fiaz

Thesis committee

Promotors
Prof. Dr. ir. J.L. van Leeuwen
Professor of Experimental Zoology
Wageningen University

Prof. Dr. S. Schulte-Merker
Professor of Molecular Developmental Zoology
Wageningen University

Co-promotor
Dr. ir. S. Kranenbarg
Assistent Professor, Experimental Zoology Group
Wageningen University

Other members
Prof. Dr. A.H.J. Bisseling, Wageningen University
Prof. Dr. ir. T.H. Smit, VU University Amsterdam
Dr. A.H. Meijer, University of Leiden
Dr. M.W. Hale, University of Chicago, United States of America

This research was conducted under the auspices of the Graduate School of Animal Sciences

Swim-training affects zebrafish development: from molecules to function

Ansa W. Fiaz

Thesis
submitted in fulfilment of the requirements for the degree of doctor
at Wageningen University
by the authority of the Rector Magnificus
Prof. Dr. M.J. Kropff,
in the presence of the
Thesis Committee appointed by the Academic Board
to be defended in public
on Friday 20 September 2013
at 4 p.m. in the Aula.

Ansa W. Fiaz
Swim-training affects zebrafish development: from molecules to function

PhD thesis, Wageningen University, Wageningen, NL (2013)
With references, with summaries in Dutch and English

ISBN 978-94-6173-646-8

For Florian and Zinedine
For the Beginning and the End

Contents

1 Introduction **1**

1.1 Zebrafish as vertebrate model 2

1.1.1 History 2

1.1.2 Phylogeny and the zebrafish genome 3

1.1.3 Natural habitat 3

1.1.4 Embryonic and larval development 4

1.2 Role of mechanical forces during development 8

1.3 Mechanotransduction 8

1.4 Subjecting zebrafish to swim-training 9

1.4.1 Swim training set-ups and methods 9

1.4.2 Effect of swim-training on fish 10

1.5 Thesis outline and aim 11

2 Phenotypic plasticity and mechano-transduction in the teleost skeleton **15**

2.1 Introduction 17

2.2 Sensing mechanostimuli in birds and mammals 18

2.3 Sensing mechanostimuli in teleosts 20

2.4 Conclusion 21

3 Quantification of swimming kinematics of larval zebrafish (*Danio rerio*) in varying flow conditions **25**

3.1 Introduction 27

3.2 Materials and methods 28

3.2.1 Husbandry 28

3.2.2 Flow set-up 28

3.2.3 High-speed recordings 29

3.2.4 Analysis of flow velocity 30

3.2.5 Model of the shape of the body 32

3.2.6 Analysis of swimming kinematics 33

3.2.7 Statistical analysis 34

3.3 Results 34

3.4 Discussion 39

4 Swim-training changes the spatio-temporal dynamics of skeletogenesis in zebrafish larvae (*Danio rerio*) 45
4.1 Introduction 47
4.2 Results 48
4.2.1 Swim behaviour and growth during swim-training 48
4.2.2 Effect of swim-training on chondrogenesis 49
4.2.3 Effect of swim-training on osteogenesis 53
4.3 Discussion 57
4.4 Materials and Methods 61
4.4.1 Husbandry 61
4.4.2 Ethics Statement 61
4.4.3 Swim-training setup 61
4.4.4 Training regime 62
4.4.5 Sampling and length measurements 64
4.4.6 Swimming behaviour 64
4.4.7 Burst frequency 65
4.4.8 Cartilage and bone staining 65
4.4.9 Statistical analysis of cartilage and bone formation 66
4.A Supplemental Figures and Multimedia 69

5 Exploring the effect of exercise on the transcriptome of zebrafish larvae (*Danio rerio*) 73
5.1 Introduction 75
5.2 Materials and methods 76
5.2.1 Husbandry 76
5.2.2 Swim-training set-up and regime 76
5.2.3 Whole genome microarray analysis 77
5.2.4 In situ hybridization 79
5.2.5 qRT-PCR analysis of muscle growth and structure 80
5.3 Results and Discussion 81
5.3.1 Effect of swim-training on swim behaviour and growth 81
5.3.2 Effect of swim-training on the transcriptome 81
5.3.3 Effect of swim-training on expression of genes involved in muscle growth and structure 87
5.4 General Discussion 88
5.4.1 Swim-training did not affect growth and survival 88
5.4.2 Swim-training induces molecular changes in the gastrointestinal system 89
5.4.3 Swim-training induces molecular changes in muscle growth and structure 89
5.A Supplemental data 91

6 Exploring the molecular link between swim-training and caudal fin development in zebrafish larvae (*Danio rerio*) 95
6.1 Introduction . . . 97
6.2 Materials and methods . . . 98
6.2.1 Husbandry . . . 98
6.2.2 Swim-training set-up and regime . . . 98
6.2.3 Whole genome microarray analysis . . . 99
6.2.4 In situ hybridization . . . 100
6.2.5 qRT-PCR analysis . . . 101
6.3 Results and Discussion . . . 102
6.3.1 Swim-training increases expression of muscle specific genes during caudal fin development . . . 102
6.4 Conclusion and Perspectives . . . 107
6.A Supplemental data . . . 109

7 General discussion 113
7.1 Introduction . . . 114
7.2 Zebrafish as exercise model for vertebrate development . . . 114
7.2.1 Swim-training increases swimming activity and intensity during larval development . . . 114
7.2.2 Swim-training affects larval growth and development . . . 115
7.3 Caudal fin as model structure to examine mechanotransduction during development *in vivo* . . . 116
7.4 Concluding remarks and perspectives . . . 117

References 120

Summary 141

Samenvatting 143

Acknowledgements 146

Personalia 151

”This book of mine has little need of preface, for indeed it is ”all preface” from beginning to end.”

D’Arcy Wentworth Thompson

Chapter 1

Introduction

A century ago, developmental processes were largely explained from a mechanical viewpoint [207]. Cells and tissues were described as 3D architectural structures which had to obey the same physical and mathematical laws as manmade constructions [87, 207]. With the advent and progress on the field of molecular biology and chemistry, the focus shifted to genes and proteins to explain developmental process. This provided a wealth of detailed information on how genes and proteins interact and control developmental processes. However, in the past decades, it has become clear that not only molecular signals but also mechanical forces are important for the regulation of developmental mechanisms. *In vitro* studies have described a diverse range of molecular pathways via which mechanical forces regulate development. *In vivo* studies, however, have just started to reveal the molecular link between mechanical forces and development. The *ex utero* development of fish makes them a much more accessible experimental system than mammalians to investigate developmental processes *in vivo*. To contribute to a better understanding of the molecular link between mechanical forces and development *in vivo*, we subjected larval zebrafish to swim-training (which presumably increases mechanical loads). Subsequently, we analyzed the swimming kinematics of zebrafish larvae subjected to flow and performed a morphological and molecular analysis of the effect of swim-training on zebrafish larval development.

In the following section, I will first discuss the history and development of the zebrafish. Subsequently, I will give a short review on the role of mechanical forces during development and mechanotransduction. This will be followed by a description of swim-training set-ups and methods used in previous studies. I will end with an overview of the aim and outline of this thesis.

1.1 Zebrafish as vertebrate model

1.1.1 History

The zebrafish has been used as a (classic) developmental model since the 1930s due to the transparent embryos allowing embryological manipulations and tracking morphogenesis during vertebrate development (see also the review by Laale *et al.* [110]). The zebrafish was first used as vertebrate model for genetic analysis in the 1970s by George Streisinger, who is acknowledged by many within the field as the founding father of zebrafish research [101, 149]. George Streisinger had worked previously on bacteriophage genetics and wanted to apply that knowledge on the analysis of the genetics and development in a vertebrate [101]. He chose the zebrafish as a model system, because he knew by experience as a fish hobbyist that zebrafish were easy to maintain and raise (e.g. in a petridish during the first days) and developed rapidly. The zebrafish offered the opportunity to perform genetic analysis due to large offspring numbers and to apply embryological methods such as transplantations due to the *ex utero* development and the relatively large size and transparency of the embryo [101, 149]. In a seminal paper he describes the use of zebrafish for genetic manipulation and production of mutants [200]. This study inspired the large-scale mutagenic screens that identified about 2000 mutants [149, 150, 229]. These mutants have greatly contributed to the establishment of the zebrafish as a model for vertebrate development [121, 150]. The zebrafish rose further in popularity due to the sequencing of the genome and the ability to generate transgenic lines which allows to follow specific cell types during morphogenesis *in vivo* [121, 149].

In addition, the zebrafish is not only being used to analyze embryonic development but also increasingly as a model for several human diseases [121]. The analysis of the latest version of the zebrafish genome showed that 70% of human genes have a zebrafish orthologue [83]. The zebrafish offers the ability to examine the course of the disease *in vivo* via e.g. transgenic lines and to perform chemical screens on whole animals for drug discovery and therapies [121].

Currently, more than 500 laboratories over the world use the zebrafish for their research and more than 1000 papers are published on zebrafish per year [121]. The zebrafish is also increasingly being used in other fields of research (e.g. proteomics, physiology, immunology, toxicology, fish swimming biomechanics) and at different stages (larvae, juvenile and adult). Correspondingly, a diverse range of techniques and methods are currently available to investigate developmental processes at different levels (e.g. molecular, cellular, organ) and stages in zebrafish.

1.1.2 Phylogeny and the zebrafish genome

Zebrafish belong to the class of Actinopterygii (the ray-finned fishes). The Actinopterygii shared a common ancestor with mammals which lived about 450 million years ago. Within the Actinopterygii, the zebrafish belongs to the division of Teleosts (modern bony fish). Within the teleosts, the zebrafish is part of the freshwater family of Cyprinidae which also consists of (among others) carps and minnows [149, 194]. Teleosts fish underwent an additional round of genome duplication compared to other vertebrates such as the mammals [134]. The zebrafish genome consist of around 1.4 gigabases [83] which is less than half the size of the human genome (around 3.1 gigabases, GRCh37 February 2009 assembly by Genome Reference Centrum). It contains around 26.000 protein-coding genes (the human genome contains around 20.000 protein-coding genes, GRCh37 February 2009 assembly by Genome Reference Centrum) and 69 % of zebrafish genes have at least one human orthologue [83].

1.1.3 Natural habitat

The natural distribution of the zebrafish occurs at several locations on the Indian subcontinent (e.g. Pakistan, Nepal, India and Bangladesh) [4, 51, 194]. The name Danio derives from the Bengali name '*dhani*' meaning 'of the rice field' [194]. Zebrafish have been found in a diverse range of waterbodies (rice paddies, small streams, channels, rivers) with speeds ranging from 0-13.9 cm/s, at 12.3–38.6°C and pH ranging from 5.9–9.8 [4, 51]. The natural habitat of larval and juvenile zebrafish and the life history of the zebrafish in the wild is less wel documented. It has been observed that larval zebrafish were found in still, shallow waters with a silt- or sand-covered bottom [4, 51].

1.1.4 Embryonic and larval development

As stated before, zebrafish develop rapidly. Within a couple of days, development of certain organs and structures has taken place which are similar to higher vertebrates although in a minimalistic version such as the gut and the vertebral column. In the following paragraphs, I will provide a short overview of the embryonic and larval development of the zebrafish to illustrate the rapid development and to provide a background (with a focus on muscle and bone development) on zebrafish development for the following chapters.

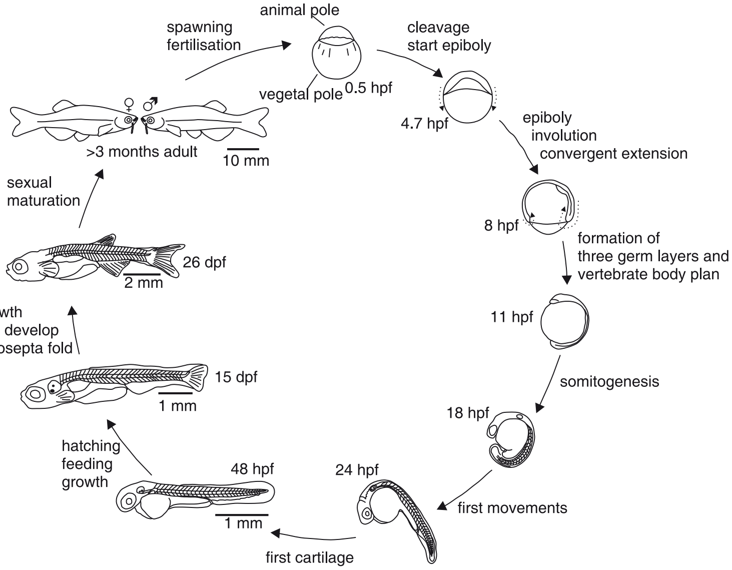
animal pole
spawning
fertilisation
cleavage
start epiboly
vegetal pole
0.5 hpf
4.7 hpf
♀ ♂
>3 months adult
10 mm
epiboly
involution
convergent extension
sexual
maturation
8 hpf
formation of
three germ layers and
vertebrate body plan
26 dpf
2 mm
11 hpf
growth
fins develop
myosepta fold
15 dpf
1 mm
somitogenesis
18 hpf
hatching
feeding
growth
48 hpf
24 hpf
first movements
1 mm
first cartilage

Figure 1.1. Schematic representation of zebrafish life history at 28.5°C (modified from [132]). Fertilization activates the segregation of the non-yolk cytoplasm at the animal pole and cytoplasm rich in yolk granules at the vegetal pole of the zygote. Within a couple of hours, cells at the animal pole starts to spread over the yolk (epiboly). In parallel to epiboly, these cells undergo gastrulation which is a process consisting of cell movements of involution, convergence and extension. Gastrulation leads to the formation of the primary three germ layers and the embryonic axis. See text for a description of the other stages.

During embryonic development, the primary three germ layers (ectoderm, mesoderm and endoderm) and the embryonic axes (first dorso-ventral and then antero-posterior) have formed within 10–11 hours post fertilization (hpf) (Figure 1.1). At this stage, part of the ectoderm has differentiated into the neural plate and somitogenesis is about to commence in the mesoderm [98, 149]. The endoderm will give rise to the digestive system and associated organs e.g. liver. The mesoderm will differentiate into among others the notochord (hydrostatic rod-like structure) and somites. Within a day, initial elements of the primary organs have formed, somitogenesis is complete and myotomes are arranged in a V-shape from a lateral viewpoint [132]. The so-called horizontal myosepta, sheets of connective tissue running along the anterior-posterior axis, divide each myotome in a ventral and dorsal half [98, 149]. The first movements appear at around 17–18 hpf as side-to-side contractions of the tail (Figure 1.1) (embryos raised at 28.5°C, [183]. At this stage, slow-twitch red and fast-twitch white muscle fibers can already be distinguished [42]. Red muscle fibers are located laterally to the notochord. At 21 hpf, the embryo's also respond to touch with rapid coiling behaviour. By 24 hpf, red muscle fibers have migrated to the periphery and constitute a superficial sheet under the skin [42]. At this stage, both fast and slow muscle fibers are recruited during coiling behaviour [21]. After 26 hpf these responses are followed by swimming episodes [183].

The first cartilaginous structures develop in the cranium between 1 and 2 dpf (e.g. Meckel's cartilage, Figure 1.1 and 1.2) [36]. At this stage, the heart starts beating and blood starts to circulate in the closed system of arteries and veins and the median finfold (forming collagenous strengthening structures called actinotrichia) forms. The intestine has formed a cord with radially aligned cells and a small lumen is visible [152]. At 2 dpf, the embryo has developed the classic vertebrate Bauplan (Figure 1.1) [98]. Between 2 and 3 dpf, embryos start hatching. The first cartilage condensations are visible in the supportive girdle structure (Figure 1.2). The first bone structure of the pectoral girdle, the cleithrum, is also apparent, which attaches to the occipital region of the skull (Figure 1.2) [98]. The first bone structures of the skull appear in the opercular region (opercle) (Figure 1.2). The differentation of the intestinal epithelium into specialized intestinal cells commences around 3 dpf.

Zebrafish are termed larvae from the third day of development until 30 dpf [149]. At the end of 3 dpf, morphogenesis of many basic organ systems has been completed. The mouth has shifted anteriorly and dorsally and the first active movements of the jaws become apparent. Around 4 dpf, the intestinal epithelium consists of absorptive, goblet and endocrine cells which form a microvillar brush border and peristaltic contractions become apparent [152, 215]. In addition, hepatic blood flow and the pancreas are apparant at 4 dpf [152]. Around 5 dpf, the gastrointestinal system becomes functional and larvae are able to survive on exogenous food and the swim-bladder inflates. During early larval development, larvae switch from cutaneous respiration to gill respiration. At 7 dpf, gills are required for ionregulation and at 14 dpf gills are required for oxygen uptake [180]. The larvae now mainly increase in size and the yolk has reduced significantly [98, 149].

Swimming activity gradually increases with age. Directly after hatching, fish spend most of the time on the bottom of the tank and swimming bouts often start while lying on their side. Directly after hatching, zebrafish exhibit mainly cyclic swimming behaviour. From 4-5 dpf, larvae are gradually able to maintain directional stability and swim with an intermittent swimming pattern (burst and coast behaviour) [137, 138].

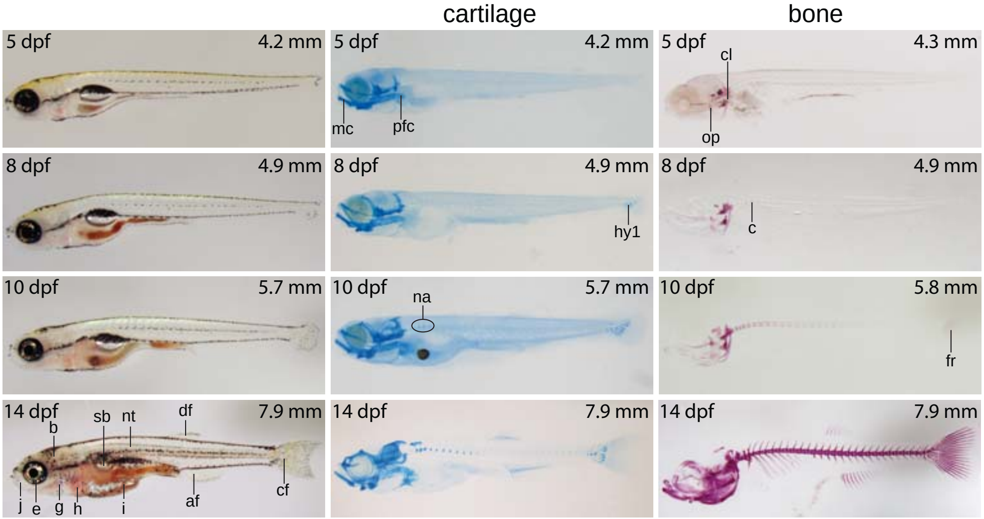

Figure 1.2. Overview of overall, cartilage and bone development of zebrafish larvae. The range of stages are shown that were also investigated in this study. Measured standard length is shown in the top right corner of each panel. Cartilage staining (middle images) were performed on fish shown with brightfield illuminiation (left images). af, anal fin; b, brain; c, centra; cf, caudal fin; cl, cleithrum; df, dorsal fin; e, eye; fr, finrays; g, gills; h, heart; i, intestine; j, jaw; mc, Meckel's cartilage; na, neural arches (part of Weberian apparatus); nt, neural tube; op, opercle; pfc, pectoral fin cartilage; sb, swimbladder.

The proliferation of the slow and fast twitch muscle fibers in the somites continues during larval development. By 7 dpf, differences in muscle fiber physiology (ATPase reactivity, succinate dehydrogenase activity and mitochondrial content) are distinguished between slow (red) and fast (white) muscle fibers [174]. Muscle growth can take place via hyperplasia (cell division) or hypertrophy (cell growth) in zebrafish. Red muscle fibers increase in number until adulthood, whereas white and intermediate muscle fibers increase in number until a total length of about 20 mm is reached. Muscle growth via hypertrophy shows a steady increase from a total length of 15 mm onwards [173]. At 15 dpf, red muscle fibers are located in a wedgelike insertion near the horizontal septum. Intermediate fibers are located in a thin strip between the red and white muscle fibers [163].

Skeletal development in zebrafish is a relatively late event compared to higher vertebrates. The onset of many cartilage and bone structures of the zebrafish skeleton lies within the first two weeks. The zebrafish skeleton consists of bones which form directly from mesenchymal condensations (direct ossification, dermal or membrane bones) or from cartilage precursors (perichondral or endochondral bones) [13, 36]. In dermal or membrane bones, bone matrix is deposited directly in the connective tissue. In perichondral bones, bone matrix is deposited on the surface of the cartilage precursor whereas in endochondral bones, bone matrix is deposited within the cartilage precursor [36, 74, 84].

Cartilage matrix is formed by chondrocytes whereas the unmineralized bone matrix (osteoid) is secreted by osteoblasts [65, 94]. Both chondrocytes and osteoblasts derive from mesenchymal precursors [103]. Osteoblasts cells also produce alkaline phosphatase which stimulates the deposition of calcium salts leading to the mineralization of the bone matrix [65, 94]. When osteoblasts become embedded in the osteoid, they transform into osteocytes [57]. Advanced teleosts have acellular bone, whereas lower teleosts such as zebrafish have cellular bone [84]. During zebrafish larval development, bone structures do not yet contain osteocytes. Only when the bone matrix has reached a certain thickness, do cells become embedded, although certain structures e.g. finrays and scales remain acellular [84].

The skull of the zebrafish is a relatively complex structure consisting of 74 skeletal elements (this is around three times more than in a human skull) [36]. Thirty of these bones form via direct ossification. Forty-three of the 74 skeletal structures in the skull form via a cartilage precursor. As described above, the first bone and cartilage structures appear in the skull and in the pectoral fin (Figure 1.2) [36]. In the following two weeks, skeletal development of the skull continues with the appearance of cartilage and bone structures in different regions of the viscerocranium and neurocranium [36]. The ossification of skeletal structures in the skull is complete around 70 dpf. Cubbage and Mabee [36] observed a general trend that bones which are involved in feeding and respiration (cleithrum, opercle) ossify earlier than bones that are part of the neurocranium (e.g. orbitosphenoid) which are assumed to experience less mechanical loading. There was no clear pattern in the sequence of ossification between dermal and cartilage bones.

The first cartilage structures of the axial skeleton, the hypurals in the caudal fin, appear around 4 mm (around 5–6 dpf) (Figure 1.2) [13]. At about the same stage, the first bone structures in the axial skeleton, the vertebral centra, appear in the anterior most part of the notochord via direct ossification (Figure 1.2). This is followed by the development of cartilage structures at the first four vertebrae, which are part of the Weberian apparatus (Figure 1.2) [13]. The Weberian apparatus plays an important role in the transmission of vibrations from the swim bladder to the inner ear [13, 69]. Around 5–6 mm (around 10 dpf), the first bone structures (the finrays) of the caudal fin appear in the axial skeleton (Figure 1.2) [13]. The posterior part of the caudal axial skeleton, the caudal peduncle, is modified to transmit forces generated by the axial muscles to the tail fin [132, 214].

After 2 weeks post-fertilization, the transition to the juvenile stage takes place (Figure 1.1). The major changes includes secondary folding of the myosepta into nested cones resulting in typical W-shaped arrangement from a lateral viewpoint, further ossification of the skeleton, development of the adult pigment pattern and development of the adult fins. Around three months post-fertilization, fish reach sexually maturity and are staged as adult fish (Figure 1.1) [149].

1.2 Role of mechanical forces during development

During development, cells experience intracellular and extracellular mechanical forces. The extracellular mechanical forces are generated by among others fluid flow, tensile and compressive loading. *In vitro* and *in vivo* studies have shown that these mechanical forces play an important role during development (reviewed by e.g. [58, 96, 125, 166]). The following examples illustrate the role of mechanical forces during development.

Arnsdorf and coworkers [3] demonstrated that mechanical forces generated by fluid flow *in vitro*, stimulated osteogenic differentiation of mesenchymal stem cells. *In vivo*, mechanical loading generated by muscle forces have a critical role during osteogenesis and chondrogenesis during embryonic development (reviewed by [53]).

In vitro studies showed that depending on the type of regime, mechanical strain can stimulate the proliferation and or differentiation of skeletal muscle cells ([25, 109]). *In vivo*, increased loading induced muscle growth via hyperplasia and hypertrophy in young mice [161].

In vivo studies showed that the abrogation of fluid shear stress (generated by blood flow) led to abnormal heart and reduced hematopoietic stem cell formation [82, 146]. In addition, the modulation of blood flow led to abnormal heart valve morphogenesis [213].

1.3 Mechanotransduction

The molecular mechanisms of mechanotransduction are extensively being investigated. The most noted mechanotransducers are mechanosensitive ion channels, primary cilia and transmembrane surface adhesion receptors [58, 125, 143, 166]. The mechanosensitive ion channels respond rapidly upon membrane stretching via blood flow and transduce the mechanical signals via influx of the second messenger Ca^{2+} [112]. Primary cilia sense forces generated by fluid flow which leads to Ca^{2+} influx and calcium-induced activation of signalling pathways [141, 171]. Transmembrane surface adhesion receptors such as integrins and cadherins play an important role in mechanosensing and transduction because these receptors transduce forces from extracellular matrix to the cytoskeleton and neighbouring cells and vice versa (reviewed by [58, 86, 125, 126, 143, 166]). These receptors transduce mechanical forces via adhesion complexes to downstream signalling pathways, to the actin cytoskeleton or the nucleus. This leads to changes in downstream signalling pathways, in the actin cytoskeleton tension or in the nucleus structure which in turn (directly or indirectly) can affect transcription.

A diverse range of signalling pathways and transcription factors have been described, which are affected by mechanical forces [125]. In particular, the Rho-family of small GTPases and protein kinase (e.g mitogen-activated protein kinase (MAPK)) signalling pathways, which play an important role in the regulation of many cellular processes (e.g. growth, differentiation and migration) [124, 125, 143]. The Rho-family of small GTPases regulate cytoskeletal structure and cytoskeletal tension via modulation of actomyosin contractility [124, 143]. *In vitro* studies have shown that RhoA (a member of the Rho-family of GTPases) (and cytoskeleton tension) is crucial for transduction of mechanical forces from the extracellular matrix via integrin receptors to the nucleus (leading to transcription) [3, 129, 162]. Furthermore, it has been shown that mechanical forces activate MAPK signalling pathways by stimulating focal adhesion kinase via focal adhesions [16, 89]. MAPK signalling pathways in turn activate transcription factors such as RUNX2 (a key transcription factor for osteogenesis) upon mechanical stimulation [92, 105, 140].

In vitro studies have contributed an important part to the understanding of the molecular link between mechanical forces and developmental processes. However, the complex interaction between mechanical and molecular signals is just starting to be uncovered via *in vivo* studies. With this study we would like to contribute to unravelling the molecular link between mechanical forces and development *in vivo*. The zebrafish as a vertebrate model provides many possibilities to gain a comprehensive understanding of this molecular link due to the diverse range of available tools and analyses. In addition, the zebrafish experiences relatively large morphological changes and mechanical loads during early vertebrate development (with respect to higher vertebrates). To investigate the molecular link between mechanical forces and development, we subjected zebrafish larvae to swim-training, which presumably increases mechanical loads. Swim-training has been used mainly to investigate the effect of exercise on (adult) fish. Several studies have investigated the effect of swim-training on larval development. In the following sections, I will provide a short literature overview of the methods and regimes used to subject fish to swim-training and the effects of swim-training on fish metabolism and development (with a focus on zebrafish).

1.4 Subjecting zebrafish to swim-training

1.4.1 Swim training set-ups and methods

Several different swim-training set-ups and methods have been used to measure swimming performance, oxygen consumption in fish and to subject fish to swim-training. Bainbridge built a fish wheel to measure the swimming kinematics of adult trout, goldfish and dace and later also endurance performance [6, 7]. Brett introduced the swim tunnel to measure endurance performance and oxygen consumption [18]. With this type of swim tunnel the critical swimming speed (the maximum swimming speed a fish can swim for a certain time) was determined and oxygen consumption could be measured in relation to swimming speed. Similar swim tunnels have been used to measure endurance performance and oxygen consumption in adult zebrafish and subject to swim-training [131, 155, 167]. A gravity-fed swim-training set-up consisting of several parallel tubes has been used to measure endurance performance, oxygen consumption in larval zebrafish and subject to swim-training [5, 106, 163].

Zebrafish have been subjected to a variety of training regimes at different developmental stages. McClelland *et al.* [131] subjected adult fish to swim-training two times 3 hours per day, 6 days/4 weeks. Fish were subjected to 2 BL/s (Body Length) which increased every week with 1 BL/s until 5 BL/s. Palstra *et al.* [155] trained adult zebrafish for 6 hours a day, 4 days/week, 4 weeks long at 13 BL/s. Van der Meulen et al. [133] subjected fish from 14–84 dpf to a swimming regime of 6 hours a day, starting with 3 BL/s and ending with 4.2 BL/s. Bagatto *et al.* [5] subjected zebrafish larvae of 3–32 dpf to water velocities of 2 or 5 BL/s for 15 hours (during the night). Pelster *et al.* [163] and Kopp *et al.* [106] used the same swim-training set-up and subjected fish to swim-training for 12–15 hours from 9–32 dpf at 5 BL/s.

1.4.2 Effect of swim-training on fish

In salmonid species, swim-training is known, among other effects, to stimulate growth and food conversion efficiency at low swimming speeds (1–2.5 BL/s) [40, 154]. In general, in most studies, in teleosts, swim-training stimulates muscle growth of red muscle fibers via hypertrophy (cell diameter/size) and hyperplasia (cell number) (reviewed by [41, 154, 184]). Depending on the fish species and training regime, swim-training can lead to changes in lipid-, glucose- or protein metabolism [41, 154, 184].

Swim-training increases the aerobic capacity of skeletal muscle in fish. The improved aerobic capacity is due to an increase in capillarity of muscle tissue, mitochondrial content and activity of aerobic enzymes [40, 52, 91, 131, 184]. Recently, Totland and coworkers showed that in salmon swim-training stimulates an increase in bone mass and strength [210].

Several studies have investigated the effect of swim-training during larval development. Cloutier *et al.* [32] showed that swim-training accelerated the onset of chondrogenesis and osteogenesis in the median fins in the Artic Charr (*Salvelinus alpinus*). In our lab, we have shown that swim-training accelerated the onset of osteogenesis in the caudal fin during late larval and juvenile zebrafish development [132]. In addition, in larval and juvenile zebrafish, swim-training increases aerobic muscle performance via an increased expression of slow fiber markers and an increase in red muscle mass (increased total cross sectional area) and a shift in cardiac muscle to faster muscle phenotype [133]. Bagatto *et al.* [5] showed that swim-training decreased active oxygen consumption in free-swimming zebrafish larvae and juveniles which indicates that swim-training increased swimming efficiency. The Pelster lab continued with this research and showed that swim-training led to an increased mitochondrial content in the red and intermediate fibers in larval and early juvenile zebrafish (15 and 32 dpf) while an increased capillarization of the muscle fibers in the tail fin and increased vascularization index of muscle tissue caudal of the anus was found only in early juveniles [163]. They further showed that the hypoxic signalling pathway did not play an important role in the shift to a more aerobic phenotype in response to swim-training [106]. Recently, it was shown that swim-training also affected circadian rhythms in zebrafish larvae [50]. These studies demonstrated that swim-training leads to significant changes during zebrafish larval development.

1.5 Thesis outline and aim

As stated before, the zebrafish is a versatile system which offers the possibilities to perform analyses on various levels and with diverse range of tools and genetic analyses. In this thesis, we took advantage of opportunities that the zebrafish offer and analyzed the effect of swim-training on the swimming kinematics, skeletal development and gene expression.

In Chapter 2, we review the current understanding of mechanotransduction during adult and embryonic skeletal development in birds, mammals and teleosts. As stated before, mechanical loading imposed by muscle forces does not only affect bone growth and maintenance in adult vertebrates but also affects embryonic bone development. Furthermore, mechanotransduction in adult mammalian and avian skeletal development has been extensively investigated, however less is known about mechanotransduction during embryonic skeletal development as a consequence of their *in utero*/*in ovo* development. Thus, due to the *ex utero* development and genetic analyses, the zebrafish as vertebrate model can provide a better understanding of mechanotransduction during early skeletal development. In the following chapters, we subject zebrafish to swim-training (which presumably increases mechanical loading) and perform a kinematic, morphological and molecular analysis of the effect of swim-training, to investigate how swim-training affects development *in vivo* and via which molecular pathways this effect is mediated.

To investigate how swim-training affects swim-kinematics, we perform in Chapter 3 a quantitative analysis of the swim-kinematics of zebrafish larvae in different flow conditions. We record the swimming behaviour of zebrafish larvae at 10 dpf with and without flow with high-speed video cameras (in an orthogonal set-up) and analyze the data using a 3D in-house developed automated fish tracker. This demonstrates that fish subjected to flow swim faster and longer, have higher tail beat frequencies and maximum normalized curvatures in the caudal fin.

In Chapter 4, we explore the effect of swim-training on zebrafish cranial, axial and appendicular skeletal development. We subject zebrafish to swim-training, which presumably increases mechanical load, from 5–14 dpf and show that swim-training increases frequency of swimming bursts and prioritizes the formation of cartilage and bone structures in among others the head and the anal, dorsal and caudal fin.

Subsequently, to investigate via which molecular pathways swim-training affects larval development, we explore the effect of swim-training on the transcriptome in zebrafish larvae in Chapter 5. We perform a whole genome microarray analysis of zebrafish subjected to swim-training and control fish sampled at 10 dpf. In addition, we also investigate the effect of swim-training on muscle growth and structure in trained and control fish sampled at 5 and 14 dpf. We show that swim-training leads to molecular changes already after 5 days of swim-training in a variety of organ systems, and that muscle can shift to a slow aerobic phenotype already during zebrafish larval development.

The caudal fin experiences relatively large morphological changes during larval development and the results from Chapters 3 and 4 indicate that mechanical load plays an important role during caudal fin skeletal development. Therefore, in Chapter 6, we focus on the caudal fin and explore the molecular link between swim-training and caudal fin development. We perform a whole genome microarray analysis on caudal fins of zebrafish subjected to swim-training and control fish at 10 dpf. We identify two muscle specific genes which show an increased expression exclusively in the caudal fin.

In the last Chapter, 7, we synthesise the results from this thesis. We discuss the findings of this thesis with respect to other studies and how these findings could contribute to a better understanding of mechanotransduction during development *in vivo*. Furthermore, we provide suggestions on future studies which could shed more light on the molecular link between mechanical forces and developmental processes *in vivo*.

”However, when I realized that zebrafish was a system that might allow us to exploit the genetic approach in a vertebrate, I saw a fascinating challenge, [...].”

Christiane Nüsslein-Volhard

Chapter 2

Phenotypic plasticity and mechano-transduction in the teleost skeleton

Ansa W. Fiaz[1], J. L. van Leeuwen[1], S. Kranenbarg[1]

Journal of Applied Ichtyology, 2010 (26), 289–293

---

[1] Experimental Zoology Group, Department of Animal Sciences, Wageningen University and Research Centre, Wageningen, The Netherlands

Summary

The proper formation, growth and maintenance of many bones depends on the mechanical loads generated by gravity and muscles. Mechanical loading by muscle forces does not only affect bone growth and maintenance in adult and juvenile vertebrates, but also affects larval and embryonic bone development. We have reviewed the current understanding of mechanotransduction in birds and mammals and compared it to teleosts. The major mechanosensing cells in the adult mammalian and avian skeleton are osteocytes. They are interconnected via cell processes and are contained within a canalicular network. Basal teleosts have osteocytes but their connectivity is questionable and the presence of a functional canalicular network is unlikely. Advanced teleosts have acellular bone and therefore lack osteocytes. Yet the skeleton of teleosts does show adaptive responses to changes in mechanical load. In these animals it is likely that osteoblasts, bone surface cells and chondrocytes act as mechanosensors. The factors expressed by osteocytes upon mechanical stimulation have been extensively investigated *in vitro* and *in vivo* in adult mammals and birds. Less is, however, known about the mechanotransduction pathway during embryonic bone development. The zebrafish presents new opportunities to analyze the mechanotransduction pathway during early (larval) bone formation due to the *ex utero* development and genetic analyses.

2.1 Introduction

The proper formation, growth and maintenance of many bones depends on the mechanical loads generated by gravity and muscles. Microgravity leads to a decrease in bone mass at a rate of approximately 1 % per month in man in the weight-bearing skeletal sites [117]. Increased skeletal loading stimulates an increase in bone mass and strength [35]. These examples show that the mammalian skeleton is not static but a dynamic structure that continuously remodels itself to adapt to its mechanical environment.

Deformities of the vertebral column show that the teleost skeleton also responds to changes in mechanical loading. Lordosis -an abnormal ventrad curvature of the vertebral column- is a ubiquitous vertebral deformity in wild and farmed teleosts. Although it has a multifactorial etiology, excessive mechanical loading plays an important role in the development of lordosis [97]. MicroCT analysis of lordotic vertebrae in the European sea bass (*Dicentrarchus labrax*) showed an increase in bone volume and second moment of area in affected vertebrae [108]. This suggests the lordotic vertebral morphology to be an adaptation to increased mechanical loading. This suggestion was further substantiated by a finite element analysis showing an attenuating effect of the increased bone volume on strain energy density.

Mechanical loading by muscle forces does not only affect bone growth and maintenance in adult and juvenile vertebrates, but also affects larval and embryonic bone development. The following examples illustrate the crucial role of mechanical loading via muscle activity during embryonic bone development.

Rodríguez et al. [178] showed in a radiographic and histological study that human fetal immobility, due to neuromuscular disorders, led to thin, hypomineralized, and slender long bones. Furthermore, multiple fractures were found through the growth plate and the diaphysis. The authors also found a significant decrease in bone mass and in the cortical thickness and area of the long bones [179]. A decrease in the mechanical load on developing bones due to fetal immobility, muscle atrophy and hypotonia was suggested to be the cause of these thin, fragile bones [178].

Skeletal analysis of Myo-D and Myf-5 mutant mice showed that mechanical loading by muscle activity during embryonic development influences the basic shape of bone elements [68]. Myo-D and Myf-5 mutant mice do not develop functional skeletal muscles. These mice do not generate any active movement *in utero*, and die shortly after birth [182]. The whole femur of these mutant mice was less mineralized and had shorter mineralization zones. Furthermore, the mutant humeri lacked the curvature of wildtype (WT) humeri and mutant mice had 2–4 times more osteoclasts in the limb bones than their WT siblings [68].

In vivo paralysis of chick embryos markedly decreases osteogenesis. Paralysis of chick embryos from 6–20 days after fertilization led to cartilaginous (after day 13) and bony fusion (after day 17) of the cervical vertebrae [81, 139]. There was a slight delay in the onset of mineralisation of regions appearing in the later stage of incubation (after 16 days) such as the neural arch of the thoracic vertebrae [81]. Decrease of bone growth in paralyzed chick embryos was greatest in the extremities. Analysis of the bone and cartilage regions showed that there was a significant reduction of the bone surface area in the hind limbs, with the greatest reduction in the femur (57 % at day 18) [111].

Larval zebrafish also respond to changing mechanical loads. The axial muscle of zebrafish larvae subjected to endurance swim training showed a shift towards a slow aerobic phenotype [133]. Furthermore, the trained larvae showed an acceleration of ossification onset in the tail bones [132].

While the molecular and cellular mechanisms of vertebrate osteogenesis are rapidly elucidated (e.g. 115, 120, 197, 225), our understanding of the mechanism through which mechanical loads affect osteogenesis is still limited. Despite this lack of knowledge, we can assume the mechanism to contain: (i) sensors that detect the mechanical input signals; (ii) processing units that translate the sensor output into recognizable instructions; and (iii) actuators that interpret the instructions and act accordingly. Herein, we review current understanding of the importance of mechanotransduction in birds and mammals and compare it to teleosts.

2.2 Sensing mechanostimuli in birds and mammals

In adult mammals and birds, the major mechanosensing cells in bone are osteocytes, which represent 90–95 % of the cells in bone (e.g. 14, 20, 57, 102, 113, 203). Osteocytes derive from osteoblasts which have stopped producing bone matrix and become entombed in the bone matrix [142, 157]. The cellular and molecular mechanism of how osteocytes exactly become buried in the bone matrix is not yet clear (see [57] for a recent review). It is known that the osteoblast differentiates into an osteocyte via a decrease in size and reduction in the number of cell organelles (e.g. the endoplasmatic reticulum and mitochondria, 47). During the process of transformation and isolation, the osteocyte remains connected to other osteocytes and osteoblasts on the bone surface via cell processes. The extracellular matrix mineralizes, leaving a small lacuna containing the osteocyte body, and small tubular channels or canaliculi around the cell processes [156, 157]. Small molecules and electrical signals are exchanged between cells via gap junctions at the most distal part of the cell processes [44, 158, 187]. We refer the reader to Knothe Tate et al. [102] and Kogianni and Noble [104] for recent reviews on this topic.

The cellular mechanism via which the osteocyte detects mechanical stimuli is still under debate. According to the lacuno-canalicular flow hypothesis [34, 220], the flow of interstitial fluid in the complex 3-dimensional network of lacunae and canaliculi plays an important role in mechanotransduction. The application of a load on an intact bone leads to the deformation of the bone matrix and flow of the interstitial fluid. This strain-driven motion of the fluid likely produces shear forces at the cell processes which stimulate the osteocyte. The deformation of the bone matrix, however, could also stimulate the osteocyte via the deformation of the cell processes and/or cell body via tethering elements [14].

The signals released once a mechanical stimulus is detected have been extensively investigated. The first signal to be released by osteocytes is nitric oxide (NO). Klein-Nulend et al. [99] showed that pulsating fluid flow stimulated the production of NO in *in vitro* cultured chick osteocytes and mouse bone cells. The production of NO was maximal 5 min after onset of the pulsating flow. The fluid flow also stimulated a significant increase in prostaglandin (PG) E_2 production after 10 min, which lasted for 60 min. Inhibition of NO production prevented the increase of PGE_2 production [99]. This suggests that the transient increase in NO production might transduce the signal into a more sustained response with the increase in PGE_2 production.

Vatsa et al. [212] showed that upon *in vitro* mechanical stimulation in mouse long bone osteocytes NO production was increased in the cell processes and the main body of the osteocyte. This study shows that both the cell processes and the main body of the osteocyte might be involved in mechanotransduction.

NO is synthesized by nitric oxide synthase (NOS) enzymes. *In vivo* inhibition of NOS with L-NAME reduced the rate of bone formation by 66 % in rat tibiae subjected to mechanical bending [211]. Another study by Chow and Chambers [28] showed that *in vivo* inhibition of prostaglandins with indomethacin reduced the rate of bone formation by 66 % in rat caudal vertebrae subjected to mechanical load. Interestingly, bone formation due to increased mechanical loading was suppressed when indomethacin was administred before loading and not after loading [28]. These results indicate that NO and prostaglandins play an important role in the early transduction of mechanical signals to bone formation.

Insulin-like growth factor I (*Igf-I*) showed an increased expression within 30 min in osteocytes in compressed rat caudal vertebrae, which continued up to 6 h after the mechanical stimulus. Expression of *Igf-I* was suppressed by indomethacin [116], suggesting that this factor is regulated by prostaglandins and is a later player in the mechanotransduction pathway than NO and PGE_2.

In vivo mechanical loading by compression (5 min) of the 8th caudal vertebrae in rats increased the expression of *c-Fos* mRNA after 1 h in cortical osteocytes. These experiments also showed that 5 min of loading were sufficient to stimulate bone formation in metaphyseal trabecular bone [85]. The expression of *c-Fos* was not suppressed by indomethacin [116]. These results and the increased expression of *c-Fos* shortly after stimulation suggest that *c-Fos* plays an important role in the early response to mechanical loading, yet via another pathway than prostaglandins.

Osteopontin (OPN), a major noncollagenous bone matrix protein, plays an important role in bone formation, resorption, and bone remodelling (reviewed by [144]. *Opn* mRNA expression showed a 4-fold increase in rat tibia at 6 and 24 h after mechanical loading [136]. Mechanical stress on the interradicular septum (IRS) of rat molars, by experimental tooth movement, led to increased *Opn* expression in osteocytes on the distal side. The proportion of *Opn* expressing osteocytes increased to 87.5 % after 48 h of mechanical loading on the distal side of the IRS while in control rats the proportion of *Opn* expressing osteocytes was only 3.3 % [204].

Besides osteocytes, several studies have indicated that chondrocytes, osteoblasts and bone surface cells can also act as mechanosensors and express factors which promote osteogenesis upon mechanical stimulation [226–228].

Primary chondrocytes, isolated from bovine calf humeral head cartilage and subjected to cyclic tensile strain *in vitro*, showed an increased expression of several hypertrophic markers such as *collagen type X* and *Runx/Cbfa1* [226]. RUNX is regarded as a master transcription factor in osteogenesis [105]. Chondrocytes isolated from embryonic chick sternum and subjected to cyclic stretch induced matrix deformation *in vitro*, showed an increased expression of *Indian Hedgehog* (*IHH*), *Collagen type X* and *Cartilage Matrix Protein* (*Matrilin-1*). Indian Hedgehog is a key signalling molecule in chondrocyte proliferation and differentiation. The expression of *IHH* coincided with the expression of the *cartilage matrix protein* (*matrilin-1*), which is a marker of mature chondrocytes. The blocking of *IHH* completely inhibited the mechanical stimulation of chondrocyte proliferation and differentiation. Thus, *IHH* is necessary for the mechanical stimulation of chondrocyte proliferation and maturation [227, 228].

NO production was upregulated in osteoblasts upon *in vitro* mechanical stimulation [212]. Bone surface cells or bone lining cells are osteoblasts that have undergone terminal differentiation. Expression of *c-Fos* was increased in bone surface cells on trabecular bone surfaces by mechanical stimulation and was resistant to indomethacin [116]. *Opn* expression was increased in osteoblasts and bone surface cells on the distal side of the interradicular septum in rat molars subjected to mechanical loading [204].

Despite the extensive knowledge about mechanotransduction in adult mammals and birds, less is known about the pathway of mechanotransduction during embryonic bone development, especially *in vivo*. Nowlan et al. [148], however, recently discovered that *Indian Hedgehog* and *Collagen type X* respond to altered mechanical loading during embryonic bone development in chick hind limb *in vivo*. Using finite element analysis and in situ hybridizations these authors showed a clear correlation between the expression patterns of these genes and patterns of the biophysical stimuli in the tibiotarsus between normal and immobilized chick embryos.

2.3 Sensing mechanostimuli in teleosts

Osteocytes with cell processes, chondrocytes, and bone surface cells are also present in the teleost skeleton [84]. It is, however, unclear whether the teleost osteocytes form an interconnected network. Furthermore, the bone of advanced teleosts (neoteleosts) lacks osteocytes altogether [159], thus precluding the main mammalian type of mechanosensation (likely mediated by canalicular flow) [37]. Despite the absence of osteocytes, acellular bone does show an adaptive response to altered mechanical loads [107]. The strongest mechanical stimuli calculated by strain energy densities in the lordotic vertebrae of sea bass were found in the central part of the vertebrae, whereas major bone deposition occurred at the articular surface of the lordotic vertebrae. A comparable phenomenon of appositional bone growth is seen at the articular surfaces of compressed vertebrae of the Altantic salmon (*Salmo salar*) [224]. This adaptive response of teleost bone in the absence of a lacunocanalicular network is probably mediated by osteoblasts and bone surface cells that act as mechanosensors [225].

Kranenbarg et al. [107] and Witten et al. [224] also observed chondroid or cartilage formation in between two vertebrae in response to a compressive mechanical environment environment. This is in accordance with Pauwels' theory of tissue differentiation, which states that compression is the specific stimulus for the development of cartilaginous tissue [172]. Chordoblasts and intervertebral ligament cells likely show a mechanically induced transdifferentiation into a cartilaginous phenotype.

In teleosts, the skeleton develops relatively late in ontogeny compared to mammals and birds (e.g. [188, 223]. In zebrafish embryos, the first movements appear around 17–19 hours post fertilization as side to side contractions of the trunk and precede coordinated patterns of swimming behaviour [183]. The first bony structures in the head skeleton of the zebrafish appear at 3 days post fertilization and at 5 days post fertilization in the axial skeleton [13].

Van der Meulen [132] showed that zebrafish larvae subjected to endurance swim training showed an acceleration of the ossification of cartilage precursors in the tail. Most fin rays and hypurals were ossified at 20 days post fertilization in trained fish while ossification in control fish was observed at 35 days post fertilization. These observations suggest that the chondrocytes of the cartilage precursor act as mechanosensors in larval zebrafish.

In all teleosts, the formation of the vertebral bodies starts with the mineralization of the notochordal sheath. The mineralized notochordal sheath is acellular [71, 88, 145]. Stemple [198] concluded that the notochord is a tissue very similar to cartilage, containing both cells (chordoblasts) and an extracellular matrix (the notochordal sheath). It expresses several cartilage specific genes such as collagen type II, type IX and SOX9. The deposition of collagen type X signals the onset of ossification in both cartilage and the notochord [198]. The role of the notochord as a mechanosensor has yet to be explored, but it can possibly mediate a proper spatial and temporal development of the vertebrae in response to the axial loads caused by swimming.

2.4 Conclusion

Mammals, birds and teleost fish share the mechanosensitive nature of their skeleton. The skeleton is able to respond to changes in its mechanical environment and to adapt accordingly. The main mechanosensors, however, are markedly different between mammals/birds and teleosts. Osteocytes are the main mechanosensor in birds and mammals. They are interconnected via cell processes and are contained within a canalicular network. This presents a global mechanosensing and transducing system in which the location at which the stimulus is sensed does not have to be at the location where the adaptive response takes place.

Basal teleosts do have osteocytes but their connectivity is questionable and the presence of a functional canalicular network is unlikely. Advanced teleosts have acellular bone and therefore lack osteocytes, as do larval teleosts. Yet, the skeleton of teleosts does show adaptive responses to changes in mechanical load. Probably osteoblasts, bone surface cells, and chondrocytes act as mechanosensors. This would present a *local* mechanosensing system in which signal detection and response are co-localized.

The factors expressed by osteocytes upon mechanical stimulation have been extensively investigated *in vitro* and *in vivo* in adult mammals and birds. Analyses of embryonic mechanostransduction *in vivo* are hampered by the *in utero* development in mammals and *in ovo* development in birds (though see [148]. The zebrafish presents an excellent model for analyses of mechanotransduction during early (larval) bone formation because of its *ex utero* development, ease and speed of reproduction, translucent embryos and fully sequenced genome. Therefore, we are currently trying to elucidate which are the key genes and proteins in translating mechanical load into bone formation in larval zebrafish by a combined biomechanical and molecular approach.

”I believe the day must come when the biologist will – without being a mathematician– not hesitate to use mathematical analysis when requires it.”

Karl Pearson

Chapter 3

Quantification of swimming kinematics of larval zebrafish (*Danio rerio*) in varying flow conditions

Ansa W. Fiaz[1], Remco P.M. Pieters[1], Cees J. Voesenek[1], Johan L. van Leeuwen[1]

---

[1] Experimental Zoology Group, Department of Animal Sciences, Wageningen University and Research Centre, Wageningen, The Netherlands

Abstract

During development, fish larvae experience various environmental challenges such as predation and varying flow conditions. Studies have shown that fish larvae exhibit adaptive changes in response to an increased flow via swim-training. Swim-training accelerated skeletal development of the head and median fins and increased growth, swimming efficiency and aerobic muscle performance. It is likely that the applied flow increases swimming activity which leads to these adaptations. Therefore, we performed a detailed analysis of the swim-kinematics of zebrafish larvae in varying flow conditions.

With a two camera set-up, we made synchronized high-speed video recordings of zebrafish at 10 days post-fertilization that swam in a tube with either no flow or an average flow speed of 14.2 mm/s. Subsequently, to quantify the swimming kinematics, we analyzed the obtained high-speed recordings of the fish with in-house developed 3D automatic tracker software. In addition, using Particle Image Velocimetry (PIV) and Computational Fluid Dynamics (CFD) analyses we showed that flow in the tube approximated a Hagan-Poisseuille flow profile at the location of the recordings and used this information to derive the actual swimming speed of the fish.

The analysis of the swimming kinematics of fish in varying flow conditions demonstrated that the presence of flow increased tail beat frequency and the duration of individual swimming bouts. In addition, fish subjected to flow swam faster and generated higher peak curvatures in the caudal fin. These findings suggest that flow increased the swimming intensity during a swimming burst.

This study is the first to quantify the swimming kinematics of zebrafish larvae in varying flow conditions. These data could help to unravel how a flow-induced increase in swimming activity could lead to morphological and metabolic adaptations. Furthermore, it may provide input for future CFD analyses to investigate how altered environmental conditions change the distribution of forces along the body of the fish larvae.

Keywords: high-speed video, 3D fish tracker, tail beat frequency, body curvature, swimming velocity

3.1 Introduction

During larval development, a fast increase in swimming performance is important to escape from predators and to maintain position in varying flow conditions. Studies have shown that fish larvae that are subjected to an increased flow via swim-training show an adaptive response [5, 50, 54, 133, 163]. Swim-training, which presumably increases mechanical loads, prioritized the formation of cartilage and bone structures in the head and tail region as well as the formation of skeletal elements in the anal and dorsal fins [54]. In addition, swim-training has been shown to improve growth [54, 133], swimming efficiency [5], aerobic muscle performance [133, 163] and affects circadian rhythms [50]. In a previous study, we showed that swim-training increased the overall frequency of swimming bursts (here, a burst represents a forward movement consisting of several tail beats followed by coasting) in zebrafish larvae [54]. However, it is unknown whether e.g. maximum body curvatures increase as a result of the swim-training. The analysis of swimming kinematics of fish in varying flow conditions could contribute to a better understanding of how an increased swimming activity via swim-training can lead to the morphological and metabolical adaptations. In addition, the quantified body deformations can be used to compute the force distribution on the body surface using Computational Fluid Dynamics (CFD) [119], and thus shed new light on the external loading of the body.

Several studies have described the locomotor patterns and swimming kinematics of swimming bursts of zebrafish larvae in stagnant water. During larval development, zebrafish change their swimming style. Directly after hatching, zebrafish swim mainly cyclicly and switch to burst and coast behaviour around 4 mm BL (total body length, > 5 dpf) [138]. Zebrafish larvae experience a transitional flow regime ($Re = 50$–1200) (according to our lab observations). The dimensionless Reynolds number (Re) indicates the relative importance of inertial over viscous forces [10]. Zebrafish larvae exhibit normalized swimming speeds of 2.4–55.3 BL/s (normalized by total body length (BL)) and tail beat frequencies of 31–100 Hz [19, 59, 137, 209].

Müller and Van Leeuwen [137] demonstrated that, during burst and coast behaviour, peak curvatures were located in the post-anal region (in fish longer than >4 mm at >0.7 BL position along the body). In addition, Li *et al.* [119] demonstrated, via CFD analysis of the pressure and shear distributions along the body of a zebrafish larvae, that the highest left-right pressure differences were located at the posterior body of zebrafish larvae (during cyclic swimming at 5 dpf) which indicated that this part generated the highest force peaks and most of the thrust. Thus, taken together, these data indicate that the tail motion makes an important contribution to the propulsion in larval zebrafish.

Here, we made high-speed recordings of spontaneous routine swimming behaviour of zebrafish larvae at 10 dpf (≈ 5 mm standard length) because at this stage important morphological transitions take place [13, 160]. We demonstrated in previous studies that at this stage, swim-training induced significant molecular and morphological changes in the caudal fin ([54], Chapter 6). Furthermore, the first ossified structures (hypurals and finrays) appear around 10 dpf in the caudal fin [54, 160]. This makes it an interesting stage to investigate how flow affects swimming kinematics.

In a previous study by Fontaine *et al.* [55], an automated fish tracker was used to investigate the effect of an increasing stiffness of the vertebral column on swimming performance during zebrafish development. However, this tracker cannot accommodate pitch and roll motions (fish make often considerable pitch and roll angles) and cannot track the tail with sufficient accuracy for our purposes. We used a dual high-speed camera set-up and a new in-house developed 3D automated fish tracker (this software package will be described in detail elsewhere) to accomodate pitch and roll angles and to track the tail with sufficient accuracy. We made simultaneous recordings from the bottom and lateral side of a square tube since pitch and roll angles cannot be captured by a single camera. With our new software, it is possible to track fish in 3D, including movements of the tail fin, by using multiple synchronized video sequences from different angles of view.

In addition, the flow profile in the tube is often not taken into account when determining the swimming speed of fish larvae which can lead to over- or underestimation of the actual swimming speeds. Therefore, we performed Particle Image Velocimetry (PIV) and CFD analyses to characterize the flow within the tube to determine the ambient flow velocity near the position of the fish. These analyses indicated that the flow approached an almost fully developed Hagan-Poisseuille flow profile at the location of the recordings. This enabled us to calculate the actual swimming velocity of fish subjected to flow. Our study is the first to perform this correction of the swimming velocity of fish larvae subjected to flow.

Here, we demonstrate that flow leads to significant changes in swimming kinematics of zebrafish larvae. Fish subjected to flow swam faster and longer and had a higher tail beat frequency. Furthermore, maximum normalized curvatures in the caudal fin were larger. These findings indicate that the presence of flow increased the swimming intensity during individual swimming bursts.

3.2 Materials and methods

3.2.1 Husbandry

Wildtype zebrafish were reared at the fish facility of Wageningen University under standard conditions at 27±0.5°C [222]. Eggs were collected by allowing two males to mate with three females. Eggs were kept in small containers in a water bath at the breeding facility at 29±0.5°C. The high-speed recording experiments were approved by the Wageningen University Animal Experiments Committee (protocol nr. 2012022e). Fish were fed *Paramecium* (until 9 dpf) and *Artemia* (from 8–10 dpf) *ad libitum*. Fish were fed before the recordings.

3.2.2 Flow set-up

The set-up for subjecting fish to flow consisted of a gravity-fed system which was located in a temperature controlled room (26°C, Figure 3.1A–C). Fish were retained in a square tube (251 mm × 20 mm × 20 mm) by a fine nylon mesh (0.4 mm × 0.4 mm, from core to core of the wires, thickness of wires is 0.20 mm) on each end of the tube. A parallel array of tightly packed straws (inner diameter of 1.40 mm, outer diameter of 2.50 mm, Derlon), with fine nylon mesh at both ends, was placed at the entrance of the tube to create an approximately uniform flow velocity at the inlet. Swimming behaviour was recorded in a specific section of the tube, indicated with an asterisk in Figure 3.1C.

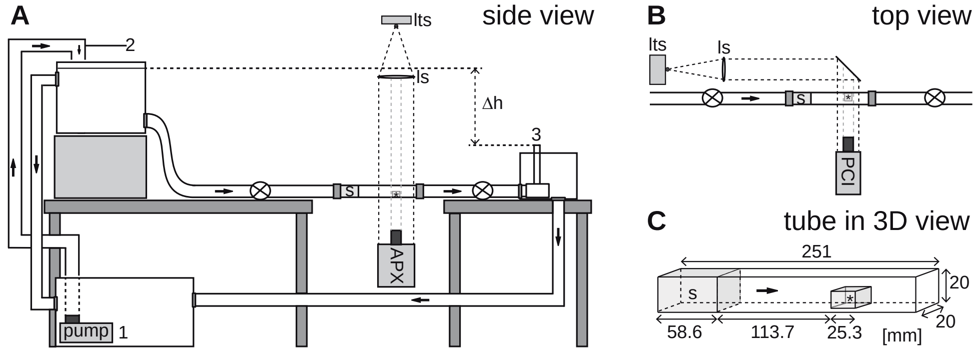

Figure 3.1. Schematic representation of the high-speed video (hsv) set-up. Arrows indicates the direction of the flow. Swimming behaviour was recorded in a specific section of the tube indicated with an asterisk. The section containing the parallel array of tightly packed straws is indicated with an S. ls = lens, lts = light source. **A**: Side view of the hsv set-up. The recordings from the bottom of the tube were recorded with the FASTCAM-APX RS camera (APX). Water was pumped (1) to the top aquarium (2) and flowed back into the reservoir via the square tube and outflow tube (3) due to gravity. The difference in water level, Δ h, between the top aquarium (1) and the outflow tube (2) determined the flow velocity in the square tube. **B**: Top view of a section of the hsv set-up indicating position of the FASTCAM-1024 PCI camera (PCI) for the recordings from the lateral side of the tube. **C**: 3D schematic representation of the square tube including the dimensions of the tube and of specific sections. The small grey box, indicated with an asterisk, represents the volume where recordings were made of the swimming behaviour of zebrafish larvae.

3.2.3 High-speed recordings

Twenty fish were placed in the tube and allowed to acclimate (15–30 min) before starting the recordings. We first made high-speed recordings of swimming behaviour without flow. Subsequently, recordings were made of the swimming behaviour of fish subjected to an average flow velocity over the cross-section of the tube of 14.2 mm/s (25 % of the critical flow velocity, [54]). Note that the actual flow velocity that the fish larvae experience is different from this average flow velocity.

A parallel lightbeam (produced by a KL150B lightsource, 150W, Schott AG, Germany) was projected at the specific section of the tube where the swimming behaviour was recorded (Figure 3.1). The swimming behaviour was recorded from the lateral side of the tube with a FASTCAM-1024 PCI high-speed camera (PHOTRON Ltd., Japan; 1000 frames s^{-1}, 1024×1024 pixels, exposure time 250 µs) and a 105 mm Nikon lens (AF MICRO NIKKOR, 1:2.8d, Nikon Corporation Inc., Japan). Swimming behaviour was recorded from below with a FASTCAM-APX RS high-speed camera (PHOTRON Ltd., Japan; 1000 frames s^{-1}, 1024×1024 pixels, exposure time 250 µs) and a 120 mm Nikon lens (Medical-NIKKOR Micro, 1:4, Nikon Corporation Inc., Japan) with a 27.5 mm Nikon extension ring (Nikon Corporation Inc., Japan). With this set-up using parallel beams of backlight, we made recordings of the silhouettes of the fish. For each experimental condition (without flow or with flow), 19 swimming sequences were further analyzed. Each sequence consisted of one swimming burst, which is a forward movement consisting of several tail beats.

3.2.4 Analysis of flow velocity

To determine the flow velocity profile in the section of the tube where the recordings were made (Figure 3.1C), we performed Particle Image Velocimetry (PIV) analysis of the flow. The recordings were made from the bottom of the tube with the FASTCAM-APX RS high-speed camera (60 frames s^{-1}, 1024×1024 pixels, exposure time 10 ms) and a 120 mm Nikon lens (1:4) with a 27.5 mm Nikon extension ring. To visualize the flow, the fluid was seeded with Conduct-O-Fill® silver-coated hollow glass spheres (SH400S20, Potters Industries Inc., USA; average diameter 13 µm) which were illuminated by a laser sheet produced with a continuous Excel 2.0W laser (Laser Quantum Ltd., United Kingdom; wavelength of 532 nm) and a cylindrical lens (focal length -12.5 mm). The laser sheet was projected horizontally at 10 mm above the bottom of the tube and we analyzed the flow at 13.9 mm/s.

The PIV recordings were analyzed with DaVis (version 7.4.0.120-64, LaVision GmbH, Germany) to calculate the actual flow velocity. The size of the initial sub-image for the PIVs correlation procedure was 64 × 64 pixels, and reduced to 32 × 32 pixels for the second and final correlation (overlap between sub-images was 50 %). We took a time-average of the PIV velocity field to smoothen the velocity vectors. One hundred subsequent frames were recorded to calculate a time average of the velocity profile. A velocity profile of this analysis is shown in Figure 3.2C (red curve).

In addition, we used Computational Fluid Dynamics (CFD) to simulate the flow in the square tube. We used the steady state solver of Fluent (version 6.3.26, Fluent Inc., USA) for this purpose. These flow velocity profiles were verified with the unsteady solver of Fluent, which yielded the same results. For the CFD analyses of the flow velocity it was assumed that at the entrance of the tube (starting from the end of the section with the straws) the flow had an uniform velocity over the cross-section (Figure 3.2A, left side). We included in the CFD analyses that, at the outflow of the tube, the flow had a nearly uniform flow velocity profile due to the mesh located at the outflow of the tube. This was simulated with a constant loss coefficient of 10 over the outlet surface. Substantial changes of the value of this coefficient had a negligible effect on the flow velocities in the region where we made the recordings. The CFD analyses indicated that at the location where the recordings were made, the flow profile approximated a Hagan-Poisseuille flow profile (Figure 3.2A, B). The cross-section of the flow profile and the position of fish at this location indicated that fish were mainly located in the boundary layer.

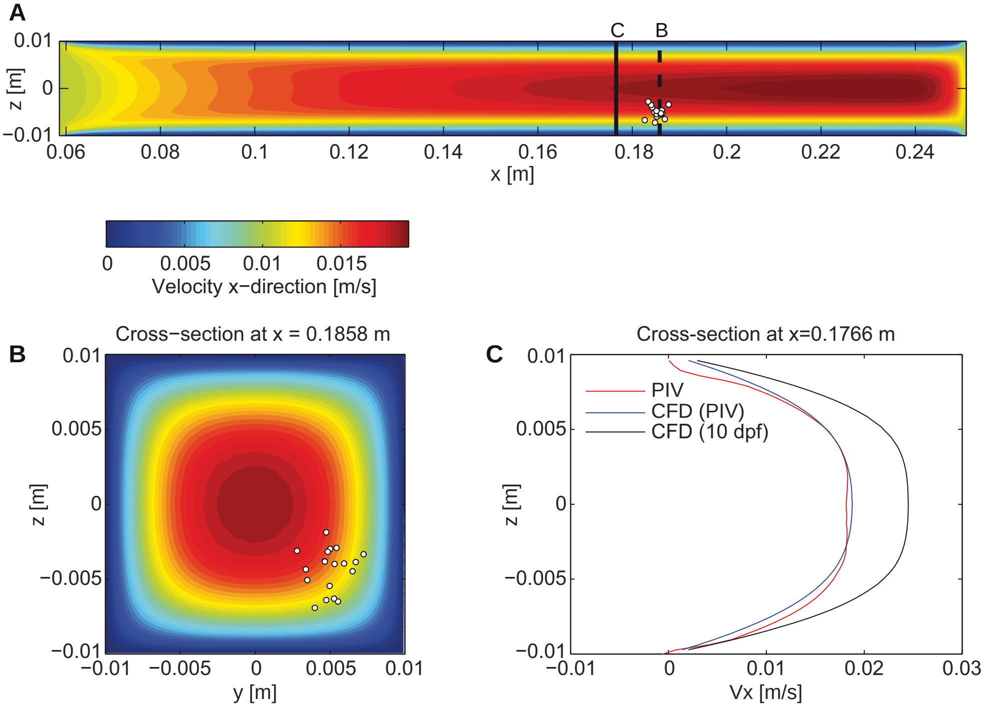

Figure 3.2. PIV and CFD analyses of flow velocity profiles of the square tube. **A**: Side view of flow velocity profile of the square tube determined with CFD analysis with an average flow velocity of 0.0142 m/s. The flow profile was visualized starting from the right end of the section with the straws (x = 0.06 m). It was assumed that at this point the flow profile started with a uniform flow velocity over the cross-section. The direction of flow was from left to right. The black vertical line indicates the position of the mid-horizontal velocity profiles shown in C. The black dashed line indicates the position of the cross-section shown in B. **B**: Cross-section of flow velocity profile (location indicated in A) with the position of the fish (of the 19 analyzed swimming events) indicated with white dots. **C**: PIV and CFD analyses of flow velocity profile at the location indicated in A. The CFD analyses (blue curve) adjusted to match the PIV data (red curve). The CFD analyses of the flow profile at 10 dpf (black curve) was used to correct the swimming speed of fish subjected to flow. See also text for further explanation of PIV and CFD analyses of flow velocity profiles. The white dots in A and B indicate position of fish subjected to flow of the recorded swimming bursts.

The CFD flow predictions were validated with the flow velocity analysis from the PIV recordings (Figure 3.2C). These CFD inflow conditions agreed with the measured average flow velocity observed in the PIV analyses. The CFD flow prediction is shown at the section of interest with a blue curve (Figure 3.2C). During the high speed recordings of fish subjected to flow, we used slightly higher flow velocities. These flow velocities were used to compute the flow profile by CFD (Figure 3.2C, black curve). These results were used as input for the fish tracker to correct the swimming speed of the fish subjected to flow.

3.2.5 Model of the shape of the body

The swimming kinematics of the fish in different flow conditions were analyzed with an in-house developed 3D automated fish tracker implemented in Matlab (R2012a, The Mathworks, Inc., USA) (the tracker software will be described elsewhere). A 3D body model of the fish is needed to track the fish in the high-speed recordings with the tracker software. Three-dimensional body models of fish were made based on images taken from the lateral and dorsal side of wildtype zebrafish larvae at 10 dpf. Images were taken with an Olympus DP50 digital camera (Olympus Corporation Inc., Japan) mounted on a Zeiss Stemi SV11 microscope (Carl Zeiss AG, Germany) and with Analysis^{D} software (version 2.2, Soft Imaging System GmbH, Germany). In the dorsal images, we digitized the longitudinal axis (from the snout to tail tip) and traced the outlines of the head and trunk (with and without pectoral fins) and eyes (tracing both eyes as one structure). In the lateral images, we digitized the longitudinal axis (from snout to tail tip), the positions where the abdomen had the greatest width and traced the outlines of the head and trunk, the eyes and the median finfold. The skin outlines were fitted at 51 equidistant points along the body and a 3D model of the shape of the body (with and without pectoral fins) was constructed with an in-house developed program in Matlab (Figure 3.3).

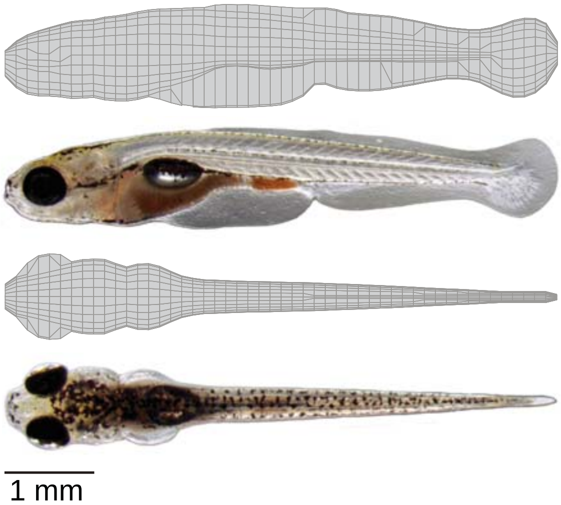

Figure 3.3. Example of a 3D model of the shape of the body (without pectoral fins) of a 10 dpf wildtype zebrafish. The model of the shape of the body was based on the image shown below the model. Top = lateral view, bottom = dorsal view.

The details of this program will be described elsewhere. Based on the length of the fish in the high-speed recording a body model of a fish was chosen which had similar dimensions. This model was subsequently isometrically scaled to make it identical in size to the fish in the high-speed recordings. In the video frames where the fish kept the pectoral fins along the body, a body model including the pectoral fins was used to track the fish. In the other frames, the fish was tracked with a body model excluding the pectoral fins.

3.2.6 Analysis of swimming kinematics

The output of the fish tracker software are positions, rotations (roll, pitch, yaw) and body angles of the fish as function of time. These parameters have been smoothed for further analysis by fitting the data with the cubic B-spline using the method of least squares (with the Matlab routine SPLINEFIT [122]). The level of smoothing is controlled by the number of breakpoints. Setting a breakpoint at every fifth frame achieved optimal smoothing, as indicated by the absence of high frequency irregularities, while retaining the physical signal.

Subsequently, we used the smoothed position, rotation and body angles to calculate the following kinematic parameters. First, the centre of mass (CoM) was computed from the mass distribution, assuming equal density throughout the fish. Furthermore, swimming velocity was calculated by differentiating the displacement of the CoM between consecutive frames. The velocity of the CoM was corrected for the local ambient flow velocity in the earth-bound frame (see also section 3.2.4). The forward and lateral velocity components of the mid-tail (0.94 BL) were determined with respect to the instantaneous velocity of the CoM. We also computed the forward speed of the mid-tail in the moving frame of the CoM by subtracting the velocity of the CoM from the forward velocity in the earth-bound frame (Figure 3.7).

Lateral displacement of the tail tip was determined in a head-attached coordinate system by calculating the distance of the tail tip to the centre line through the head (the latter was assumed to be rigid) (See also Figure 3.6A). The lateral speed of the tail tip in the head-bound frame was calculated by differentiating the lateral displacement of the tail tip between consecutive frames. The number of half beats was determined via the lateral displacements of the tail tip (with respect to the centre line through the head) (see also Figure 3.6). The lateral displacement of the tail tip between two zero-crossings which was larger than 0.05 BL was counted as a half beat.

The tail beat frequency was determined as follows. We first determined the extremes in the lateral displacement plots of the tail tip (only the extremes of half beats larger than 0.05 BL with respect to the centre line through the head). Subsequently, the time interval between two extremes was calculated. The half beat frequency was calculated by dividing 1 by the average of the time intervals between two extremes during a swimming bout. The tail beat frequency was calculated by dividing the half beat frequency by two.

The duration of the swimming bout was defined as the time between the first movement of the tail until the moment that the tail had just returned to the mid-line in the head-attached frame after the last lateral excursion of the tail. The curvature was calculated by taking the derivative of the local body angle with respect to the distance along the central body axis. Swimming velocity, lateral speeds and forward speeds of the tail (in the earth-based frame of reference), lateral displacements and lateral speeds of tail tip (with respect to the centre line through the head) and curvatures were normalized by the total body length (BL).

3.2.7 Statistical analysis

To explore significant differences ($p < 0.05$) between the swimming kinematics of zebrafish larvae subjected to an increased flow and without flow, we evaluated the kinematic data with an independent t-test, when data had a normal distribution, with SPSS (version 19.0.0.1, IBM, USA). To assess the normality of data, we performed a Q-Q plot analysis, histogram of frequency distribution and Shapiro-Wilk test in SPSS. The following kinematic parameters had a normal distribution: tail beat frequency, duration of swimming burst and maximum normalized curvature of a swimming burst and average maximum normalized curvatures of the first three half beats. The other kinematic parameters (normalized swimming velocity, maximum normalized lateral displacements and lateral speeds and position of maximum normalized curvature within a swimming burst and position of average maximum normalized curvature over three half beats) and pitch angle did not have a normal distribution and therefore a Mann-Whitney U test was used to explore significant differences with SPSS. Note that multiple recordings could have been made of the same fish. However, since we could not determine whether it was the same fish or an another fish, we regarded each recording as an independent observation.

3.3 Results

During the high-speed recordings of the swimming behaviour of fish in the tube without flow, fish swam throughout the tube. However, when fish were subjected to flow, fish swam mostly upstream near the walls of the tube. During both recording sessions fish showed intermittent swimming behaviour: short bursts of tail beats alternated with coasting. Occasionally, fish subjected to flow would adhere to the wall or stick against the mesh at the outflow of the tube to maintain position.

Furthermore, fish subjected to flow demonstrated swimming bouts consisting of several swimming bursts (a forward movement consisting of several tail beats followed by coasting) directly one after another. After such a swimming bout (consisting of several swimming bursts) fish shortly went with the flow before starting a new swimming bout. We only analyzed individual swimming bursts of fish subjected to flow and without flow.

To illustrate high-speed recordings of fish swimming with flow and without flow, we selected representative swimming sequences which had tail beat frequencies, pitch angles and maximum curvatures (of all half beats) near the average values (Figure 3.4). The analysis of these recordings with the automated fish tracker (for the same frames) are shown in Figure 3.5. This demonstrates (among others) that the motion of the tail fin was accurately tracked (>0.9 BL).

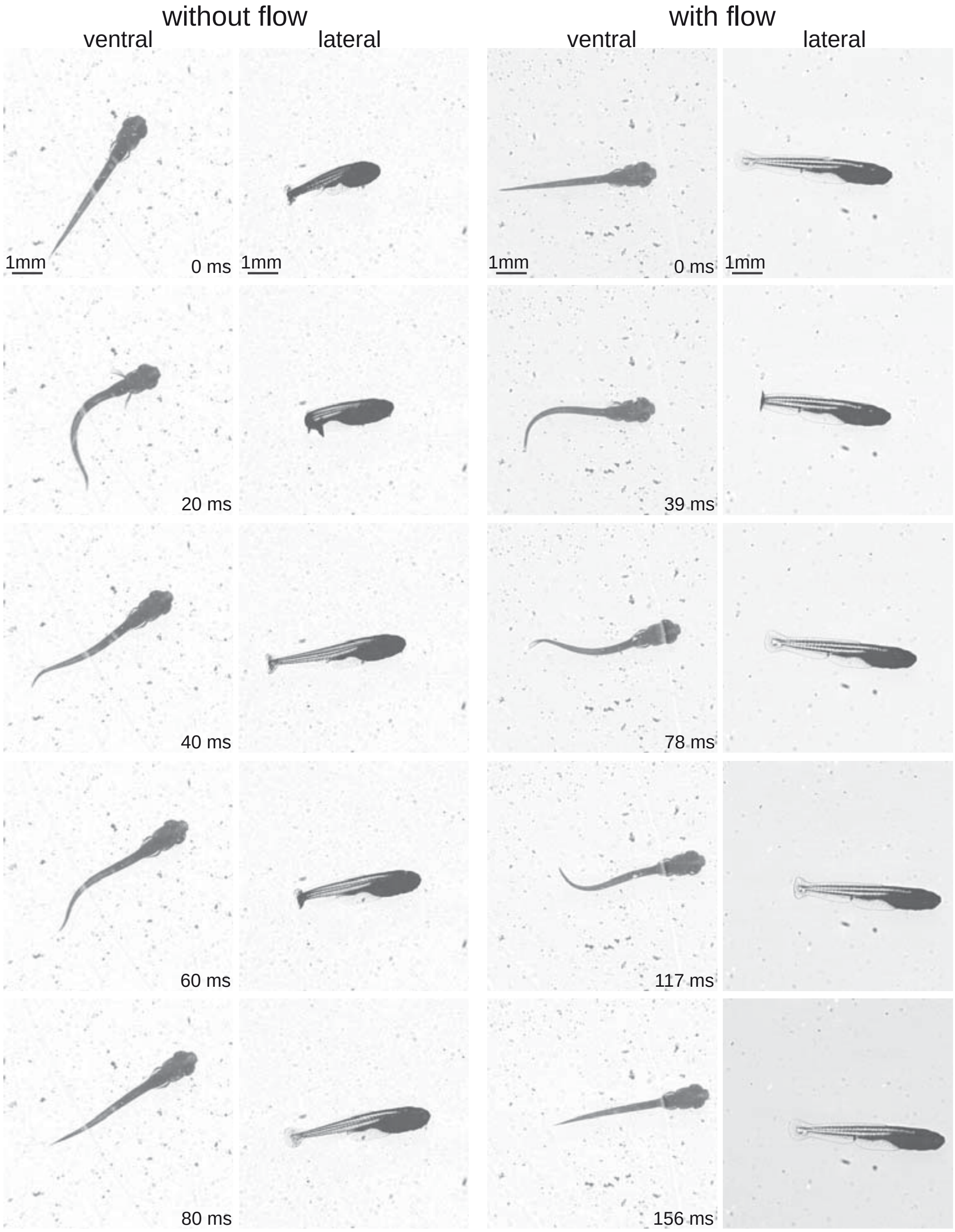
without flow
ventral
lateral
with flow
ventral
lateral
1mm
0 ms
1mm
1mm
0 ms
1mm
20 ms
39 ms
40 ms
78 ms
60 ms
117 ms
80 ms
156 ms

Figure 3.4. Representative frames from high-speed recordings illustrating a complete swimming burst with and without flow, from the bottom and lateral side of the tube. Total body length: 5.8 mm (without flow), 5.2 mm (with flow). Kinematic analyses of these high-speed recordings are shown in subsequent figures.

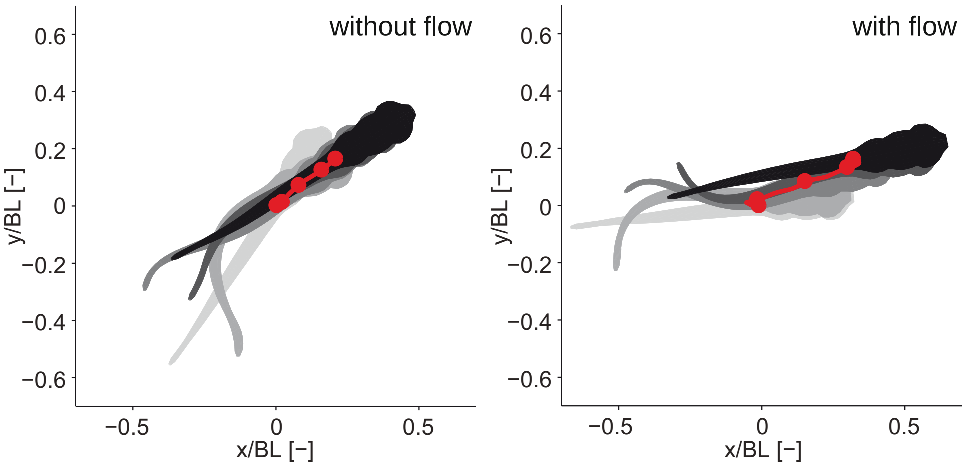

Figure 3.5. Tracking results of the frames of the high-speed recordings shown in Figure 3.4 with the automated fish tracker. The red curve with the red dots indicates the path of the CoM (red dot). The colour of the body model indicates the tracking in time, thus, the first frame corresponds with the light grey model, the last frame with the black body model.

The maximum magnitude of the pitch angle in the recordings illustrated in Figure 3.4 was 12 degrees for the fish which did not experience flow whereas this was 8 degrees for the fish subjected to flow. The maximum magnitude of the pitch angles, on average, was not significantly different between fish which did not experience flow and fish subjected to flow ($p > 0.05$, Table 3.1). The range of maximum magnitude of the pitch angles was 1.62–27.99 degrees in fish which did not experience flow whereas this was 1.52–11.75 degrees in fish subjected to flow.

Table 3.1. Kinematic parameters of zebrafish larvae in varying flow conditions, Part I

Flow conditions	BL [mm]	θ [°]	d [ms]	*half beats*
No flow	5.45±0.45	10.85±6.74	95.37±9.09	3.11±0.32
Flow	5.37±0.24	7.51±2.52	127.68±16.49*	6.21±1.27*

Values represents averages ± standard deviation of swimming bursts, n = 19. Asterisks indicates significant difference ($p < 0.05$). *BL*, total body length; *pitch*, maximum magnitude of pitch angle; *d*, duration of a swimming burst; *half beats*, number of half beats.

Figure 3.4 and Table 3.1 also shows that the duration of the swimming burst was longer in fish subjected to flow than without flow. In the example shown in Figure 3.6, the fish which did not experience flow, exhibited three half beats (Figure 3.6B) and had a tail beat frequency of 22 Hz whereas the fish subjected to flow exhibited eight half beats and had a tail beat frequency of 30 Hz (Figure 3.6C). The average number of half beats and the tail beat frequency during a swimming burst was larger in fish subjected to flow ($p < 0.05$, Table 3.1 and Table 3.2).

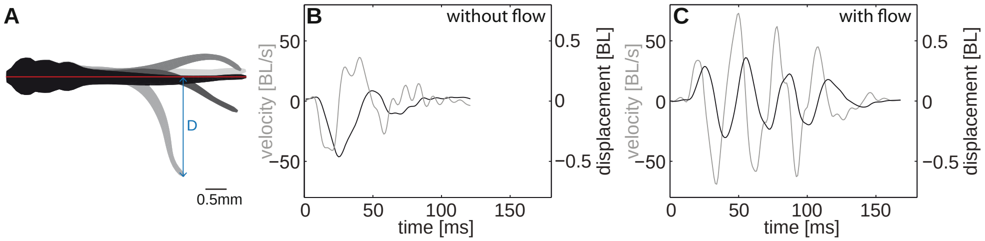

Figure 3.6. Flow increases tail beat frequency and lateral velocities of the tail tip. **A**: Lateral displacement of the tail tip was determined by calculating the distance of the tail tip to the centre line through the head (indicated here with a up down blue arrow and D). The red line indicates the centre line through the head. The number of half beats were determined by counting the lateral displacements of the tail tip between two zero-crossing which were larger than 0.05 BL. **B,C**: Normalized lateral displacement and lateral velocities of the tail tip of the recordings shown in Figure 3.4. Normalized lateral displacement of the tail tip is indicated with a black curve, normalized lateral speed of tail tip is indicated with a grey curve.

Table 3.2. Kinematic parameters of zebrafish larvae in varying flow conditions, Part II

Flow conditions	*f* [Hz]	*D(tailtip)* [BL]	*v(tailtip)* [BL/s]
No flow	23.20±2.72	0.39±0.16	46.87±18.32
Flow	31.96±4.15*	0.38±0.11	96.28±38.54*

Values represents averages ± standard deviation of swimming bursts, n = 19. Asterisks indicates significant difference ($p < 0.05$). *BL*, total body length; *f*, tail beat frequency; *D(tailtip)*, maximum amplitude of normalized lateral displacement of the tail tip (in a head-bound frame); *v(tailtip)*, maximum amplitude of normalized lateral speed of the tail (in a head-bound frame).

In the example recordings, the maximum amplitude of the normalized lateral displacement of the tail tip of the fish which did not experience flow was 0.47 BL whereas this was 0.35 BL for the fish subjected to flow (Figure 3.6). On average, there was not a significant difference between the maximum amplitudes of the lateral displacement of the tail tip between fish subjected to flow and which did not experience flow ($p > 0.05$, Table 3.2).

In Figure 3.6, the maximum amplitude of the normalized lateral speed of the tail tip was 40.86 BL/s for the fish which did not experience flow, whereas the fish subjected to flow had a larger maximum amplitude of 76.38 BL/s. On average, maximum amplitude of the normalized lateral speed of the tail tip was larger in fish subjected to flow (Figure 3.6, $p < 0.05$, Table 3.2). As expected, during both sessions, the lateral speed of the tail tip reached maximum amplitudes before the lateral displacement of the tail tip reached maximum amplitudes.

In the example shown in Figure 3.7, the fish which did not experience a flow had a maximum normalized swimming speed of 6.9 BL/s, whereas the fish subjected to flow had a maximum normalized swimming speed of 9.8 BL/s. On average, fish subjected to flow swam faster than fish which did not experience flow ($p < 0.05$, Table 3.3).

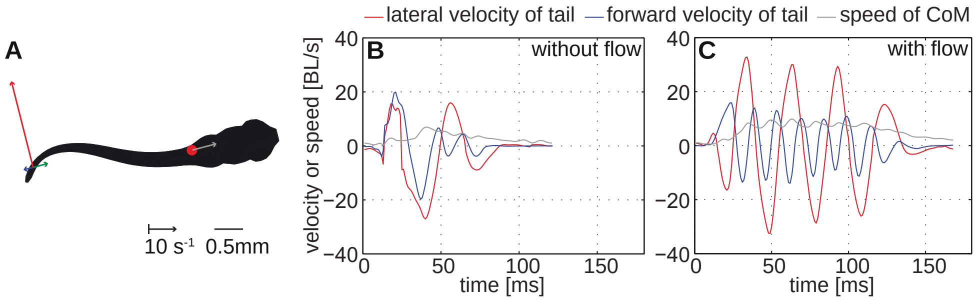

Figure 3.7. Flow leads to higher swimming speeds and the mid-tail contributes an important part in the forward thrust. **A**: Schematic representation of the forward and lateral velocity components of the mid-tail with respect to the velocity of the CoM at 47 ms (with flow). Colours of the velocity vectors correspond with the colours of the velocity versus time plots in B and C. **B, C**: Normalized forward and lateral velocities of the mid-tail and speed of the CoM of the recordings shown in Figure 3.4.

Table 3.3. Kinematic parameters of zebrafish larvae in varying flow conditions, part III

Flow	*U* [BL/s]	*curvature*	*pos-curvature* BL	*curv-three*	*pos-curv-three* BL
No Flow	6.05±1.92	9.29±1.44	0.93±0.04	8.22±1.10	0.93±0.02
Flow	11.61±3.92*	12.03±1.42*	0.94±0.02	9.95±0.98*	0.93±0.01

Data represent averages ± standard deviation of a swimming burst unless otherwise indicated, n = 19. Asterisks indicates significant differences ($p < 0.05$). *U*, maximum speed of CoM; *curvature*, normalized maximum curvature of all half beats; *pos-curvature*, position along the body of the maximum normalized curvature of all half beats; *curv-three*, normalized maximum curvatures averaged over the first three half beats; *pos-curv-three*, position along the body of maximum normalized curvature averaged over the first three half beats, BL = total body length.

The analysis of the velocity components of the mid-tail with respect to the velocity of the CoM of the recordings showed that lateral speed of the mid-tail and speed of the CoM reached maximum amplitudes at similar moments (Figure 3.7). The forward velocity of the mid-tail showed a shift with respect to the speed of the CoM. Maximum forward velocity of the mid-tail was reached at or near the maximum deceleration of the CoM, whereas the reverse occurred for the minimum in the forward velocity (which in fact represents a backward velocity of the tail with respect to the CoM).

There were significant differences in curvature between fish subjected to flow and without flow (Figure 3.8). In fish subjected to flow, the increase of curvature along the body axis was more steep. Furthermore, the transition (in time) between peak curvatures was narrower and steeper. We computed non-dimensional curvatures by multiplying curvature by body length. In the example recordings in Figure 3.8, the fish subjected to flow had maximum normalized curvature of 12.26 during a swimming burst whereas the fish which did not experience a flow had maximum normalized curvature of 9.89 during a swimming burst. Furthermore, the maximum normalized curvature averaged over three consecutive half beats was also larger in the fish subjected to flow (10.66 vs 8.77 in the fish which did not experience a flow).

On average, fish subjected to flow had larger maximum normalized curvatures during a swimming burst and averaged over three half beats ($p > 0.05$, Table 3.3). The location of these maximum normalized curvatures was similar between fish subjected to flow and without flow and was located around 0.93–0.94 BL (Table 3.3). This location corresponds with the mid-tail. Thus, this indicates that the mid-tail experienced higher peak curvatures when fish were subjected to flow.

3.4 Discussion

Our study is the first to demonstrate that flow induces significant changes in swimming kinematics of zebrafish larvae. Previous findings demonstrated that flow-induced swim-training increased the burst frequency in fish subjected to flow, thus increasing swimming activity [54]. The current study shows that flow not only increases the time spent on swimming but also increases the swimming intensity during a swimming burst. Furthermore, we showed that it is important to make recordings from multiple angles of view since fish made considerable pitch angles. The range of maximum magnitude of pitch angles was 1.52–27.99 degrees (in fish subjected to flow and without flow). By taking the pitch angles into account, it was possible to obtain a correct fit of the body model in the high-speed video recordings. The substantial pitch and roll angles of larval fish have been a serious limitation of previous manual and automated tracking procedures.

With PIV and CFD analyses, we were able to calculate the actual swimming speeds of fish subjected to flow. This showed that although fish were subjected to an average flow velocity of 14.2 mm/s (corresponding to a normalized velocity of 2.64 BL/s) fish swam at 62.4±2.16 mm/s or 11.61±3.92 BL/s. The flow velocity profile approximated a Hagan-Poisseuille profile and fish had to swim in this parabolic flow profile (Figure 3.2). The flow speeds in this location were in the range of about 10.0–15.0 mm/s. Thus, our study demonstrates that fish experience a range of flow velocities while swimming in a tube with constant average flow velocity. They also swam at higher speeds than the applied average flow speed in the tube.

In a previous study from our lab, larval zebrafish kinematics of cyclic swimming and slow starts were investigated from 2–14 dpf in stagnant water [137]. Swimming speeds ranged between 9.3–55.3 BL/s during cyclic swimming whereas during slow starts swimming speeds ranged between 3.9–7.0 BL/s. Tail beat frequency during cyclic swimming ranged between 31–100 Hz whereas during slow starts this ranged

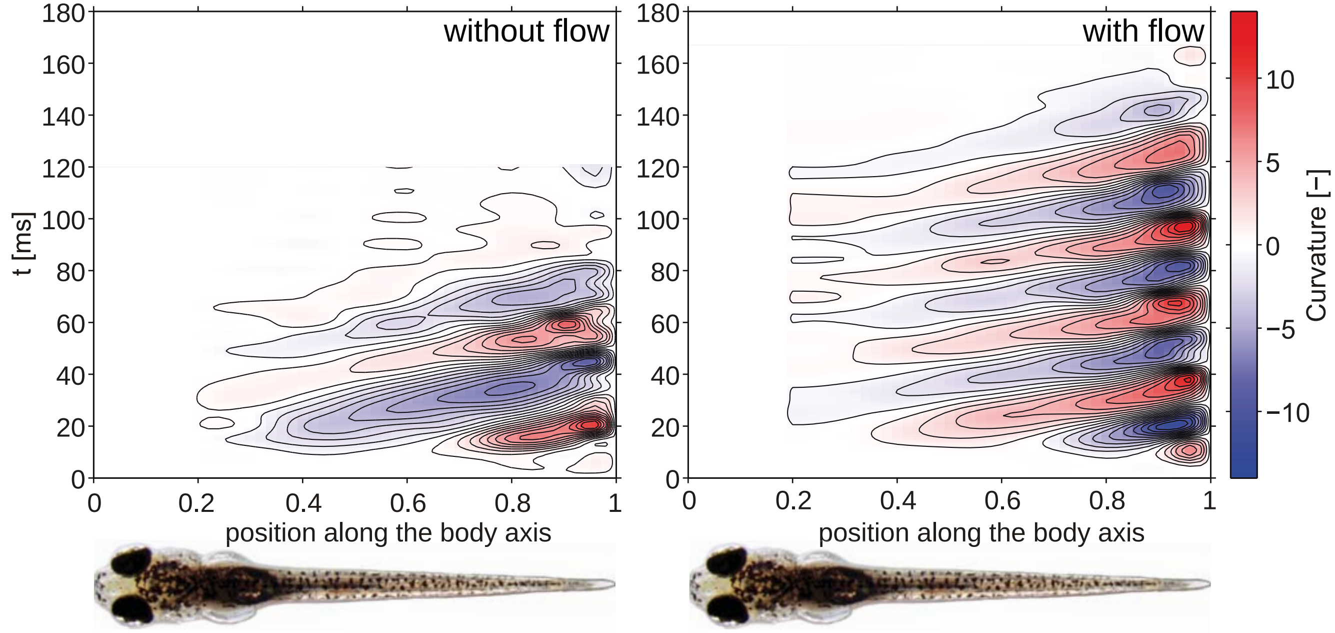

Figure 3.8. Flow leads to higher peak curvatures in the caudal fin. Normalized curvature plots of the recordings shown in Figure 3.4 which represent two typical examples.

between 28–61 Hz. Based on these kinematic parameters, the swimming behaviour exhibited by the fish which did not experience a flow were categorized into slow starts and of the fish subjected to flow to cyclic swimming. We observed a discrepancy between the previous study and this study with respect to the curvature data. During slow starts (4–14 dpf), peak curvatures were located between 0.8–0.9 BL and were smaller than in our study (maximum normalized curvatures = 6). During cyclic swimming (2–7 dpf), peak curvatures were mostly located around 0.8 BL and were about twice as small as in our study (maximum normalized curvatures = 5). This could be due to the stronger level of smoothing applied in that study than our study. It could also be due to differences in developmental stages that were analyzed. In our study, the swimming kinematics of fish at 10 dpf were analyzed whereas in the study by Müller and Van Leeuwen [137] the swimming kinematics of different stages (2, 3, 4, 5, 7, 14 dpf) but not 10 dpf were analyzed. In a future study, we will include a similar range of stages, allowing us to compare the two studies.

Fish subjected to flow showed an increase in tail beat frequency, but the maximum amplitudes of the normalized lateral displacement of the tail tip were similar. The maximum amplitudes of the normalized lateral speeds of the tail tip were larger in fish subjected to flow, which corresponds to the higher tail beat frequencies that we observed. In addition, the backward velocity of the mid-tail (0.94 BL) was maximal when the CoM reached its maximum forward acceleration and vice versa. This indicates that the mid-tail made an important contribution to the forward thrust. This was observed both in fish subjected to flow and in fish which did not experience flow.

The flow that was applied in the tube induced larger maximum normalized curvatures during a swimming burst and averaged over the first half beats. Maximum normalized curvatures were located around 0.93–0.94 BL which corresponds with the caudal fin. In a previous study, we showed that flow-induced swim-training prioritized the development of skeletal elements in the caudal fin. In that study, fish were subjected to a higher flow velocity (50 % U_{crit}) than in the current study. We expect similar effects on peak curvatures in the caudal fin at this higher velocity. The increased curvatures in the caudal fin indicates that the caudal fin experienced increased mechanical loading during swim-training. This increased loading could have stimulated the prioritization of the development of skeletal structures in the caudal fin (observed in our previous study [54]). The kinematic data obtained in this study could be used as input for computational fluid dynamics to investigate how flow leads to changes in the distribution of forces along the body [61, 119] and to what extent this leads to higher peak forces on the caudal fin. Additionally, the analysis of swim-kinematics of zebrafish larvae at different developmental stages in varying flow conditions could provide a better understanding of the link between functional performance and morphological development.

Acknowledgments

We thank Jos van den Boogaart, Björn Elzer and Eric Karruppannan for the support with building the high-speed recording set-up and the preliminary experiments. We are especially grateful to the members of the Zebrafish Facility at Wageningen University for providing help and taking care of the zebrafish. We would also like to thank Sander Kranenbarg for his input on the experimental design and critical reading of the manuscript.

”Just keep swimming. Just keep swimming. Just keep swimming, swimming, swimming. What do we do? We swim, swim.”

Dory (in Nemo)

Chapter 4

Swim-training changes the spatio-temporal dynamics of skeletogenesis in zebrafish larvae (*Danio rerio*)

Ansa W. Fiaz[1], Karen M. Léon-Kloosterziel[1], Gerrit Gort[2], Stefan Schulte-Merker[1,3], Johan L. van Leeuwen[1], Sander Kranenbarg[1]

Plos One, 2012 (7), e34072

---

[1] Experimental Zoology Group, Department of Animal Sciences, Wageningen University and Research Centre, Wageningen, The Netherlands

[2] Biometris, Wageningen University and Research Centre, Wageningen, The Netherlands

[3] Hubrecht Institute-KNAW & UMC Utrecht, Utrecht, The Netherlands

Abstract

Fish larvae experience many environmental challenges during development such as variation in water velocity, food availability and predation. The rapid development of structures involved in feeding, respiration and swimming increases the chance of survival. It has been hypothesized that mechanical loading induced by muscle forces plays a role in prioritizing the development of these structures. Mechanical loading by muscle forces has been shown to affect larval and embryonic bone development in vertebrates, but these investigations were limited to the appendicular skeleton. To explore the role of mechanical load during chondrogenesis and osteogenesis of the cranial, axial and appendicular skeleton, we subjected zebrafish larvae to swim-training, which increases physical exercise levels and presumably also mechanical loads, from 5 until 14 days post fertilization. Here we show that an increased swimming activity accelerated growth, chondrogenesis and osteogenesis during larval development in zebrafish. Interestingly, swim-training accelerated both perichondral and intramembranous ossification. Furthermore, swim-training prioritized the formation of cartilage and bone structures in the head and tail region as well as the formation of elements in the anal and dorsal fins. This suggests that an increased swimming activity prioritized the development of structures which play an important role in swimming and thereby increasing the chance of survival in an environment where water velocity increases. Our study is the first to show that already during early zebrafish larval development, skeletal tissue in the cranial, axial and appendicular skeleton is competent to respond to swim-training due to increased water velocities. It demonstrates that changes in water flow conditions can result into significant spatio-temporal changes in skeletogenesis.

Keywords: mechanical load, swim-training, zebrafish, osteogenesis, chondrogenesis

4.1 Introduction

Fish larvae are the smallest free-living vertebrates. They encounter many environmental challenges during development such as variation in water velocity, food availability and predation. Osse and van den Boogaart [151] hypothesized that developmental patterns of form change and growth in larval fish which optimize survival chances are maintained during the course of evolution. Moreover, Fuiman [60] and Osse and van den Boogaart [151] showed that growth of the head and tail area were prioritized over the growth of the trunk area during fish larval development. In fish larvae, the first skeletal elements to develop are structures involved in feeding (e.g. cleithrum, 5th branchial arch), respiration (e.g. opercular bones) and swimming (e.g. hypurals) [13, 36, 75, 221]. The rapid development of structures involved in feeding and swimming is important for survival on exogenous food and to escape predation.

Weisel[221] investigated early bone development in the sucker *Catostomus macrocheilus* and found that the bones which formed earliest were associated with movement such as feeding, respiration and swimming rather than protection. This suggests that mechanical loading induced by muscle forces plays a role in prioritizing the development of these structures.

Mechanical loading by muscle forces has been shown to affect embryonic and larval bone development in vertebrates, but these investigations have been limited to the appendicular skeleton. In humans, Rodríguez *et al.*[178] demonstrated in a radiographic and histological study that fetal immobility led to thin, hypomineralized, and slender long bones. In avian and murine embryos, *in vivo* experiments with decreased mechanical loading led to a reduction in mineralization, bone surface area, chondrocyte proliferation and glycosaminglycan content of cartilage in long bone rudiments [62, 68, 111, 135, 147]. Increased *in vivo* mechanical loading led to longer leg bones in chick embryos [73, 77]. In addition, *in vitro* experiments showed that increased mechanical loading increased the rate of bone and cartilage formation in chick bone rudiments and calcification of the cartilage growth plate in mouse long bone rudiments [66, 100]. In fish, Cloutier *et al.* [32] showed that swim-training accelerated the onset of chondrogenesis and osteogenesis in the median fins in the Artic Charr (*Salvelinus alpinus*). Previous work from our lab showed that swim-training accelerated osteogenesis of the tail bones during late larval and juvenile development in zebrafish [132]. Analysis of the tail region showed that the onset of osteogenesis of the hypurals and spines of the caudal peduncle appeared earlier in the trained fish than in the control fish.

To investigate the role of mechanical loading in prioritizing the development of structures involved in feeding, respiration and swimming, we analyzed the effect of swim-training during early skeletal development in zebrafish. It is likely that swim-training increases mechanical loading via increased muscle activity. The *ex utero* development and the relatively late skeletal development of the zebrafish makes it possible to investigate the effect of swim-training on the onset of chondrogenesis and osteogenesis *in vivo*. We investigated the time of appearance of cartilage and bone structures in the cranial, axial and appendicular skeleton. In zebrafish embryos, coordinated patterns of swimming appear before the development of many skeletal elements. The first movements appear around 17-19 hours post-fertilization (hpf,[183]) as side-to-side contractions of the trunk and precede coordinated patterns of swimming behaviour. The onset of chondrification and ossification of many skeletal elements lies between 5-14 dpf [13, 36]. The transition from a notochord to a vertebral column also takes place in this period. Therefore, zebrafish larvae were subjected to swim-training from 5-14 dpf. From 72 hpf until 29 dpf (approximately 3.5 mm-10 mm total length), zebrafish are staged as larva [98, 149].

Our study is the first one to investigate the effect of increased swimming activity on osteogenesis and chondrogenesis of the cranial, axial and appendicular skeleton during early fish larval development. Our study shows that increased swimming activity increases growth in zebrafish larvae and prioritizes the formation of skeletal elements that are involved in feeding, respiration and swimming. This reveals a previously unknown plasticity in early vertebrate chondrogenesis and osteogenesis of the cranial, axial and appendicular skeleton in response to an increased water velocity [22, 32, 38, 186, 225].

4.2 Results

4.2.1 Swim behaviour and growth during swim-training

Zebrafish larvae were subjected to swim-training for 9 hours per day from 5-14 dpf. Trained fish were kept in tubes in a custom built swim-training setup and subjected to 50 % of the critical flow velocity (see also Materials and Methods and Figure 4.6). Control fish were kept in identical tubes in the same swim-training setup but with a continuous water flow of less than 0.1 Bl/s for refreshment. During the swim-training we observed the swimming behaviour of control and trained fish (see also Supplementary Movies 4.A.1 and 4.A.2 of the swimming behaviour of control and trained fish). Until 12 dpf more than 80 % of the trained fish swam along the wall of the tube. At 13 dpf this decreased to 76 % and at 14 dpf further to 42 %. At these stages, trained fish swam more in the central part of the tube. The number of trained fish swimming in the front part of the tubes (closer to the inflow of water) also decreased at 13 and 14 dpf. Until 12 dpf, on average, 47 % of the trained fish swam in the front part of the tube, at 13 dpf this was 36 % and at 14 dpf 13 %. In the younger stages, trained fish adhered to the wall of the tube for more than 3 seconds (7 %-1% from 5-8 dpf, respectively) to maintain position. Trained fish older than 8 dpf did not show this behaviour. During the swim-training, only occasionally did trained fish stick for more than 3 seconds against the mesh (<1 %, 6 and 10 dpf). The control fish swam in all directions throughout the tube.

Both trained and control fish showed intermittent swim behaviour; short bursts of tail beats alternated with coasting. To investigate if trained fish had a higher burst frequency than control fish, we analyzed the number of bursts per second. Note that one burst represents several tail beats. Statistical analysis of the burst frequency showed that no relationship with age could be found (Figure 4.1A, ANCOVA, $p > 0.05$). However, trained fish had on average a higher burst frequency (3.5 bursts/s) during the swim-training than control fish (2.5 bursts/s, t-test, $p < 0.05$). During the breaks trained fish swam within 5 minutes throughout the tube like the control fish, indicating that trained fish recovered quickly from the training. Mortality ranged between 2-40 % and was not significantly different between control and trained fish which indicates that swim-training did not influence survival.

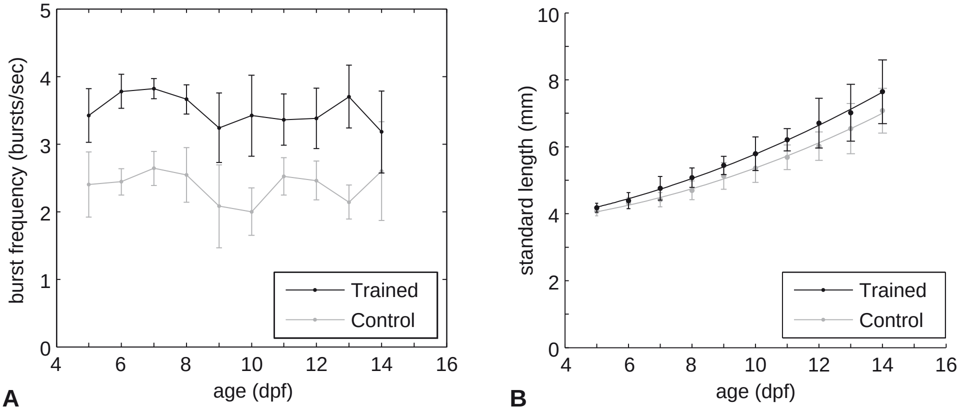

Figure 4.1. Swim-training increased burst frequency and growth in trained fish. **A**: Average number of bursts per second ± standard deviation as a function of age in days post fertilization (dpf). **B**: Average standard lengths (dots) ± standard deviation (with quadratic regression fit) as a function of age (dpf).

Swim-training increased growth in trained fish compared to control fish (Figure 4.1B), as shown by quadratic regression of the standard length measurements on age in the two groups. A significant difference ($p < 0.05$) between the coefficients of the linear terms for trained and control fishes was found. The curvature was not significantly different between the two groups, nor were the intercepts. These results indicate that length differences between trained and control groups increased linearly with age.

4.2.2 Effect of swim-training on chondrogenesis

The onset of chondrogenesis for each cartilage structure (trained and control fish) was estimated by the age or body length at which 50 % of the fish showed the presence of a specific cartilage structure. We refer to the estimates of age as $CF50_{age}$ (Cartilage Forming) and to the estimates of body length as $CF50_{lgt}$. $CF50_{age}$ and $CF50_{lgt}$ values were calculated from logistic regressions of the binary presence or absence data of cartilage structures (see also Materials and Methods). Plotting the $CF50_{age}$ values of trained fish against the $CF50_{age}$ values of control fish showed that swim-training accelerated chondrogenesis (Figure 4.2A, P<0.0001). Almost all of the $CF50_{age}$ values were located below the reference line, which indicates that cartilage structures appeared earlier in trained fish. However, plotting the CF50$_{lgt}$ values of trained fish against the CF50$_{lgt}$ values of control fish showed that trained fish were slightly longer at the onset of chondrogenesis during early development (Figure 4.2B, P<0.0001). This difference in CF50$_{lgt}$ values between trained and control fish decreased with increasing length (P<0.0001).

In teleosts, bones can form via intramembranous or perichondral ossification. During intramembranous ossification, bones form directly from mesenchymal precursors whereas during perichondral ossification, bony matrix forms around a cartilage model [13]. We refer to the phase from the onset of chondrogenesis until the onset of osteogenesis as the cartilage phase. The duration of the cartilage phase in cartilage structures was calculated by subtracting the CF50$_{age}$ values from the BF50$_{age}$ values in control and trained fish. Plotting the duration of the cartilage phase (in days) against the CF50$_{age}$ and CF50$_{lgt}$ values showed that the duration of the cartilage phase decreases with increasing age and length, both in control and trained fish (Figure 4.2C and D, $p < 0.05$).

In the control fish, some structures already appear before 5 dpf (e.g. Meckel's cartilage, ceratobrancials 1-5, basihyal and hyosympletic (Supplemental Figure 4.A.1) and the CF50$_{age}$ values of these structures could therefore not be calculated from our data. The cartilage structures to appear between 5-8 dpf were the parhypural, hypural 1-3 and the pectoral fin endoskeleton (Figure 4.3A and Supplemental Figure 4.A.1). Chondrogenesis proceeded with the appearance of the neural arches 3-5, epibranchials (ep) 3-4, hypobranchial (hb) 3, hypural 4, hemal arch and spine of preural vertebra (pu) 2 and the posterior part of the exoccipital between 8-10 dpf. The first structures of the Weberian apparatus and the first anal proximal radials (apr) 3-4 appeared between 10-12 dpf. Other cartilage structures which also appeared between 10-12 dpf were the ep 1-2, basibranchial 4, parapophyses (pop) 5, hypural 5, haemal arch 28, neural arch of pu 2-3 and haemal arch of pu 3. The paraphophyses appeared in an anterior to posterior direction. The proximal and distal radials of the anal and dorsal fin, however, appeared anteriorly and posteriorly to the third and fourth radial. The following cartilage structures appeared between 12-14 dpf: hb 4, pharyngobranchials (pb) 1-4, supraneural 2-3, roofing cartilage, parapophyses 6-12,

Figure 4.2 ***(following page).*** Swim-training accelerated both chondrogenesis and osteogenesis. **A**: CF50$_{age}$ values of trained fish plotted against CF50$_{age}$ values of control fish with a linear regression fit (solid line). Dashed line is a reference line which indicates the CF50$_{age}$ values which are not different between control and trained fish. Plus signs indicate cartilage structures without BF50$_{age}$ values, squares are with BF50$_{age}$ values. **B**: Similar plot as in A but with CF50$_{lgt}$ values. **C**: Duration of cartilage phase for cartilage bones (in days, indicated with squares in A and E) plotted against the CF50$_{age}$ values of control and trained fish with a linear regression fit (solid lines) (trained fish: black dots and black regression line, control fish: grey dots with grey regression line). **D**: Similar plot as in C but with duration of cartilage phase (days) plotted against the CF50$_{lgt}$ values of control and trained fish. **E**: Similar plot as in A but with BF50$_{age}$ values. Red dots indicates BF50$_{age}$ values of dermal bones, plus signs of cartilage bones without CF50$_{age}$ values, squares of cartilage bones with CF50$_{age}$ values. Dashed line see A. **F**: Similar plot as in E but with BF50$_{lgt}$ values.

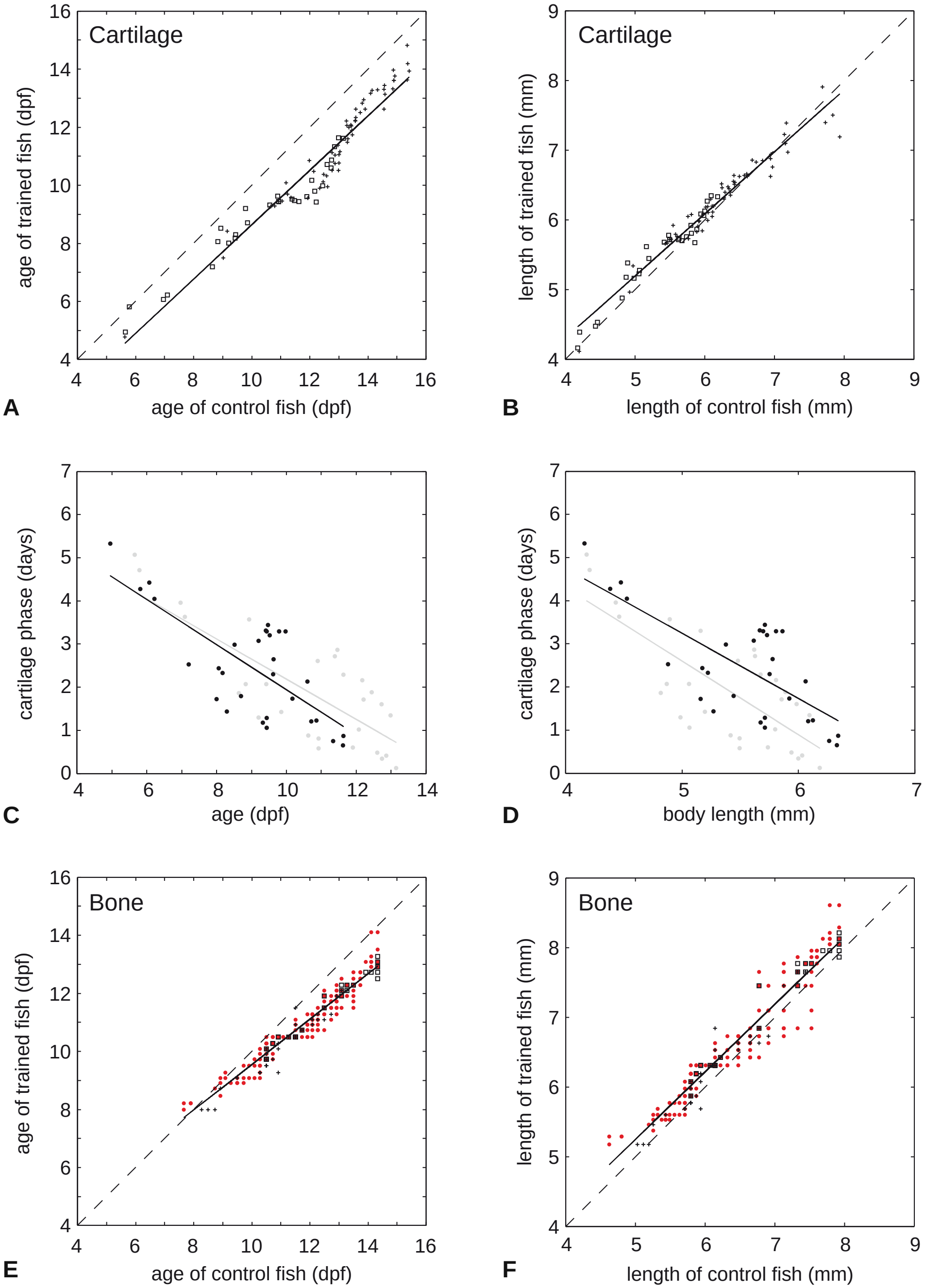
Cartilage
age of trained fish (dpf)
age of control fish (dpf)
4
6
8
10
12
14
16
A
Cartilage
length of trained fish (mm)
length of control fish (mm)
4
5
6
7
8
9
B
cartilage phase (days)
age (dpf)
0
1
2
3
4
5
6
7
4
6
8
10
12
14
C
cartilage phase (days)
body length (mm)
0
1
2
3
4
5
6
7
4
5
6
7
D
Bone
age of trained fish (dpf)
age of control fish (dpf)
4
6
8
10
12
14
16
E
Bone
length of trained fish (mm)
length of control fish (mm)
4
5
6
7
8
9
F

apr 1-2, 5-10, anal distal radials (adr) 2-6 (with adr 4 as the first), dorsal proximal radials (dpr) 1-8, neural arch 27-28, haemal spine 28, neural spine of pu2 and neural and haemal spine of pu3. The cartilage structures to appear at 14 dpf and later were pop 13, supraneural 5, apr 11-13, adr 1, 7-10 and dorsal distal radials (ddr) 1-7.

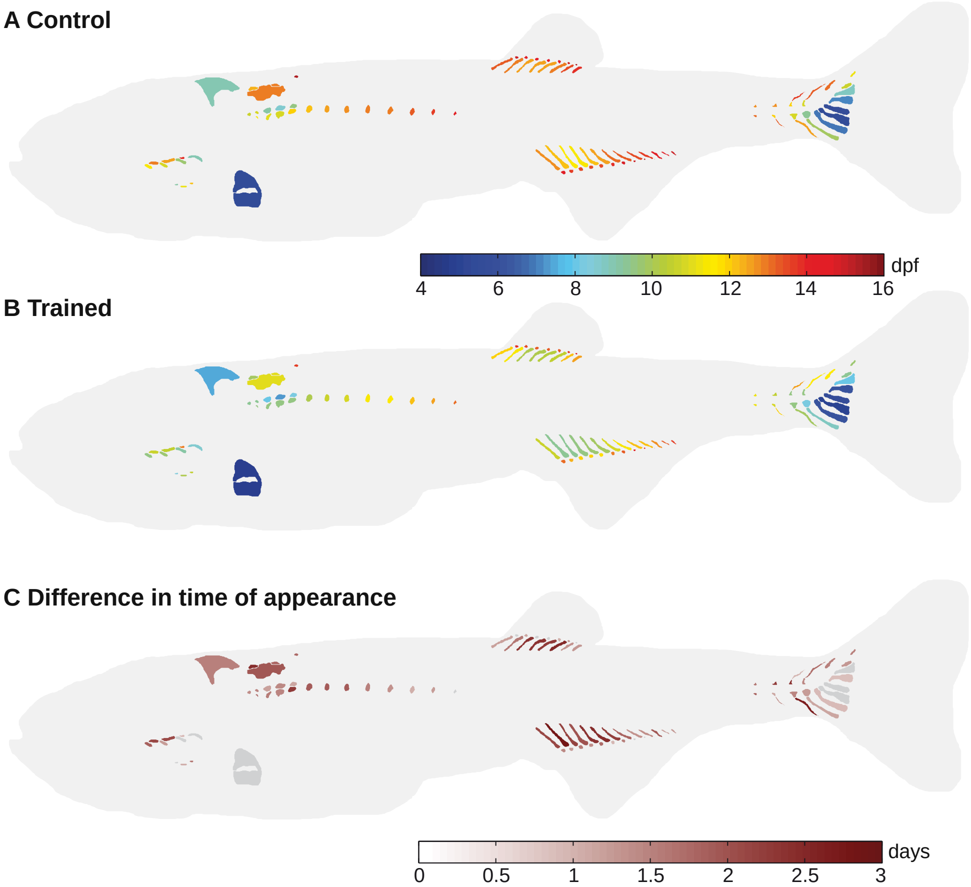

Figure 4.3. Swim-training had a differential effect on the age at appearance of cartilage structures between control and trained fish. **A,B**: CF50$_{age}$ values visualized in the corresponding structures in control fish (A) and trained fish (B). **C**: Differences in CF50$_{age}$ values between control and trained fish. Positive values indicate that structures appear earlier in the trained fish. Structures with a difference less than twice the standard error are indicated in grey.

Analysis of the difference in the CF50$_{age}$ values (temporal shift) between control and trained fish showed that swim-training had a differential effect on the temporal shift of cartilage structures (Figure 4.3C). The average standard error of the CF50$_{age}$ values was slightly higher in the control fish (0.34 days) than in trained fish (0.31 days). The minimum and maximum standard errors were also higher in the control fish than in trained fish (control: min 0.29 days, max 0.66 days; trained: min 0.29 days, max 0.52 days). Of the 92 cartilage elements analyzed in total, 77 cartilage elements showed a temporal shift which was larger than 2x SED (standard error of the difference). The minimum temporal shift of these 77 elements was 0.9 days and the maximum was 2.8 days. Chondrogenesis in these elements occurred on average 1.6 days earlier. In the cranial skeleton (11 elements examined in total), 8 elements had a temporal shift larger than 2x SED such as the epibranchials 1-2. In the axial skeleton (26 elements examined in total), 25 elements had a temporal shift larger than 2x SED such as the Weberian apparatus (e.g. tripus, supraneurals 2,3,5) and parapophyses 5-12. In the appendicular skeleton (55 elements examined in total), 44 elements had a temporal shift larger than 2x SED such as the anal and dorsal radials and cartilage structures in the caudal peduncle (e.g. epural, haemal and neural spines and arches of pu 2 and 3).

Analysis of the difference in order of appearance (rank shift, based on $CF50_{age}$) of cartilage structures between control and trained fish showed that swim-training had also a differential effect on the rank shift of cartilage structures (Figure 4.4A). Of the 92 cartilage elements analyzed in total, 42 elements showed a forward rank shift in the order of appearance in the trained fish versus the control fish. In the cranial skeleton (11 elements examined in total), 3 elements showed a forward rank shift such as epibranchial 1. In the axial skeleton (26 elements examined in total), 11 elements showed a forward rank shift such as structures in the Weberian apparatus and haemal arch 27. The paraphophyses on the other hand showed a negative rank shift. In the appendicular skeleton (55 elements examined in total), 28 elements showed a forward rank shift which are associated with swimming such as the anal and dorsal proximal radials and haemal spines of preural centra 2 and 3. The difference in the order of appearance of cartilage structures based on $CF50_{lgt}$ values between trained and control fish was similar to the difference in the order of appearance of cartilage structures based on $CF50_{age}$ values between trained and control fish (data not shown).

4.2.3 Effect of swim-training on osteogenesis

The onset of osteogenesis for each bone structure (trained and control fish) was estimated by the age or body length at which 50 % of the fish showed the presence of a bone structure. We refer to the estimates of age as $BF50_{age}$ (Bone Forming) and to the estimates of body length as $BF50_{lgt}$. $BF50_{age}$ and $BF50_{lgt}$ values were calculated from logistic regressions of the binary presence or absence data of bone structures (see also Materials and Methods). Plotting the $BF50_{age}$ values of the trained fish against the $BF50_{age}$ values of control fish showed that swim-training also accelerated osteogenesis (Figure 4.2E). Most of the $BF50_{age}$ values were located below the reference line, which indicates that bone structures appeared earlier in trained fish. The difference in $BF50_{age}$ values between trained and control fish increased with age. This difference in $BF50_{age}$ values between control and trained fish increased to more than 1 day at 12 dpf and onwards. Swim-training accelerated both intramembranous and perichondral ossification. However, plotting the $BF50_{lgt}$ values of trained fish against the BF50$_{lgt}$ values of control fish showed that trained fish were slightly longer at the onset of osteogenesis (Figure 4.2F, $P<0.0001$).

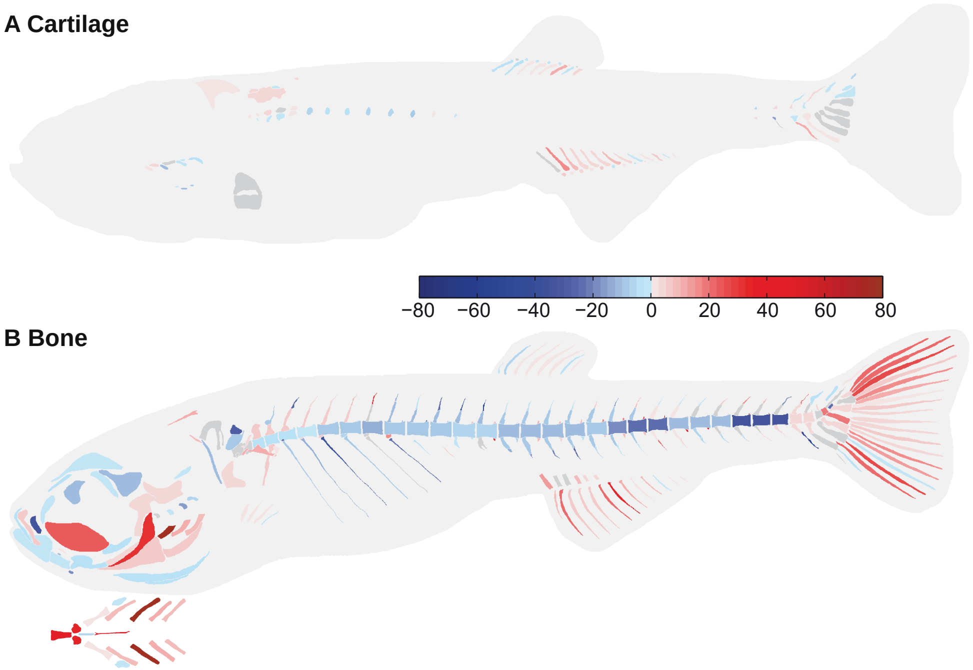

Figure 4.4. Swim-training had a differential effect on the order of appearance of cartilage and bone structures between control and trained fish. **A,B**: Difference in the rank of cartilage (A) and bone (B) structures between control and trained fish. Red structures indicate a forward shift in the order of appearance, blue structures a delay. Structures which did not show a difference are indicated in grey.

In the control fish, some structures already appear before 5 dpf (e.g. cleithrum, opercle and parasphenoid (Supplemental Figure 4.A.2)and the BF50$_{age}$ values of these structures could therefore not be calculated from our data. The bone structures to ossify in the control fish between 5-8 dpf were the anterior-most 5 centra and branchiostegal ray 2 (Figure 4.5A and Supplemental Figure 4.A.2). Osteogenesis proceeded (8-10 dpf) with the ossification of the first caudal finrays, centra 6-12 and structures in the cranial skeleton (maxillary, dentary, quadrate, entopterygoid, hyomandibular, pro-otic, ceratohyal, branchiostegalray 3, interopercle, subopercle and basioccipital). The following structures ossified between 10-12 dpf in the axial skeleton: structures of the Weberian apparatus (e.g. claustrum, intercalarium, tripus), centra 13-28, ribs 4-7, the haemal arches (14-28) and spines (18,20-21), neural arches (3-28) and postzygapophyses (pstz, 15-18), many structures of the caudal peduncle (e.g. (pre)urals, hypurals, spines and arches on the preural vertebrae 2 and 3) and the caudal finrays. In the cranial skeleton, the following structures ossified between 10-12

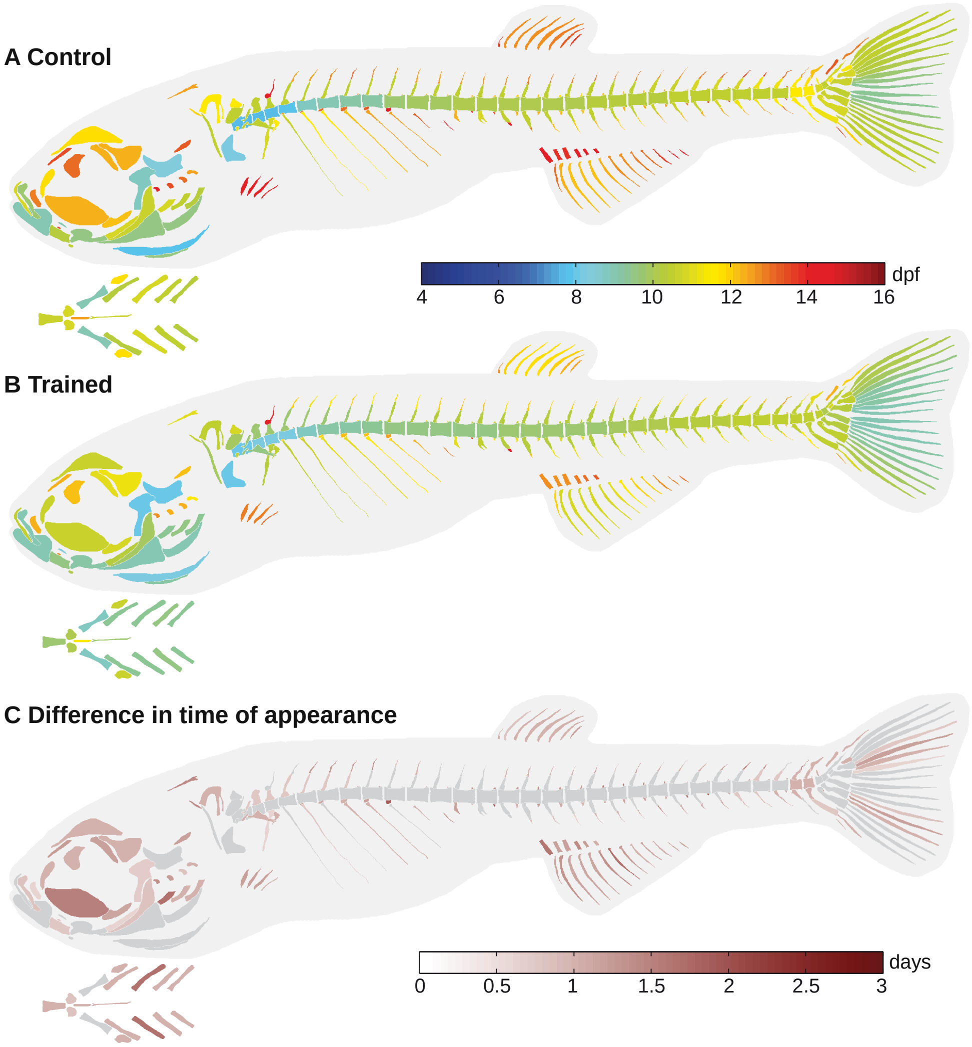

Figure 4.5. Swim-training had a differential effect on on the age at appearance of bone structures between control and trained fish. **A,B**: BF50$_{age}$ values visualized in the corresponding structures in control fish (A) and trained fish (B). The branchial region is indicated separately, ventral view. **C**: Differences in BF50$_{age}$ values between control and trained fish. Positive values indicate that structures appear earlier in the trained fish. Structures with a difference less than twice the standard error are indicated in grey.

dpf: premaxillary, lateral ethmoid, frontal, anguloarticular, retro-articular, sympletic, preopercle, basihyal, urohyal, ventral hypohyal, epihyal, ceratobranchials 1-4, posttemporal, exoccipital and supracleithrum. The following structures ossified between 12-14 dpf in the axial skeleton: parapophyses (pop, 5-9), ribs (8-11), haemal arch (13) and spines (16-17, 19, 22-28), neural spines (5-28), haemal (14-28) and neural pstz (6-14, 19-28), anal fin rays (5-11), dorsal finrays (1-8), anal proximal radials (apr, 2,3), neural spines of pu 2 and 3 and their respective caudal finrays. In the cranial skeleton, the following structures ossified between 12-14 dpf: infraorbital 1, supraorbital, orbitosphenoid, pterosphenoid, sphenotic, pterotic, supraoccipital, ectopterygoid, metapterygoid, coronomeckelian, basibranchial and epibranchial 2-4. The bones which appeared at 14 dpf and later were epibranchial 1, neural spine 4, pop 10, rib 12, haemal spine 15, neural pstz 2, 5, haemal pstz 13, pectoral finrays, apr 1, 4-6 and anal finrays 12-13.

Analysis of the difference in $\mathrm{BF50}_{age}$ values (temporal shift) between control and trained fish showed that swim training had a differential effect on the temporal shift of bone structures (Figure 4.5C). The average standard error of all $\mathrm{BF50}_{age}$ values in the trained and control fish was similar (0.22 days). The minimum and maximum standard errors were also similar (control: min 0.20 days, max 0.26 days; trained: min 0.20 days, max 0.25 days). Of the 292 bone elements analyzed in total, 186 showed a temporal shift larger than 2x SED. The minimum temporal shift of these bone elements was 0.64 days, the maximum temporal shift was 2.00 days. On average osteogenesis in these elements occurred 1.1 days earlier in the trained fish. In the cranial skeleton (45 elements examined in total), 32 elements had a temporal shift larger than 2x SED such as the ceratobranchials 1-4, epibranchials 1-4, hyomandibular, maxillary and frontal. In the axial skeleton (171 elements examined in total), 99 elements had a temporal shift larger than 2x SED such as structures in the Weberian apparatus, ribs and paraphophyses, hemal and neural spines, hemal and neural pstz, na (3-8, 27-28) and ha (13, 26-28). In the appendicular skeleton (76 elements examined in total), 55 elements had a temporal shift larger than 2x SED such as the anal proximal radials and fin rays, dorsal finrays, pectoral finrays, structures in the caudal peduncle and caudal finrays.

Analysis of the difference in order of appearance (rank shift, based on $\mathrm{BF50}_{age}$) of bone structures between control and trained fish showed that swim training had also a differential effect on the rank shift of bone structures (Figure 4.4B). Of the 292 bone elements analyzed in total, 137 elements showed a forward rank shift in the order of appearance in the trained fish versus the control fish. In the cranial skeleton (45 elements examined in total), 13 of the 20 elements which showed a forward rank shift are associated with ventilation and feeding such as the ceratobranchials 1-4, opercular bones and hymandibular. Elements in the neurocranium and lower jaw on the other hand showed a negative rank shift. In the axial skeleton (171 elements examined in total), 62 elements showed a forward rank shift and are associated among others with the elevation of the head such as the first 6 neural arches in the precaudal skeleton or in the articulation between the vertebrae such as the zygapophyses. The ribs and centra, however, showed a negative rank shift. In the appendicular skeleton (76 elements examined in total), 55 elements showed a forward rank shift and are associated with swimming such as the anal and caudal finrays. The difference in the order of appearance of bone structures based on $\mathrm{BF50}_{lgt}$ values between trained and control fish was similar to the difference in the order of appearance of bone structures based on BF50$_{age}$ values between trained and control fish (data not shown).

4.3 Discussion

Our study is the first one to show that swim-training increased growth already during early larval development in zebrafish (Figure 4.1). Previous work from our lab showed that swim-training transiently increased growth during late larval and juvenile development in zebrafish [132] and Palstra *et al.* [155] recently demonstrated that exercise training also increased growth in adult zebrafish. Furthermore, previous work on training in salmonids has shown that exercise at low swimming speeds (<1.5 BL/s) increased growth (reviewed by Davison [39]). The increased growth was related to an increased food intake and a better food conversion efficiency. Our results are, however, in contrast to the study performed by Bagatto *et al.*[5], where swim-training did not affect growth during early development. This could be due to the lower exercise intensity employed in our study. Mortality was also lower in our study. Bagatto *et al.* [5] argued that the high mortality was due to a suboptimal feeding regime during which larvae were not able to acquire sufficient *Paramecium* or *Artemia* to survive (especially the first day of) training. In our swim-training experiments, we overcame this problem by supplementing the diet of the larvae with Liquifry (a milky suspension of yeast and proteins) which increased survival in earlier pilot experiments. In summary, our study demonstrated that swim-training can already increase growth during early larval development if the training and feeding regime are carefully chosen.

In our study, skeletal development in the control fish was as reported by Cubbage and Mabee [36] and Bird and Mabee [13]. The first structures to develop in the cranial skeleton were associated with feeding and respiration. In the axial skeleton, the first regions to develop were the Weberian region and the caudal fin region. Thus, similar to the sucker *Catostomus macrocheilus*, structures which formed earliest were associated with movement rather than protection [221].

Swim training induced an earlier onset of both chondrogenesis and osteogenesis in trained fish (Figure 4.2). Interestingly, the difference in CF50$_{age}$ values (temporal shift) of cartilage structures between control and trained fish was close to constant over the range of ages investigated whereas the temporal shift of bone structures between control and trained fish became more pronounced in later stages. Cloutier *et al.*[32] also found that early forming bone elements were less responsive than late forming bone elements. The following two hypotheses can explain this observation: 1) early forming bones are more developmentally constrained than late forming bones and the latter have a higher degree of plasticity [175, 191] or 2) the time of exposure to the training regime is longer for the late forming bones, which possibly leads to larger cumulative effects on development. However, we do not observe similar effects on the formation of the cartilage structures. This suggests that swim-training has a different regulatory effect on the development of cartilage than on bone structures. Furthermore, swim-training accelerated both the onset of bone formation via perichondral ossification and via intramembranous ossification (based on $\mathrm{CF50}_{age}$ and $\mathrm{BF50}_{age}$). In addition, the duration of the cartilage phase (the phase from the onset of chondrification until the onset of ossification) of perichondral bones was not affected by swim-training. This indicates that although the onset of chondrogenesis and osteogenesis in these bones was shifted forward due to the swim-training, the duration of the cartilage phase is rather fixed.

In zebrafish, skeletal development is best correlated with size [13, 36, 160]. As mentioned above, swim-training increased growth in trained fish and accelerated chondrogenesis and osteogenesis. The analysis of the difference in $\mathrm{CF50}_{lgt}$ and $\mathrm{BF50}_{lgt}$ values between trained and control fish, however, showed that trained fish were longer than control fish at the onset of chondrogenesis and osteogenesis. These results suggest that swim-training accelerated overall larval development but growth was accelerated more than chondrogenesis and osteogenesis.

The main goal of our study was to investigate the role of mechanical loading (via swim-training) in prioritizing the development of structures involved in feeding, respiration and swimming. We therefore also analyzed the difference in order of appearance which showed if swim-training lead to a shift in priorities during chondrogenesis and osteogenesis between control and trained fish. Furthermore, this difference in order of appearance gave similar results either with the order of appearance based on the length or on age at appearance of cartilage and bone structures. The results discussed in the next paragraphs are based on the difference in order of appearance of cartilage and bone structures between control and trained fish.

We found that the development of skeletal elements associated with feeding and respiration in the cranial skeleton was prioritized during osteogenesis in trained fish (Figure 4.4). Interestingly, the development of many elements of the neurocranium was not prioritized. The skull of the zebrafish is a complex structure compared to the mammalian skull regarding the number of bones and articulations [36, 93]. Many of the bones in the splanchocranial and opercular region are involved in respiration and feeding (e.g. hyomandibular, operculars, branchial arches, hyoid arch) [36, 75, 221]. The onset of chondrification and ossification of the skeletal elements involved in feeding and respiration takes place in the first two weeks post fertilization. In this period, zebrafish larvae also make the transition from cutaneous respiration to gill respiration [180]. At 14 dpf, gills are required for O_2 uptake and ionoregulation [180]. In fish, ventilation takes place by actively pumping (via the muscular pump of the buccal cavity) water across the gills filaments [93]. The increased swimming activity by trained fish presumably increased the oxygen uptake leading to an increase in ventilation. Ballintijn [9] showed in carp that during high intensity breathing more muscles are active than during normal breathing. This suggests that an increase in ventilation due to swim-training increased muscle induced mechanical forces on cranial bones associated with respiration.

Besides those bones in the cranial skeleton that are associated with feeding, the development of bones in the dorsal part of the precaudal axial skeleton (Figure 4.4; neural arches 3-8) was also prioritized during osteogenesis in trained fish. In zebrafish larvae, a suction feeding event commences with the opening of the mouth by elevation and protraction of the hyoid by the protractor hyoideus and elevation of the head by the epaxial musculature [76]. The epaxial musculature attaches to the dorsal structures of the axial skeleton and inserts on the posterior aspect of the neurocranium (e.g. supraoccipital). The head lift and mouth opening are followed by rapid depression of the hyoid by the sternohyoideus. This muscle inserts on the hyoid via a long tendon which later ossifies into the urohyal [76]. The higher swimming activity in trained fish presumably increased the food uptake which possibly augmented the mechanical loads on these structures. Thus, this suggests that mechanical load induced by muscle forces plays an important role in prioritizing the development of the skeletal elements associated with feeding.

The formation of several elements of the Weberian apparatus was prioritized during chondrogenesis and osteogenesis (e.g. roofing cartilage, tripus, na 3 and 4, Figure 4.4). The Weberian apparatus plays an important role in the transmission of vibrations from the swim bladder to the inner ear [13, 69]. It is not known if the Weberian apparatus also has a direct role in feeding, respiration or swimming [13, 69]. Furthermore, it is also puzzling why the formation of only certain structures such as the roofing cartilage, tripus, na3 and 4 was prioritized but not the formation of the centra 1-4, scaphium and claustrum. Analysis of the distribution of mechanical load in this region during swim-training might explain the shift in priorities during skeletal development of the Weberian apparatus.

Interestingly, in the axial skeleton, the development of the postzygaphophyses was prioritized during osteogenesis in trained fish but not the development of the centra (Figure 4.4). Furthermore, the development of the ribs, which provide protection of the various organs in the visceral cavity, was also not prioritized. The axial musculature of fishes supplies the major propulsive forces for locomotion and attaches to the vertebral column [93]. It was therefore expected that the increased swimming activity would also prioritize the development of the centra. These results suggest that postzygaphophys and elements in the cranial and appendicular skeleton experienced different mechanical loads than the centra [23], which prioritized the formation of those elements over the formation of the centra. During the swim-training, the notochord develops into a vertebral column with stiff vertebrae linked by intervertebral ligaments. Zygaphophyses play an important role in the articulation between successive vertebrae and increase the stability of the vertebral column [13, 93]. They form at the posterior ends of centra and are attached with ligaments to the prezygaphophyses of the immediately posterior vertebra [13]. The development of stiff vertebrae in later stages could have altered the distribution of the mechanical load along the axial skeleton with high peak loads in the intervertebral joints. Furthermore, the swimming performance of zebrafish larvae also improves during ontogeny [137]. This might have increased the mechanical loads specifically on the postzygaphophyses during swim-training and thus prioritized their formation.

Moreover, the development of structures in the median fins was prioritized during chondrogenesis and osteogenesis in trained fish (Figure 4.4). Cloutier *et al.* [32] investigated the effect of swim-training on the onset of skeletogenesis in the median fins in the Arctic charr (*Salvelinus alpinus*). They also found that an increased swimming activity accelerated chondrogenesis and osteogenesis in the median fins. The median fins are flexible and are used for propulsion, braking and steering [214]. The posterior part of the caudal axial skeleton, the caudal peduncle, is modified to transmit forces generated by the axial muscles to the tail fin [132, 214]. The development of the median fins improves swimming performance by increasing the lateral body profile which increases thrust during swimming [64, 219]. The increased swimming activity increased the activity of the axial musculature which presumably increased the loads on skeletal elements of the median fins. This implies that an increased swimming activity prioritized the formation of skeletal elements in the median fins which probably improved swimming performance.

As stated in the Introduction, it has been shown that fish larvae show the fastest growth in the head and tail area [60][151]. Furthermore, the skeletal structures which form earliest are in the head and tail area and are essential for the survival of the fish larvae. These structures are involved in feeding, respiration and swimming. Interestingly, in our study, not only the development of elements in the head and tail area was prioritized during chondrogenesis and osteogenesis but also the development of elements in the anal and dorsal fins and axial skeleton. This suggests that an increased swimming activity gave priority to structures which play an important role in swimming and thereby increasing the chance of survival in an environment with a higher water velocity.

Our study is the first to show that during early zebrafish larval development, skeletal tissue in the cranial, axial and appendicular skeleton is competent to respond to swim-training due to increased water velocities [22, 32, 38, 186, 225]. It demonstrates that changes in water flow conditions can result into significant spatio-temporal changes in skeletogenesis. Since the zebrafish as a model system enables a diverse range of genetic analyses as well as possibilities to investigate development on a cellular, tissue and organ level, our study might facilitate in the future the connection of information about environmental influences with altered gene expression profiles and the resulting morphological changes.

4.4 Materials and Methods

4.4.1 Husbandry

Wildtype zebrafish were reared at the fish facility of Wageningen University at 27.1°C under standard conditions. Eggs were collected by mating two males with three females. Eggs were kept at 28.5°C at the breeding facility, and transferred to the fish facility at 3 dpf.

4.4.2 Ethics Statement

The swim-training experiments were approved by the Wageningen University Animal Experiments Committee (protocol nr. 2009046f).

4.4.3 Swim-training setup

The swim-training setup is a gravity-fed system (Figure 4.6A) and is located in a temperature controlled room. The part of the tubes in which the fish were kept had an internal diameter of 2 cm and a length of 20 cm for a total volume of 62.8 ml water. Fish were retained in the tubes by fine nylon mesh (0.4 mm x0.4 mm, from core to core of the wires) on each end of the tube. A parallel array of tightly packed straws (inner diameter of 6.13 mm) was placed before the first nylon mesh to create laminar flow in the tube. The water in the swim-training set-up was copper free and filtered with a biological filter system (Eheim). Water samples were taken daily from a random tube (control and trained) to measure the water quality (ammonia, nitrite, nitrate, pH and conductivity). Ammonia, nitrite and nitrate did not reach toxic levels during the swim-training (ammonia/nitrate<0.03 mg/ml, nitrate<5 mg/ml). pH (7.74±0.03) and conductivity ($884.86\pm7.78\,\mu$S/cm) also remained within the range of standard conditions. Water temperature (28.4±0.16°C) was measured daily.

The flow velocity was calculated by dividing the flow rate by the cross sectional area of the tube and thus represents the average flow velocity throughout the article unless otherwise stated. The difference in water level between the top aquarium and the outflow tubes determined the flow velocity in the training tubes (up down black arrow, Figure 4.6A). Thus, by adjusting the height of the outflow tubes, the flow velocity could be adjusted in the training tubes. Each training tube had its own outflow tube which allowed for fine adjustment of the flow velocity in each training tube.

PIV (Particle Image Velocimetry) analysis of the water velocity in the tubes showed that at the entrance of the tube the boundary layer was thin and the flow had a nearly uniform velocity over the cross-section. Near the outflow of the tube, the flow profile had developed into a Hagan-Poisseuille flow profile (Figure 4.A.3). Furthermore, the higher the flow velocity, the more time it took to fully develop a Hagan-Poisseuille flow profile.

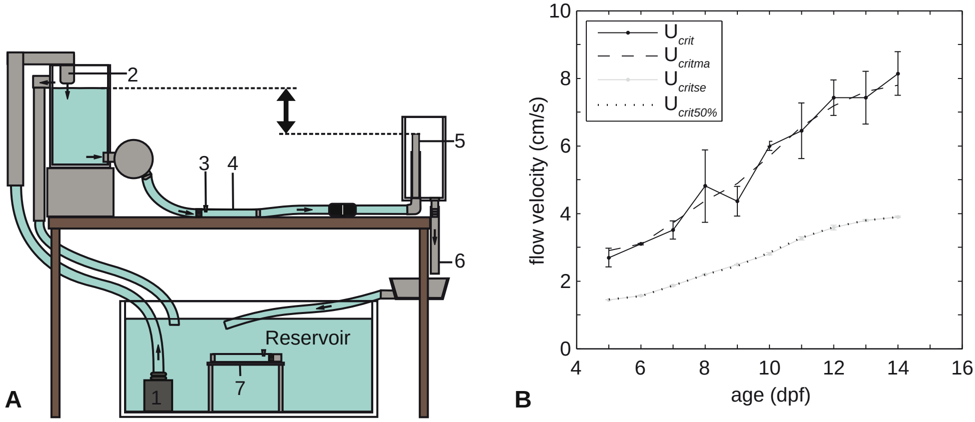

Figure 4.6. Schematic representation of the swim-training set-up in lateral view and critical flow velocity. **A**: Water was pumped (1) to the top aquarium and flowed back into the reservoir via the training tubes (4), outflow tubes (5) and outflow hoses (6) due to gravity. The difference in water level between the top aquarium and the outflow tubes (5) (indicated with up down black arrow) determined the flow velocity in the training tubes (4). Control fish were kept in similar tubes in the same set-up (7). Both the training and control section consisted of five tubes placed parallel to each other (not visible in drawing). Each tube had its own outflow tube and hose. **B**: Critical flow velocity (U_{crit}) over time and during swim-training experiments (U_{critse}). Zebrafish were subjected to 50 % ($U_{crit50\%}$) of the moving average U_{crit} (U_{critma}).

4.4.4 Training regime

We first determined the critical swimming speed of zebrafish larvae from 5-14 dpf using the method developed by Brett [18]. The critical swimming speed is a standard measurement to assess the aerobic swimming performance of fish [18, 168]. In this method, fish were subjected to intervals of swimming (for a prescribed duration) at a certain flow velocity. After each interval, the flow velocity was increased at a prescribed increment. After several intervals and increments, fish displayed symptoms of severe fatigue, did not swim anymore and were eventually swept against a mesh, indicating that fish had reached their critical flow velocity. The critical flow velocity is calculated with the following equation [18]:

$$U_{crit} = U + \left[\Delta U \times \frac{\delta T}{\Delta T} \right] \tag{4.1}$$

where U=flow velocity at the last interval where fish swam the whole interval (cm/s), ΔU=velocity increment (cm/s), δT=time that fish swam in the last interval (seconds), ΔT=duration of one interval (15min). Zebrafish larvae (n=10) were placed in a training tube and allowed to acclimate for half an hour. In the first interval of 15 min, fish were subjected to a flow velocity of 1.15 cm/s (3 body lengths per second (Bl/s), 5 dpf) to 1.91 cm/s (3 Bl/s, 14 dpf). In the next 15 min intervals, flow velocity was increased with increments of 1 Bl/s (4-7 dpf) or 2 Bl/s (8-14 dpf). After several intervals and increments, fish reached their critical flow velocity. The critical flow velocity (U_{crit}) was defined as that velocity when 50% of the fish were against the mesh at the end of the tube or held position to the wall for more than 3 seconds. These experiments were performed *in duplo* (morning and afternoon) from 5-14 dpf (Table 4.1, U_{crit} I and II). The critical flow velocity with standard deviation was plotted over time in Matlab (Figure 4.6B, U_{crit}). To smooth out the data and to highlight the trend we calculated the moving average of the critical flow velocity of 5-14 dpf (Figure 4.6B, U_{critma}). Zebrafish larvae were subjected to 50 % of this U_{critma} during the subsequent experiments (Figure 4.6B, $U_{crit50\%}$ and U_{critse}). Note that since especially the young larvae adhere to the wall of the tube, or swim close to the wall in the boundary layer, the measured critical swimming speed cannot be interpreted as the actual water velocity in which the larvae can just hold position. Our measured critical swimming speed is an overestimation of the maximum sustained swimming speed.

Table 4.1. Number of fish sampled during each stage in a swim-experiment

experiment	5 dpf	6 dpf	7 dpf	8 dpf	9 dpf	10 dpf	11 dpf	12 dpf	13 dpf	14 dpf
Ucrit I (morning)	10	10	10	10	10	10	10	10	10	10
Ucrit II (afternoon)	10	10	10	10	10	10	10	10	10	10
Cartilage I (control)	4	5	4	4	5	5	4	4	4	5
Cartilage I (trained)	3	3	3	4	1	2	3	3	4	4
Cartilage II (control)	5	4	4	3	2	3	3	2	4	3
Cartilage II (trained)	4	4	4	5	4	5	5	5	5	5
Bone I (control)	1	2	2	3	2	3	3	5	4	5
Bone I (trained)	5	5	5	4	5	5	4	4	5	5
Bone II (control)	5	4	4	5	5	5	5	5	5	5
Bone II (trained)	5	5	5	4	5	5	5	5	5	5

Bagatto *et al.* [5] subjected larval (4-14 dpf) zebrafish to a training regime at night of 2 Bl/s (yolk sac larvae, 4-6 dpf) for 24 hours and 5 Bl/s (swim up larvae, 9-14 dpf) for 15 hours. Bagatto *et al.* [5] showed that this training regime was too severe, especially for the larvae with a yolk sac. To avoid analyzing effects of the swim-training confounded by high mortality we chose for a less severe training regime. Therefore, we chose to subject the zebrafish to 50 % of the U_{critma} (Figure 4.6B, $U_{crit50\%}$) for 9 hours daily. Furthermore, to be able to monitor the swimming behaviour and the flow velocity, fish were trained during the day. During the swim-training experiments the absolute values corresponded to a relative water velocity of 3.4±0.04 Bl/s at 5 dpf to 5.1±0.6 Bl/s at 14 dpf.

At 4 dpf, 10 fish were randomly assigned to each control and training tube (5 control and 5 trained tubes) in the swim-training set-up. Fish were placed in the swim-training set-up on 4 dpf to acclimate to the conditions. From 5-14 dpf, zebrafish larvae were subjected to 3 training sessions of 3 hours (8:30-11:30, 12:00-15:00, 15:30-18:30) per day. For refreshment there was a continuous water flow of less than 0.1

Bl/s in the control tubes but only when the trained fish were subjected to swim-training. Fish were fed before the first training session and after each training session (during breaks of 30 minutes). Fish were fed *Paramecium* (until 9 dpf), Liquifry no.1 (until 7 dpf, Interpet, Surrey, England) and *Artemia* (from 8-14 dpf, live brine shrimp, Salt Lake Aquafeed, Utah, USA) *ad libitum.* Fish were always fed first *Artemia* and then *Paramecium.* During the swim experiment fish were subjected to a photoperiod regime of 12L:12D. Four swim experiments were performed in total, Cartilage I/II and Bone I/II (Table 4.1).

4.4.5 Sampling and length measurements

At the end of each training day (18:30), one fish was sampled randomly from each tube (Table 4.1, swim training experiments Cartilage I and II, Bone I and II). Subsequently, fish were euthanized with 0.1 % tricaine methane sulphonate (TMS, Crescent Research chemicals, USA) buffered with 0.08 % sodium bicarbonate (Gibco, Paisley, Scotland). Subsequently, images of sampled fish were taken in the TMS solution to measure the length. Images were taken with an Olympus DP50 digital camera mounted on a Zeiss Stemi SV11 microscope and with AnalySIS^D software (Soft Imaging System GmbH, Germany). After the length measurements, fish were fixed and stored in 4 % PFA (paraformaldehyde, Merck, Darmstadt, Germany) in PBS (phosphate buffered saline) at 4°C. Only for the bone staining, fish were transferred the following day to 70 % methanol (Merck, Darmstadt, Germany) and stored at 4°C in 70 % methanol.

Standard length was measured with the measurements tool in AnalySIS$^{\mathrm{D}}$ software of samples from four swim training experiments (Table 4.1, Cartilage I-II and Bone I-II). Standard length was measured from the anterior end of the upper jaw to the posterior end of the hypurals. In preflexion and early flexion larvae the notochord length was measured from the anterior end of the upper jaw to the posterior tip of the notochord [13]. Standard length measurements of control and trained fish in relation to age were evaluated with quadratic regression for two groups in SAS v9.2, $p < 0.05$ was accepted as significant. Average length measurements over time with standard deviation were plotted in Matlab 7.6.0.324 (R2008a, The Mathworks, Inc.).

4.4.6 Swimming behaviour

The swimming behaviour of the larvae in a randomly chosen training tube was observed for half an hour during each training session (3 training session per day, during the swim-training experiments Bone I-II, Table 4.1). An example of the swimming behaviour of control and trained fish is provided in the Supplemental Movies 4.A.1 and 4.A.2 of 11 dpf. After each minute during that half an hour the following points were noted: the number of fish swimming, position in the tube (front part or back part), number of fish swimming along the wall of the tube, attached to the wall or against the mesh (for more than 3 seconds). During each break (of half an hour), the number of fish swimming was noted directly after turning the waterflow off and then every following five minutes in a random training tube. The control fish swam in all directions throughout the tube and did not show a specific behaviour such as the trained fish.

4.4.7 Burst frequency

To analyze the burst frequency (bursts/s), the swimming behaviour of the trained and control fish was recorded with a Casio EX-F1 camera (with 30 fps in HD (1280×720)) during the 3rd training session (13:00-14:30) during the swim-training experiment Bone II (Table 4.1, Supplementary Movies 4.A.1 and 4.A.2). The number of bursts were counted of one fish per tube (n=5, control/trained) during 10 consecutive seconds (300 frames). To accurately count the number of bursts, the play back rate of the movies was decreased to 3 frames per second with the Photron Fastcam viewer 2.4. Average burst frequencies over time with standard deviation were plotted in Matlab 7.6.0.324 (R2008a, The Mathworks, Inc.). Burst frequencies of control and trained fish in relation to age were evaluated with an ANCOVA in SAS 9.2, $p < 0.05$ was accepted as significant.

4.4.8 Cartilage and bone staining

Both the cartilage and bone staining was performed essentially as described previously [197]. Fish from two independent swim-training experiments were stained for cartilage (Table 4.1, swim-training experiments Cartilage I and II). Fish from one swim-training experiment were stained for bone (Table 1, 8-14 dpf, swim-training experiment Bone II). For the bone staining, the larvae were first rehydrated in 50 % methanol, then rinsed in 0.2% Triton X100 (Sigma, St. Louis, USA) and bleached/degreased with 0.9 % H_2O_2/0.8 % KOH in 0.2 % Triton X100. Larvae of 5-9 dpf were incubated in the bleach solution for 20 min, the larvae of 10-14 dpf for 30 minutes. Larvae were then neutralized in 100 % saturated sodium tetraborate (Di-sodium tetraborate decahydrate, extra pure, Merck, Darmstadt, Germany). To make them more permeable for the alizarin red staining, larvae were digested with 0.1 g/ml trypsin (pancreas protease, Merck, Darmstadt, Germany) in 60% saturated sodium tetraborate/0.2 % Triton X100. Larvae of 5-9 dpf were incubated in the digest solution for 30 minutes, larvae of 10-14 dpf for an hour. Bones were stained with 0.04 mg/ml alizarine red (Merck, Darmstadt, Germany) in 1 % KOH. Subsequently, larvae were washed and cleared with 20 % glycerin/0.8 % KOH in 0.2% Triton X100. The larvae were rinsed with 30% glycerin and stored in 70 % glycerin/10 % KOH solution at 4°C.

For the cartilage staining, larvae were first stained with 0.15 mg/ml Alcian blue (Alcian blue 8GX, Acros Organics, New Jersey, USA) in 30 % Acetic Acid/70 % ethanol overnight. Larvae were rehydrated in 50 % and 30% ethanol and rinsed in 0.2 % Triton X100. Larvae were then bleached, neutralized, digested and stored in glycerin at 4°C according to the bone staining protocol. All experiments were performed with demineralized water and at room temperature.

Subsequently, a control or trained fish was chosen randomly and the presence or absence of a cartilage/bone structure was scored within one month. Cartilage structures were scored as present upon visualization of Alcian blue staining of the glycosaminoglycans in cartilage. Bone structures were scored as present upon visualization of Alizarine red staining of calcium in mineralized bone matrix. Images of the bone or cartilage staining of zebrafish larvae were taken with an Olympus DP50 digital camera mounted on a Zeiss Stemi SV11 microscope and with AnalySIS^{D} software (Soft Imaging System GmbH, Germany).

4.4.9 Statistical analysis of cartilage and bone formation

The onset of chondrogenesis and osteogenesis for each cartilage and bone structure (trained and control) was estimated by the age or body length at which 50 % of the fish showed the presence of a cartilage and bone element. We refer to these estimates of age as CF50$_{age}$ (Cartilage Forming) or BF50$_{age}$ (Bone Forming) values and to the estimates of body length to as CF50$_{lgt}$ or BF50$_{lgt}$ values. CF50 and BF50 values (of age and body length) were calculated from logistic regressions of the binary presence or absence data of cartilage and bone structures, using the procedure for generalized linear models (GENMOD) of SAS 9.2, employing a binomial distribution and logit link function. In the logistic regression model the probability p_{ij} of a cartilage or bone structure i to have been developed at day or body length x, in treatment group j (j=1 trained, j=2 control) is modeled as $logit(p_{ij})=a_{ij}+bx$. We used separate models for cartilage and bone structures. To keep the models simple but still usable for our purposes (i.e. to estimate CF50 and BF50 values (of age and body length)), we assumed that bone structures developed at the same rate (so have a common slope b), irrespective of the treatment. With the logistic regression models the CF50 of structure i in treatment group j was estimated as CF50$_{ij}$=-a_{ij}/b, and likewise for BF50. We excluded bones which were already present at 5 dpf in all fishes of a control or trained group, and bones which were not yet present at 14 dpf in all fishes of one of the groups, as it was impossible to calculate the CF50$_{age}$ or BF50$_{age}$ values in these cases. These bones were also excluded from the data with the estimates of the onset of chondrogenesis and osteogenesis in body length. The CF50 values (of age and body length) were average values of two swim-training experiments (Table 4.1, swim-training experiments Cartilage I and II). The BF50 values (of age and body length) were from a single swim-training experiment (Table 4.1, 8-14 dpf, swim-training experiment Bone II). The CF50 and BF50 values of the trained fish versus control fish were plotted in Matlab 7.6.0.324 (R2008a, The Mathworks, Inc.). The agreement between trained and control fishes for the different CF50 and BF50 variables was tested using the Bradley-Blackwood procedure. Significant results were followed up by a pairwise t-tests to check for systematic differences, and by t-tests of the slope.

To get an impression of the precision of the CF50$_{age}$ and BF50$_{age}$ values, we used the delta-method to compute the approximate standard errors (SE) of the CF50$_{age}$ and BF50$_{age}$ values. The delta-method can be used in case of non-linear functions of parameters, like we have here (CF50$_{ij}$=-a_{ij}/b). We used the variances and covariances of the parameters from the logistic regressions, as calculated by SAS, and imported these into R (version 2.12.2), using a tailor-made program for the delta-method. The standard error of the difference (SED) of $\mathrm{CF50_{control}}$ and $\mathrm{CF50_{trained}}$ was calculated as

$$\mathrm{SED}(\mathrm{CF50_{control}} - \mathrm{CF50_{trained}}) = \sqrt{\mathrm{SE}^2_{\mathrm{CF50_{control}}} + \mathrm{SE}^2_{\mathrm{CF50_{trained}}}} \tag{4.2}$$

The standard error of the difference of $\mathrm{BF50_{control}}$ and $\mathrm{BF50_{trained}}$ was calculated with the similar formula.

To visualize the CF50 and BF50 values with the corresponding cartilage or bone structure, each structure was traced as a separate black structure in a cartilage or bone staining of a 14 dpf trained fish with gimp v2.6. Subsequently, each of these black structures was linked to the corresponding $\mathrm{CF50}_{age}$ or $\mathrm{BF50}_{age}$ value in Matlab 7.6.0.324 (R2008a, The Mathworks, Inc.).

The difference in $\mathrm{CF50}_{age}$ values (hereafter called the temporal shift, in days) between control and trained fish was calculated by subtracting the $\mathrm{CF50}_{age}$ values of the trained fish from the $\mathrm{CF50}_{age}$ values of the control fish. The temporal shift in appearance of bone structures between control and trained fish was calculated similarly using the $\mathrm{BF50}_{age}$ values. This temporal shift between the control and trained fish was visualized with the corresponding cartilage/bone structure with the same method described in the previous paragraph in Matlab 7.6.0.324 (R2008a, The Mathworks, Inc.).

In fish, bones can form via intramembranous or perichondral ossification. During intramembranous ossification, bones form directly from mesenchymal precursors whereas during perichondral ossification, bony matrix forms around a cartilage model [13]. We call the phase from the onset of chondrogenesis until the onset of osteogenesis the cartilage phase. The duration of the cartilage phase in cartilage structures was calculated by subtracting the $\mathrm{CF50}_{age}$ values from the $\mathrm{BF50}_{age}$ values in control and trained fish. The relationship between the duration of the cartilage phase and $\mathrm{CF50}_{age}$ or $\mathrm{CF50}_{lgt}$ values (control and trained) was analyzed with linear regression in SAS 9.2, $p < 0.05$ was accepted as significant.

The order of appearance of the cartilage or bone structures in the control or trained fish was determined by assigning a rank to each cartilage or bone structure (starting with the structure which appeared first in age or body length). The shift in rank for each cartilage and bone structure was determined by subtracting the rank value of the cartilage or bone structure in the trained fish from the rank value of the cartilage or bone structure in the control fish. The shift in rank values were visualized with the corresponding cartilage or bone structure with the same method described above in Matlab 7.6.0.324 (R2008a, The Mathworks, Inc.).

Acknowledgments

We wish to thank Jos van den Boogaart for building the initial swim-setup and support with the optimization. Furthermore, we wish to thank Ramona Laurentzen and Paul Oomen for their assistance during the swim-training experiments. AWF is indebted to Henk Schipper for his advice and support with the Analysis$^{\mathrm{D}}$ software. We are especially grateful to the members of the Zebrafish Facility at Wageningen University for providing help and taking care of the zebrafish.

4.A Supplemental Figures and Multimedia

Movie 4.A.1. Swimming behaviour of control fish at 11 dpf. http://www.plosone.org/article/info%3Adoi%2F10.1371%2Fjournal.pone.0034072#s5. See also Materials and Methods for information about the recordings and analysis.

Movie 4.A.2. Swimming behaviour of trained fish at 11 dpf. http://www.plosone.org/article/info%3Adoi%2F10.1371%2Fjournal.pone.0034072#s5. See also Materials and Methods for information about the recordings and analysis.

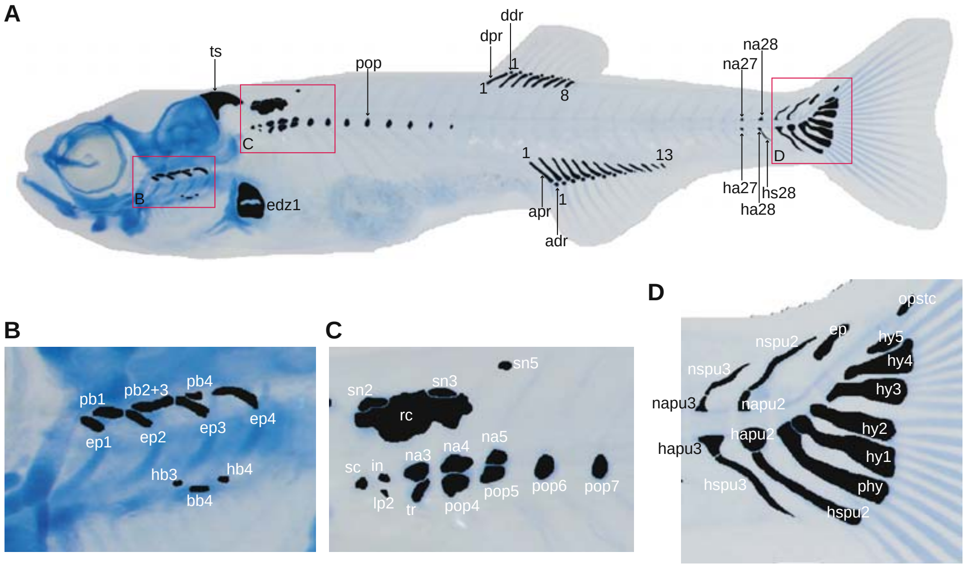
A
ts
pop
dpr
ddr
1
1
8
na27
na28
C
B
edz1
1
13
apr
1
adr
ha27
hs28
ha28
D
B
pb1
pb2+3
pb4
ep1
ep2
ep3
ep4
hb3
hb4
bb4
C
sn5
sn2
sn3
rc
na3
na4
na5
sc
in
lp2
tr
pop4
pop5
pop6
pop7
D
opstc
ep
nspu2
hy5
hy4
nspu3
napu3
napu2
hy3
hapu3
hapu2
hy2
hy1
hspu3
phy
hspu2

Figure 4.A.1. The cartilage structures, indicated here in black, which were analyzed in this study. **A**: Alcian blue staining of 14 dpf trained fish, lateral view. The areas indicated in red are shown enlarged in B, C and D. adr, anal distal radial; apr, anal proximal radial; ddr, dorsal distal radials; dpr, dorsal proximal radial; edz1, endoskeletal disc with cartilage subdivision zone 1; ha27/28, haemal arch 27/28; hs, haemal spine 28; na27/28, neural arch 27/28; pop, paraphophysis; ts, posterior end of the tectum synoticum.**B**: Branchial structures, lateral view. bb, basibranchial; ep, epibranchial; hb, hypobranchial; pb, pharyngobranchial. **C**: Weberian apparatus, lateral view. in, intercalarium; lp2, lateral process 2; na, neural arch; pop, paraphophysis; rc, roofing cartilage; sc, scaphium; sn, supraneural; tr, tripus. **D**: Caudal fin, lateral view. ep, epural; hapu, haemal arch of preural; hspu, haemal spine of preural; hy, hypural; napu, neural arch of preural; nspu, neural spine of preural; opstc, opistural cartilage; phy, parhypural. Nomenclature follows Cubbage and Mabee [36], Bird and Mabee [13] and Bensimon-Brito *et al.* [12].

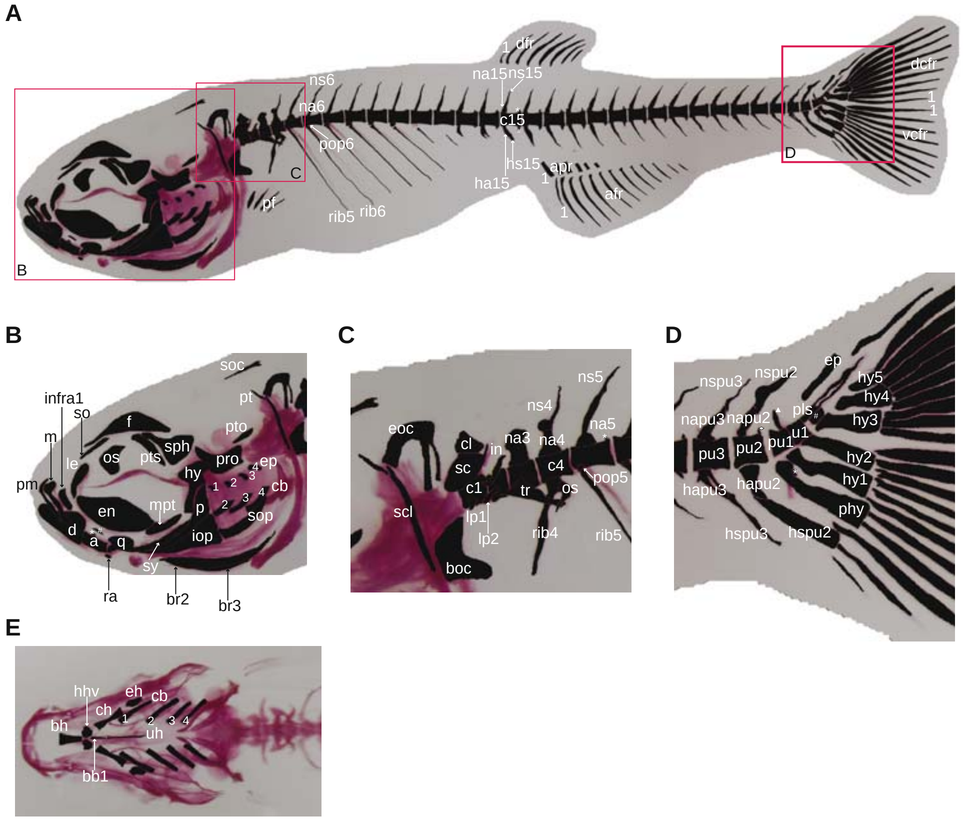
A
1 dfr
na15 ns15
ns6
na6
c15
pop6
hs15
ha15
apr
1
afr
1
pf
rib5 rib6
dcfr
1
1
vcfr
B
C
D
B
soc
pt
pto
infra1
so
f
m
le
os
pts
sph
pro
hy
ep
pm
1 2 3 4
cb
en
mpt
p
1 2 3 4
sop
d
a
q
iop
sy
ra
br2
br3
C
ns5
ns4
na5
eoc
cl
in
na3
na4
sc
c4
c1
tr
os
pop5
scl
lp1
lp2
rib4
rib5
boc
D
ep
nspu3
nspu2
hy5
hy4
napu3
napu2
pls
hy3
u1
pu3
pu2
pu1
hy2
hy1
hapu3
hapu2
phy
hspu3
hspu2
E
hhv
eh
cb
ch
bh
1 2 3 4
uh
bb1

Figure 4.A.2. The bone structures, indicated in black, which were analyzed in this study. **A**: Alizarin red staining of 14 dpf trained fish, lateral view. The areas indicated in red are shown enlarged in B, C and D. ha, haemal spine; hs, haemal spine; na, neural arch; ns, neural spine; pf, pectoral finrays; pop, paraphophysis. The haemal postzygaphophysis is marked by a pound sign and the neural postzygaphophysis by an asterisk. **B**: Cranial skeleton, lateral view. a, anguloarticular; br, branchiostegalray; cb, ceratobranchial; d, dentary; en, entopterygoid; ep, epibranchial; f, frontal; hy, hyomandibular; infra1, infraorbital 1; iop, interopercle; le, lateral ethmoid; m, maxilla; mpt, metapterygoid; os, orbitosphenoid; p, preopercle; pm, premaxilla; pro, pro-otic; pt, posttemporal; pto, pterotic; pts, pterysphenoid; q, quadrate; ra, retroarticular; so, supraorbital; soc, supraoccipital; sop, subopercle; sph, sphenotic; sy, sympletic. The coronomeckelian is marked by an asterisk and the ectopterygoid by a pound sign. **C**: Weberian apparatus, lateral view. c1/4, centrum 1/4; cl, claustrum; boc, basioccipital (posterior region); eoc, exoccipital; in, intercalarium; lp1/2, lateral process 1/2; na, neural arch; ns, neural spine; os, os suspensorium; pop, paraphophysis; sc, scaphium; scl,supracleithrum; tr, tripus. The neural postzygaphophysis is marked by an asterisk. **D**: Caudal fin, lateral view. ep, epural; hapu, haemal arch of preural; hspu, haemal spine of preural; hy, hypural; napu, neural arch of preural; nspu, neural spine; pls, pleurostyle; phy, parhypural; pu, preural; u, ural. The neural arch of the urostyle is marked by a triangle, the neural postzygaphophysis of preural 2 by a diamond, the parhypuraphophysis by an asterisk and ural 2 by a pound sign. **E**: Cranial skeleton, ventral view. bb1, basibranchial; bh, basihyal; cb, ceratobranchial; ch, ceratohyal; eh, epihyal; hhv, ventral hypohyal; uh, urohyal. Nomenclature follows Cubbage and Mabee [36] and Bird and Mabee [13].

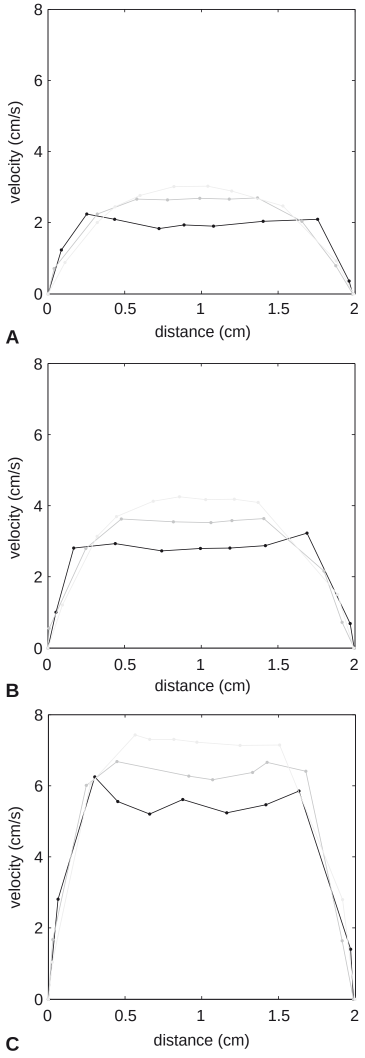

Figure 4.A.3. Flow profile in training tubes. Visualization of the flow profile with Particle Image Velocimetry at different cross sections in the tube. Black dots show the flow profile at the inflow of the tube, dark grey in the middle of the tube and light grey at the outflow of the tube. **A**: average flow velocity 5.30 cm/s. **B**: average flow velocity 2.65 cm/s, **C**: average flow velocity 1.77 cm/s.

”It is true that those we meet can change us, sometimes so profoundly that we are not the same afterwards, even unto our names.”

Yann Martel

Chapter 5

Exploring the effect of exercise on the transcriptome of zebrafish larvae (*Danio rerio*)

Ansa W. Fiaz[1], Karen M. Léon-Kloosterziel[1], Stefan Schulte-Merker[1,2], Johan L. van Leeuwen[1], Sander Kranenbarg[1]

---

[1] Experimental Zoology Group, Department of Animal Sciences, Wageningen University and Research Centre, Wageningen, The Netherlands

[2] Hubrecht Institute-KNAW & UMC Utrecht, Utrecht, The Netherlands

Abstract

In adult vertebrates, endurance training leads to physiological, metabolical and molecular adaptations which improve endurance performance. Only very few studies have focused on adaptive responses to endurance training during early vertebrate development, and molecular data is limited. Here, we explored the effect of swim-training on the transcriptome of the zebrafish during early development on a quantitative and spatial gene expression level.

We subjected larval zebrafish from 5–14 dpf (days post fertilization) to swim-training and performed a whole genome microarray analysis of trained and control fish sampled at 10 dpf. In addition, we investigated if swim-training affected the expression of genes involved in muscle growth and structure with quantitative real-time PCR in trained and control fish sampled at 5 and 14 dpf.

To obtain a general overview of the effects of swim-training on the transcriptome, we selected 52 genes from the whole genome microarray analysis based on a number of criteria. In situ hybridization demonstrated that 15 genes were specifically expressed in the brain, muscle, kidneys, liver, pancreas or intestines. Thus, swim-training led to molecular changes already after 5 days of swim-training and in a variety of organ systems. In addition, the expression of slow fiber markers was increased after ten days of swim-training, indicating that muscle can already shift towards a slow aerobic phenotype during zebrafish larval development. Taken together, this study demonstrates that significant changes occur, even at early stages, as an adaptive response to endurance training during early vertebrate development.

Keywords: swim-training, microarray, muscle, in situ hybridization

5.1 Introduction

It is well known that physical exercise such as endurance training can have many important health benefits in humans such as decreasing the risk of heart failure, preventing the onset of insulin resistance and improving muscular strength and mental fitness [33, 128, 130]. In adult vertebrates, endurance training leads to changes on the physiological, metabolical and molecular level in skeletal muscle, bone tissue, cardiovascular performance and overall energy metabolism which improve endurance performance [35, 41, 128, 130, 131, 184, 208, 210].

Only very few studies have focused on adaptive responses to endurance training during early vertebrate development. Endurance training has been shown to affect cartilage and bone development during ontogeny [32, 54, 100]. In addition, in larval and juvenile zebrafish, swim-training has also been shown to improve growth and aerobic muscle performance [54, 133]. Swim-training decreased active oxygen consumption in free-swimming zebrafish larvae and juveniles which indicates that swim-training increased swimming efficiency [5]. Pelster and coworkers showed that swim-training led to an increased mitochondrial content in the red fibers in early larval and early juvenile zebrafish (15 and 32 dpf) while an increased capillarization of the muscle fibers in the tail fin and increased vascularization index of muscle tissue caudal of the anus was found only in the early juveniles [163].

Moreover, it is poorly understood via which molecular pathways endurance training affects early vertebrate development. In a previous study from our lab, Van der Meulen *et al.* [133] showed that expression of *myogenin* (a muscle growth promotor) and total cross sectional red muscle fiber area were increased in juvenile fish subjected to swim-training (14–84 dpf). Together with the increased expression of the slow fiber markers *myosin heavy chain 1* and *troponin C1a* this suggests that axial muscle in juvenile fish shifted due to the training towards a slow aerobic phenotype [133]. Recently, it was shown that swim-training increased the expression of pyruvate dehydrogenase kinase 2, an inhibitor of pyruvate dehydrogenase, in zebrafish larvae [106]. This suggest that glucose metabolism was inhibited. In addition, the expression of enzymes involved mitochondrial ATP production was enhanced or unchanged, thus suggesting that lipid metabolism was stimulated in response to swim-training [106]. Furthermore, a recent study demonstrated that swim-training affected the transcription of the circadian genes *period1* and *clock1* in zebrafish larvae. This indicates that swim-training is a non-photic Zeitgeber which can influence circadian rhythms [50].

The lack of molecular data impedes connecting physiological and morphological data on one hand with molecular expression data on the other hand. Such a connection would contribute to our understanding of how the transcriptome of an organism changes during early development under training conditions. Here, we explored the effect of swim-training on the transcriptome of the zebrafish during early development on the quantitative and spatial gene expression level.

The zebrafish is an established model for vertebrate development due to the short generation time, *ex utero* development and the diverse range of genetic analyses. The first movements appear around 17–19 hours post fertilization (hpf, [183]) as side-to-side contractions of the trunk and precede coordinated patterns of swimming behaviour. The zebrafish shows positive rheotaxis already at the larval stage. Furthermore, the development of organ systems such as the skeletal system also takes place during this period. The onset of chondrification and ossification of many skeletal elements lies between 5 and 14 dpf (days post fertilization) and the transition from the notochord to the vertebral column also takes place in this period [13, 36]. Thus, the zebrafish is an excellent model to investigate the effect of swim-training during early development as it allows combining exercise with physiological, morphological and genetic analyses.

We subjected larval zebrafish from 5–14 dpf to swim-training and performed a whole genome microarray analysis of trained and control fish sampled at 10 dpf. We chose this stage because the first ossified structures appear around 10 dpf in the caudal fin [54]. Subsequent spatial analysis of a selected group of genes from the microarray analysis, demonstrated that swim-training led to molecular changes already after 5 days of training in several organ systems. In addition, since previous studies have shown that swim-training affects the expression of genes involved in myogenesis and sarcomeric structure in adult and juvenile zebrafish [133, 155], we investigated if similar molecular changes take place in muscle growth and sarcomeric structure during zebrafish larval development. Quantitative gene expression analysis showed that swim-training increased the expression of slow fiber markers after ten days of training. This study is the first to explore the effect of endurance training on the transcriptome during early vertebrate development on a quantitative and spatial gene expression level and demonstrates that significant changes occur, even at early stages, as an adaptive response in a variety of organ systems.

5.2 Materials and methods

5.2.1 Husbandry

Wildtype zebrafish were reared at the fish facility of Wageningen University at 27±0.5°C under standard conditions. Eggs were collected by mating two males with three females. Eggs were kept in small containers in a water bath at the breeding facility at 29±0.5°C, and transferred to the fish facility at 3 dpf. The swim-training experiments were approved by the Wageningen University Animal Experiments Committee (protocol nr.2009046f and 2011046a).

5.2.2 Swim-training set-up and regime

The swim-training setup was a gravity-fed system, located in a temperature controlled room (for a detailed description see also Fiaz *et al.* [54]). Fish were retained in transparent tubes by a fine nylon mesh on each end of the tube. Water samples were taken daily from a random tube (control and trained) to measure the water quality (ammonia, nitrite, nitrate, pH and conductivity). Ammonia, nitrite and nitrate did not reach toxic levels during the swim-training (ammonia<0.22 mg/ml, nitrite<0.03 mg/ml, nitrate<5 mg/ml). Conductivity (904.55±51.01 µS/cm) and pH (7.95±0.38) also remained within the range of standard conditions. Water temperature (28.46±0.04°C) was measured daily. Fish were subjected to swim-training as described previously in Fiaz *et al.* [54]. Briefly, fish were placed in the swim-training set-up on 4 dpf to acclimate to the conditions. From 5 dpf and onwards, zebrafish larvae were subjected to 3 training sessions of 3 hours (8:30–11:30, 12:00–15:00, 15:30–18:30) per day. Fish (trained fish) were subjected to 50 % of the critical flow velocity as determined in Fiaz *et al.* [54] (5.51±0.08 Bl/s at 10 dpf, Table 5.A.1). In a previous study, we showed that at these velocities, fish exhibit an increased swimming activity from 5–14 dpf. Furthermore, these velocities are within the range of velocities of what zebrafish larvae experience in their natural environment [51]. In the tubes with the control fish, there was a continuous water flow of less than 0.1 Bl/s for refreshment but only when the fish in the training tubes were subjected to swim-training. Fish were fed before the first training session and after each training session (during breaks of 30 minutes). Trained and control fish were fed equal volumes of *Paramecium* (9 ml, 5–9 dpf), Liquifry no.1 (1 ml, 5–7 dpf, Interpet, Surrey, England) and *Artemia* (5 ml, 8–14 dpf, live brine shrimp, Salt Lake Aquafeed, Utah, USA) *ad libitum.* During the swim experiment fish were subjected to a photoperiod regime of 12L:12D.

5.2.3 Whole genome microarray analysis

To analyze the effect of swim-training on the transcriptome, we first subjected fish to swim-training from 5 until 10 dpf as described above. Ten fish were randomly assigned to a tube (10 fish per tube, 2 tubes in total per treatment). At 10 dpf, fish (control and trained) were euthanized with 0.1 % tricaine methane sulphonate (TMS, Crescent Research chemicals, USA) buffered with 0.08 % sodium bicarbonate. Subsequently, images of sampled fish were taken in the TMS solution to measure the length. Images were taken with an Olympus DP50 digital camera mounted on a Zeiss Stemi SV11 microscope and with Analysis^{D} software (Soft Imaging System GmbH, Germany). After the length measurements, fish were immediately frozen in liquid nitrogen and stored at −80°C.

RNA was isolated from each individual fish (of 10 dpf) with the Qiagen Rneasy kit according to the manufacturer's protocol (Qiagen, Hilden, Germany). We selected 10 control and 10 trained fish for the micro array analysis with equal levels of A260/A230 ratios and RNA concentration. Micro array experiments were performed according to the manufacturer's protocol (Two-color Microarray-based gene expression analysis, version 6.0, low input quick amp labeling, Agilent Technologies, Palo Alto, USA). To obtain a pooled control RNA sample, we took 400 ng from each individual control fish (n=10) and pooled this together and to obtain a pooled trained RNA sample, we took 400 ng of RNA from each individual trained fish (n=10) and pooled this together. Subsequently, 100 ng of the pooled control RNA sample was labeled with Cy5 and Cy3 and 100 ng from the pooled trained RNA sample was labeled with Cy5 and Cy3. Equal amounts of labeled RNA of the pooled control samples were mixed with equal amounts of labeled RNA of the trained samples (control-Cy3 with trained-Cy5 and control-Cy5 with trained-Cy3). Both samples were subsequently hybridized on 4×44k Zebrafish Agilent microarrays (Zebrafish gene expression array V3, Design ID: 026437, Agilent Technologies) and placed in a hybridization chamber at 10 rpm for maximum 17 hours at 65°C. After washing and mounting, slides were scanned on a Agilent Scanner and data was extracted with Agilent Feature Extraction Software (Version 10.5.1.1). First, genes which had a red/green (Cy5/Cy3) median signal which was twice as large or more than the red/green background median signal were selected. Subsequently, the genes without a dye bias were selected for further analysis. The data discussed in this study have been deposited in NCBI's Gene Expression Omnibus [49] and are accessible through GEO Series accession number GSE42967 (http://www.ncbi.nlm.nih.gov/geo/query/acc.cgi?acc=GSE42967).

We used two strategies to select genes for further analysis (Table 5.A.2). First, we took an unbiased approach and chose the top 20 up-regulated genes. Secondly, since we are also interested via which molecular pathways mechanical signals are translated into cartilage and bone formation, we also selected 32 up-regulated genes (with a fold change of 1.75 or larger) which are, according to literature, mechanosensitive or involved in skeletal development.

The gene expression of the selected genes (total of 52 genes) was validated with quantitative real time PCR (qRT-PCR) as follows. cDNA was synthesized from the pooled RNA (trained and control) which was also used for the microarray analysis. Samples were Dnase treated with DNase I (Invitrogen, California, USA) and reverse transcribed with SuperScript III (Invitrogen) according to the manufacturer's protocol. Primers for qRT-PCR were obtained at Qiagen Gene Globe or designed with Primer 3 ([181], Table 5.A.3) and obtained at Eurogentec (Liège, Belgium). cDNA was diluted 1:10 or 1:5 for qRT-PCR. The reaction volume (total 12.5 µl) contained 6.25 µl Rotor-Gene$^{\text{TM}}$ SYBR® Green PCR Master mix (Qiagen), 1 µM of forward and reverse primer (Qiagen Primer Assay: 1.25 µl of 10×Quantitect Primer Assays, 2.5 µl nuclease free H_2O) and 2.5 µl cDNA. RT-qPCR reactions were performed in a 72-well Rotor-Gene$^{\text{TM}}$Q (Qiagen) according to the following protocol (Qiagen Quantitect Primer Assay handbook, July 2011): 5 min at 95°C (activation), followed by 40 cycles of 5 s at 95°C (denaturation) and 10 s at 60°C (combined annealing and extension). At the end of the run, a melting curve analysis was performed to check for specificity of the product: 35 cycles from 60°C to 95°C (1°C increments every cycle). Samples were run in duplo and fluorescence was measured at the end of every combined annealing and extension step. The C_t values and amplification efficiencies for each sample were obtained upon Comparative Quantitation Analysis from the Rotor-Gene$^{\text{TM}}$Q software (version 1.7). The C_t values of each gene were normalized against the C_t values of the reference genes *rps11* and $\beta actin$. The stability of the reference genes was evaluated with the BestKeeper software tool [165] and this demonstrated that gene expression of the reference genes did not differ between the trained and control samples (average absolute deviation of C_t values of control and trained samples from the mean (of trained and control values) was lower than 1: $\beta actin$=0.26

rps11=0.10). Furthermore, since *rps11* was the most stably expressed (exhibiting the lowest variation), it was chosen for further analysis. The amplification efficiency for each gene was determined by taking the average of the amplification efficiency of all samples. The relative fold change in gene expression between trained and control fish was calculated according to the Pfaffl method [164].

5.2.4 In situ hybridization

To investigate the spatial gene expression of the validated genes from the microarray analysis, we used Primer 3 software to design primers for probe synthesis ([181], Table 5.A.3) and these primers were extended with a T3, T7, or Sp6 transcription initiation site sequence on the reverse primer. cDNA from the pooled control samples or from individual fish of 10 dpf was used to perform a PCR with these primers to generate the specific coding sequences of the selected genes (0.4–1.0 kb) to use as template for the DIG labeling reaction. DIG-labeled probes were synthesized according to the manufacturer's instructions (Roche, DIG-labeling). Subsequently, DIG-labeled probes were purified with the Qiagen Rneasy kit (Protocol RNA Cleanup).

Wildtype zebrafish larvae were euthanized as described above and fixed overnight in 4 % paraformaldehyde (PFA) in phosphate-buffered saline (PBS) at 4°C. After washing with PBS (2×5min), fish were dehydrated in 100 % methanol at RT (room temperature, 2×5 min) and stored at −20°C until further use. After rehydration (75 %, 50 % and 25 % methanol/PBS, 1×5 min), fish were washed in PBST (PBS+0.1 % Tween®20, 3×5 min) and bleached in 10 % H_2O_2/PBST at RT for 100 min. Subsequently fish were washed in PBST (3×5 min) and AD (Aqua Destillata, 3×5 min). Fish were embedded in 1.5 % agar/5 % sucrose in AD and incubated overnight in 30 % sucrose/AD at 4°C. Embedded fish were frozen in liquid nitrogen and stored at −80°C. Longitudinal sections of 25 µm were made with the cryostat (Leica CM3050S) and transferred onto polysine coated slides (Menzel-Gläser, Thermo scientific). Slides were stored in a box with silica gel at −20°C or if used immediately, dried overnight at RT.

In situ hybridization was performed as described in Smith *et al.* [190] with the following modifications. Probes were diluted in hybridization buffer (50 % formamide, 5×salt [20×salt: 3 M NaCl and 0.3 M sodium citrate, pH=7.0], 0.1 % Tween®20, 9.2 µM citric acid, 0.5 mg/ml tRNA yeast (Invitrogen), 90 µl of heparin (5000 U/ml)) to a final concentration of 0.5 ng/µl. Two hundred µl of the probe solution was added to each slide and covered with Nescofilm (Bando Chemical IND., Kobe, Japan). Slides were incubated overnight at 70°C in a humid chamber. Slides were washed in solution A ((50 % formamide, 1×salt, 0.1 % Tween®20), 2×30 min, 70°C) and in 1×TBST ((0.14 M NaCl, 2.7 mM KCl, 0.025 M Tris HCl, 0.1 % Tween®20), pH=7.5), 2×30 min, RT). Subsequently, slides were incubated in 400 µl of 2 % blocking buffer (Blocking reagent, Roche, Mannheim, Germany) in 1×TBST for at least 1 h at RT. The blocking buffer was replaced with 200 µl of 1:2000 dilution of anti-DIG AP FAB fragments (Roche) in 2 % blocking buffer. The slides were covered with Nescofilm and incubated overnight at 4°C. Subsequently, slides were placed in coplin jars, washed with TBST and equilibrated with AP staining buffer ((0.1 M Tris, 0.1 % Tween®20, 0.1 M NaCl, 0.05 M $MgCl_2$), 2×10min). Slides were incubated in 400 µl of staining solution (1 ml AP staining buffer, 4.5 µl NBT and 3.5 µl BCIP) in the dark. Staining was monitored regularly and stopped with AD (2×10 min). After clearing with methanol, washing with PBS and fixation with 4 % PFA/PBS (20 min at RT), slides were mounted in Aquatex® (Merck, Darmstadt, Germany) and incubated overnight at RT to dry. Images were taken with an Olympus DP50 digital camera mounted on a Nikon Microphot-FXA microscope and Analysis^D software (Soft Imaging System GmbH, Germany).

5.2.5 qRT-PCR analysis of muscle growth and structure

Besides the whole genome microarray analysis we also performed qRT-PCR analysis of genes involved in myogenesis and sarcomeric structure in trained and control fish at 5 and 14 dpf (see also Introduction). Previous studies have shown that swim-training affects the expression of the genes involved in myogenesis (*myogenin*) and sarcomeric structure (*slow myosin heavy chain 1, slow troponin C type 1a, slow troponin C 1b, fast muscle specific myosin heavy chain 2, fast troponin C type 2, fast troponin I 2a.4*) in juvenile and adult zebrafish [133, 155]. These genes were not present in the selected list of 52 genes from the microarray analysis. To investigate if similar molecular changes take place during zebrafish larval development in muscle growth and sarcomeric structure, we examined the expression of these genes with RT-qPCR after one and ten days of swim-training (at 5 and 14 dpf).

We performed two independent swim-training experiments (experiment (exp) 1 and 2) and subjected fish to swim-training from 5 until 14 dpf as described in the section 'Swim-training set-up and regime'. During the swim-training experiments the absolute values corresponded to a relative water velocity of 3.5±0.06 Bl/s at 5 dpf to 5.62±0.04 Bl/s (exp 1) and 6.34±0.06 Bl/s (exp 2) at 14 dpf (see also Table 5.A.1). Forty fish were randomly assigned to a tube (40 fish per tube, 5 tubes in total per treatment). At the end of a training day, control and trained fish were sampled from a tube, euthanized and images were taken as described above. After the length measurements, fish were immediately frozen in liquid nitrogen and stored at −80°C. Standard length measurements (n=10–20) were taken to evaluate the growth of control and trained fish from 5–14 dpf. Standard length measurements of control and trained fish as a function of age were evaluated with quadratic regression for two groups in SAS v9.2, $p < 0.05$ was accepted as significant. Average length measurements over time with standard deviation were plotted in Matlab (version 7.12.0.635, R2011a, The Mathworks, Inc.).

RNA isolation and cDNA synthesis of each individual sampled fish (at 5 and 14 dpf) was performed as described above. Five fish were used per treatment and experiment. Primers were designed by Palstra *et al.* [155] and Van der Meulen *et al.* [133]. RT-qPCR was performed as described above. The C_t values of each gene were normalized against the C_t values of the housekeeping gene *rps11* and *rps18*. We did not use *βactin* for normalization due to technical issues when performing these qRT-PCR experiments. The stability of the reference genes was evaluated with the BestKeeper software tool [165] and this demonstrated that gene expression of the reference genes did not differ between the trained and control samples (average absolute deviation of C_t values of control and trained samples from the mean (of trained and control values) was lower than 1: *rps18*=0.27 *rps11*=0.30 (average of all experiments and stages)). Furthermore, since *rps18* was the most stably expressed (exhibiting the lowest variation), it was chosen for further analysis. The relative fold change in gene expression between trained and control fish was calculated according to the Pfaffl method [164]. Significant differences ($p < 0.05$) in relative gene expression values of muscle specific genes (versus *rps18*) between trained and control fish at 5 and 14 dpf were evaluated for each independent experiment with a Mann-Whitney U-test with IBM SPSS (version 19.0.0.1).

5.3 Results and Discussion

5.3.1 Effect of swim-training on swim behaviour and growth

Swimming behavior of zebrafish larvae was similar to the swimming behaviour of the zebrafish larvae as described in our previous study [54]. Briefly, in the younger stages, fish subjected to swim-training (trained fish) frequently adhered to the tube wall to maintain position, whereas in the older stages trained and control fish swam continuously and showed intermittent swim behavior (short bursts of tail beats alternated with coasting). During the breaks trained fish swam within 5 minutes throughout the tube like the control fish, indicating that trained fish recovered quickly from the training.

During each swim-training experiment, both trained and control fish exhibited a normal development pattern [160]. Trained and control fish sampled at 10 dpf for the whole genome microarray analysis did not significantly differ in length (control fish (5.37±0.32 mm) and trained fish (5.24±0.31 mm) (student's t-test, $p > 0.05$)). In addition, swim-training did not increase growth in trained fish compared to control fish in swim-training experiments 1 and 2 (Materials and Methods; RT-qPCR analysis of muscle growth and structure) (Figure 5.1), as shown by quadratic regression of the standard length measurements on age in the two groups. No significant difference ($p < 0.05$) was found between the coefficients of the linear and quadratic terms for trained and control fishes. Mortality ranged between 22–25.4 % in swim-training experiments 1 and 2 and was not significantly different (student's t-test, $p < 0.05$) between control and trained fish indicating that swim-training did not influence survival.

5.3.2 Effect of swim-training on the transcriptome

To obtain a general overview of the effects of swim-training on the transcriptome, we selected 52 genes (see also Materials and Methods for details of the selection process) from the whole genome microarray analysis and validated the gene expression of these genes with RT-qPCR (Table 5.A.2). Gene expression of 12 of the 52 selected genes was down-regulated according to the qRT-PCR analysis in trained fish whereas 40 of the 52 selected genes were upregulated in trained fish (normalized with *rps11*). Thus, 77 % of the selected genes from the microarray analysis were also up-regulated with qRT-PCR analysis. This suggests that the microarray analysis overestimated the number of genes which were actually up-regulated.

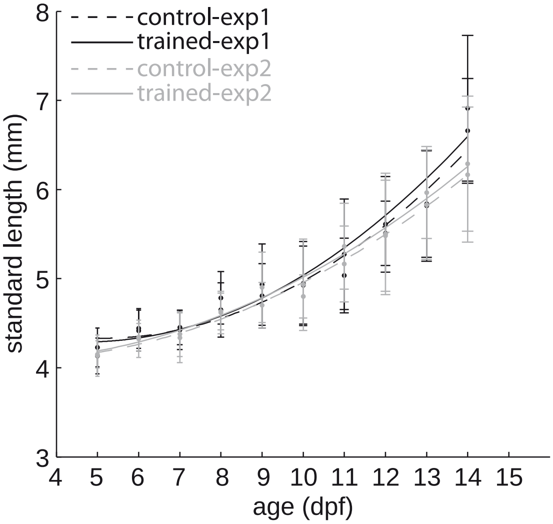

Figure 5.1. Growth was similar between trained and control fish. Average standard lengths (dots) ± standard deviation (with quadratic regression fit) as a function of age (dpf). Dashed line indicates values for control fish, solid line indicates values for trained fish. Black lines indicates experiment 1, grey lines indicates experiment 2.

We selected 23 genes which were upregulated with a fold change of 1.5 or larger in trained versus control fish in the qRT-PCR analysis (when normalized with *rps11*, Table 5.A.2) for spatial gene expression analysis with in situ hybridization. We performed in situ hybridization on longitudinal sections of 10 dpf wildtype zebrafish larvae. Out of the 23 validated genes, we observed a tissue-specific gene expression pattern for 15 genes (Table 5.1, Figure 5.2 and Figure 5.3). For the remaining 8 genes, we did not observe a tissue-specific gene expression pattern.

Seven of these 15 genes were expressed in the liver (Figure 5.2A–F; *hapb2*, *ahsg*, *itih3*, *bfb*, *si:ch211-127b11.1*, *wu:fd52f12*). The *hpx* gene was also expressed in the liver but only in a specific part of the liver (Figure 5.2G–H). Zhao *et al.* [230] and Cheng *et al.* [27] showed that *hpx* was expressed in the zebrafish in the liver of larval and adult fish, respectively. Hpx binds to heme in blood and transports it to the liver for breakdown. Hpx is produced in the liver and released into the plasma to bind heme. This suggests that swim-training stimulated the detoxification of heme.

The genes *bhlhe40*, *gadd45βa*, *ptgs2b*, *anpepb* and *LOC570571* showed a clear expression pattern in the brain (Figure 5.3A–G). The *bhlhe40* gene was expressed

Table 5.1. Gene expression values of genes selected from the genome-wide microarray analysis and which showed a specific expression pattern with in situ hybridization

Gene ID	**Gene Name**	**Gene Symbol**	***βactin***	***rps11***	**array**
NM_001025504	*prostaglandin-endoperoxide synthase 2b*	*ptgs2b*	1.68	1.78	1.78
NM_001110373	*hyaluronan binding protein 2*	*habp2*	1.47	1.56	1.83
NM_214759	*legumain*	*lgmn*	1.51	1.60	1.83
NM_001089325	*alanyl (membrane) aminopeptidase b*	*anpepb*	1.87	1.98	1.84
NM_212679	*basic helix-loop-helix family, member e40*	*bhlhe40*	1.95	2.07	1.91
NM_213031	*growth arrest and DNA-damage-inducible, beta a*	*gadd45βa*	1.54	1.63	2.02
NM_212622	*alpha-2-HS-glycoprotein*	*ahsg*	2.00	2.12	2.21
NM_001033104	*inter-alpha (globulin) inhibitor H3*	*itih3*	1.73	1.89	2.57
XM_684119	*si:dkey-206f10.1*	*si:dkey-206f10.1*	2.13	2.26	2.99
NM_131241	*complement component bfb*	*bfb*	2.22	2.02	3.76
XM_694069	*epoxide hydrolase 4-like*	*LOC570571*	3.03	2.75	3.95
NM_001111147	*hemopexin*	*hpx*	2.50	2.21	4.10
XM_001919784	*interferon-induced protein 44-like*	*LOC100150009*	2.45	2.23	4.37
NM_001114488	*si:ch211-127b11.1*	*si:ch211-127b11.1*	2.36	2.08	5.67
XM_003198044	*wu:fd52f12*	*wu:fd52f12*	2.48	2.19	9.91

Gene expression values represent the fold change in gene expression between trained and control fish (normalized against the gene expression of *βactin* and *rps11* (qRT-PCR analysis) and obtained from the microarray analysis (array)).

throughout the midbrain (Figure 5.3A). Bhlhe40 (Bhlhb2, also known as Dec1/ Eip1/Sharp2/Stra13/Clast5) is a transcription factor that plays a pivotal role in many biological processes such as cell differentiation, cell growth, cell death, circadian rhythm and immune systems. Chung *et al.* [30] showed in zebrafish that the expression level of *bhlhe40* was elevated in differentiated oligodendrocytes (glial cells which myelinate axons in the central nervous system (CNS)). Gadd45βa and Gadd45βb are both involved in somite segmentation during zebrafish embryonic development and are very similar to the mammalian GADD45β proteins [95]. Furthermore, Ma *et al.* [123] showed that *Gadd45β* plays an essential role in neural activity-dependent neurogenesis in the hippocampus of adult mice. Physical exercise increased the expression of *Gadd45β* and neural progenitor proliferation in adult WT mice. In addition, in *Gadd45β* knockout mice neural progenitor proliferation was significantly less effective compared to WT mice in response to training [123]. Several studies in adult mammals have shown that physical exercise stimulates neurogenesis [33, 123, 169, 170]. Interestingly, neurogenesis was only observed in the hippocampus, an area important for learning and memory. In the zebrafish, the dorsolateral part of the telencephalon corresponds to the mammalian hippocampus. In this study, 5 out of the 14 genes analyzed were expressed in the brain. The expression of *bhlhe40* and *gadd45βa* was, however, not restricted to the dorsolateral part of the telencephalon. Thus, the increased expression of *bhlhe40* and *gadd45βa* in the brain suggests that swim-training stimulated neurogenesis.

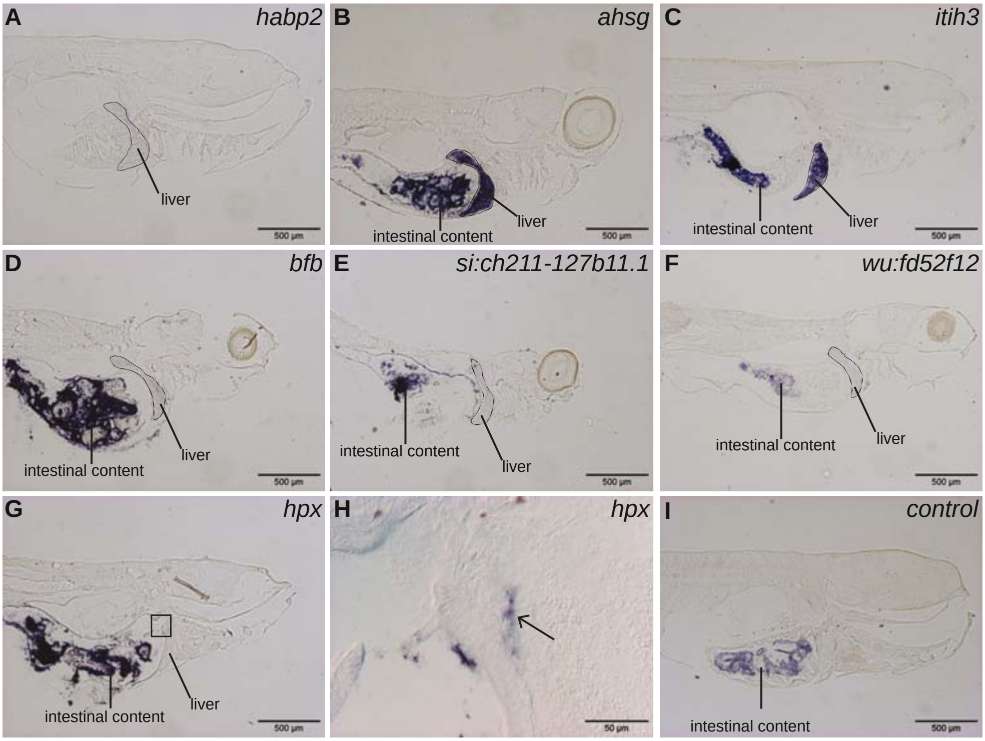
A
habp2
liver
500 µm
B
ahsg
intestinal content
liver
500 µm
C
itih3
intestinal content
liver
500 µm
D
bfb
intestinal content
liver
500 µm
E
si:ch211-127b11.1
intestinal content
liver
500 µm
F
wu:fd52f12
intestinal content
liver
500 µm
G
hpx
intestinal content
liver
500 µm
H
hpx
50 µm
I
control
intestinal content
500 µm

Figure 5.2. Swim-training induces molecular changes in the liver (**A**–**F**). Gene expression is visualized in longitudinal sections of 10 dpf wildtype zebrafish, anterior is to the right. Representative sections are shown. See Table 5.1 for abbreviations of the gene names. **A**–**F**: All genes were specifically expressed throughout the liver. **G**: *hpx* shows localized expression in a specific part of the liver (indicated with a black-lined box). **H**: higher magnification of area indicated by the black-lined box in G, arrow indicates specific expression of *hpx*. **I**: control sample (without the probe) showed staining of intestinal content which indicated that this was non-specific staining in the samples with probe. The staining intensity of intestinal content varied due to intestinal content and staining time.

The gene *anpepb* was not only expressed in the midbrain but also in the epithelial layer of the intestines and in the kidneys (Figure 5.3D–F). Anpepb belongs to the family of membrane alanyl aminopeptidases which remove N-terminal neutral, acidic or basic residues. Members of this family catalyze the removal of amino acids from small peptides and might play a role in the final digestion of these peptides [176]. In addition, the gene *lgmn* was also specifically expressed in the epithelial layer of the intestines (Figure 5.3H, K) and belongs to the asparaginyl endopeptidase or legumain family. Legumains specifically hydrolyze asparaginyl bonds [26, 193]. Sojka and coworkers identified a novel legumain in the gut of the hard tick *Ixodes ricinus* and showed that it was involved in the degradation of hemoglobin [193]. In addition, it has also been shown that in human B-cell lines, an asparaginyl endopeptidase similar to the human legumain, is involved in processing of microbial antigens [127]. Interestingly, *lgmn* was specifically expressed in the caudal intestine whereas *anpepb* was also expressed in the rostral, mid and caudal intestine (data not shown). This could be related to the different functional regions in the intestines [217]. All together, the increased expression of *anpepb* and *lgmn* in the epithelial layer of the intestine suggests that swim-training increased the digestion of peptides.

The gene *LOC570571* was not only expressed in the brain but also in tissue surrounding the cranial cartilage structures and kidneys (Figure 5.3G, J). It is predicted to encode an epoxide hydrolase 4-like protein but nothing is known about the actual biological function of this gene.

The gene *si:dkey-206f10.1* was specifically expressed in the pancreas (Figure 5.3I, L). It contains an adenylyl-/guanylyl cyclase catalytic domain but nothing is known about the actual biological function of this gene. The pancreas secretes digestive enzymes into the intestines and hormones into the bloodstream (insulin and glucagon) to regulate glucose homeostasis [189]. The expression of *si:dkey-206f10.1* might have been increased (leading to an increase in secretion of digestive enzymes or hormones) to meet the increased demands for energy by the active muscles in trained fish.

The gene *LOC100150009* was expressed at the opposite ends of muscle fibers in axial and heart musculature (Figure 5.3M–O) and head musculature (data not shown). It is predicted to encode an interferon-induced protein 44-like but nothing is known about the actual biological function of this gene. In the axial musculature, a strong staining was visible in the regions near the myosepta. In axial musculature, muscle fibers are connected to adjacent muscle fibers in the neighboring myomere via myotendinous junctions (MTJs) in the myosepta. Myotendious junctions connect the actin micro filaments that extend from the terminal Z-line in the muscle fibers to the collagen fibril rich matrix in the myosepta. Furthermore, MTJs are important sites for myofibril assembly and growth. A higher level of myosin heavy chain mRNA was observed at the MTJs in stretched hyperthropied rabbit skeletal muscle[43]. Dur-

Figure 5.3 *(following page).* Swim-training induces molecular changes in brain, kidneys, pancreas, intestines and muscle (**A**–**O**). Gene expression is visualized in longitudinal sections of 10 dpf wildtype zebrafish, anterior is to the right. Representative sections are shown. See Table 5.1 for abbreviations of the gene names. **A**–**C**: *bhlhe40*, *ptgs2b* and *gadd45βa* are specifically expressed in the midbrain. **D**–**F**: *anpepb* is specifically expressed in the midbrain, intestines and kidney, a higher magnification of the intestines and kidneys is shown in E and F, respectively. **G**–**J** *LOC570571* is specifically expressed in brain, kidneys and in tissue surrounding cranial cartilage structures, a higher magnification of the basihyal area is shown in J. **H**–**K**: *lgmn* is specifically expressed in the intestines, a higher magnification of the intestines is shown in K. **I**–**L**: *si:dkey-206f10.1* is specifically expressed in the pancreas (black-lined box), a higher magnification of this area is shown in L. **M**–**O**: *LOC100150009* is specifically expressed in muscle fibers in the axial, cranial and heart musculature, a higher magnification of the axial and heart muscle fibers is shown in N and O, respectively. Black-lined boxes indicate the area which are shown with a higher magnification, arrows indicate the specific expression pattern of the respective genes.

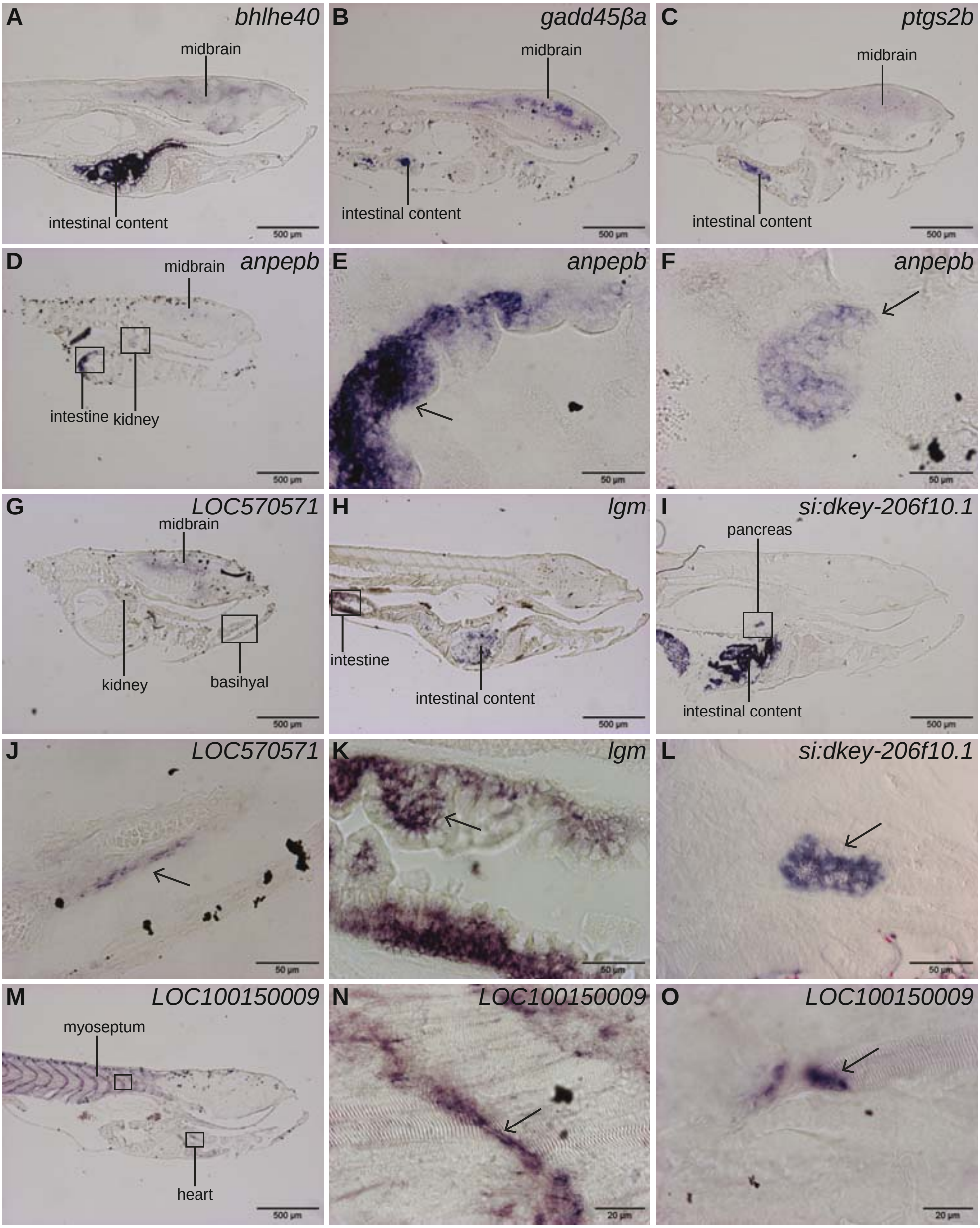
A
bhlhe40
midbrain
intestinal content
500 µm
B
gadd45βa
midbrain
intestinal content
500 µm
C
ptgs2b
midbrain
intestinal content
500 µm
D
anpepb
midbrain
intestine
kidney
500 µm
E
anpepb
50 µm
F
anpepb
50 µm
G
LOC570571
midbrain
kidney
basihyal
500 µm
H
lgm
intestine
intestinal content
500 µm
I
si:dkey-206f10.1
pancreas
intestinal content
500 µm
J
LOC570571
50 µm
K
lgm
50 µm
L
si:dkey-206f10.1
50 µm
M
LOC100150009
myoseptum
heart
500 µm
N
LOC100150009
20 µm
O
LOC100150009
20 µm

ing swimming, muscular forces are transmitted via myotendinous junctions in the myosepta to axial structures [24, 195]. The increased swimming activity in trained fish could have increased the load or duration of load on the MTJs. Thus, the increased expression of *LOC100150009* suggests that swim-training could have induced molecular changes in the MTJs for a better resistance to the increased load. The exact function of *LOC100150009*, however, remains to be investigated.

5.3.3 Effect of swim-training on expression of genes involved in muscle growth and structure

Based on previous studies we expected to find molecular changes in myogenesis and sarcomeric structure in response to swim-training (see also Introduction). We therefore analyzed the gene expression of the following set of genes involved in myogenesis and sarcomeric structure with qRT-PCR in trained and control fish at 5 and 14 dpf (Figure 5.4): *myogenin (myog), slow myosin heavy chain 1 (smyhc1), slow troponin C type 1a (stnnc1a), slow troponin C 1b (stnnc1b), fast muscle specific myosin heavy chain 2 (myhz2), fast troponin C type 2 (tnnc2), fast troponin I 2a.4 (tnni2a.4).* These genes are specifically expressed in muscle tissue in the zebrafish [45, 46, 133, 192, 205, 206].

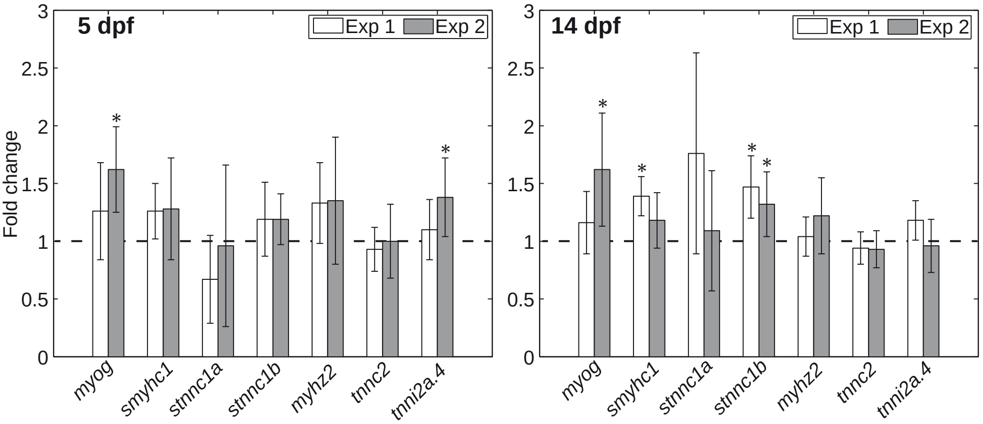

Figure 5.4. Swim-training induces molecular changes in myogenesis and sarcomeric structure in zebrafish larvae at 5 and 14 dpf. Values represent the fold change in gene expression between trained and control fish and are normalized against the gene expression of *rps18*. The dashed line indicates a relative gene expression level of one. Values are average ± standard deviation (n=5). Asterisks indicates a significant difference between trained and control fish ($p < 0.05$). See text for abbreviations of the gene names

The fold change in gene expression between trained and control fish were similar between both experiments (exp 1 and 2) for all genes at 5 dpf and for 4 genes at 14 dpf. However, *myog*, *smyhc1* and *stnnc1a* showed significant differences in fold change in gene expression (of trained versus control) between exp 1 and 2 at 14 dpf. The reasons for these differences are unclear since the experimental set-ups were similar.

Interestingly, swim-training increased the expression of the muscle growth promotor *myogenin* and fast muscle fiber marker *tnni2a.4* in trained versus control fish already at 5 dpf in experiment 2 ($p < 0.05$, Figure 5.4). Swim-training did not change the gene expression of the muscle growth or structure in experiment 1. Thus, the results from experiment 2 indicates that swim-training can already have significant effects on muscle growth and sarcomeric structure (on gene expression level) after one day of training.

At 14 dpf, swim-training increased the expression of the slow fiber markers *smyhc1* and *stnnc1b* in experiment 1 and the expression of *myogenin* and *stnnc1b* in experiment 2 in trained versus control fish ($p < 0.05$, Figure 5.4). The increased expression of the slow fiber markers suggest that muscle tissue shifted finally to a slow fiber phenotype in response to swim-training during zebrafish larval development.

5.4 General Discussion

5.4.1 Swim-training did not affect growth and survival

In this study, we examined the effects of endurance training in an early vertebrate embryo, focusing on the molecular changes induced by swim-training in the zebrafish larva. Exercise did not adversely affect growth and survival. This indicates that trained fish were able to acquire sufficient food and thus energy for growth, survival and swimming. In a previous study swim-training did increase growth rate in trained fish (versus control fish reared at the same density) [54]. The only difference between this study and the previous study was the number of fish in the tubes during the swim-training (40 and 10 fish per tube, 13 and 3 fish/20 ml, respectively). This suggests that, although the fish were fed *ad libitum*, the density of fish in a tube affects the growth rate. In fact, in this study, control fish of 10 dpf (sampled for the microarray analysis, 10 fish per tube) were significantly longer than control fish of 10 dpf from experiment 1 and 2 (40 fish per tube). In addition, Parichy *et al.* [160] showed that zebrafish larvae reared at different densities resulted in significantly different growth rates. Fish reared at low densities (1–2 fish/L) grew faster than fish reared at high densities (≈54 fish/L). In our previous study, we concluded that swim-training can increase growth rates during early larval development if the training and feeding regime are carefully chosen. In our present study, we show that, to increase growth rate in response to swim-training during early larval development, not only the training and feeding regime but also the density of fish should be carefully chosen.

5.4.2 Swim-training induces molecular changes in the gastrointestinal system

In the present study, 52 genes were selected based on a number of criteria for validation with qRT-PCR and spatial expression analysis with in situ hybridization. Fifteen genes were found to be specifically expressed in the brain, muscle, kidneys, liver, pancreas or intestines. This indicates that swim-training led to molecular changes already after 5 days of training and in a variety of organ systems. These molecular changes are likely to have led, at least in part, to physiological adaptations to meet the increasing demands for energy by the active muscles.

In mammals, endurance training also increases the share of fatty acid metabolism to meet the energy requirements [48, 80, 128, 130]. During prolonged exercise in humans, fatty acids provide 80 % of these energy requirements [130]. In fish, it is not as clear as in mammals how endurance training influences overall energy metabolism. Depending on the fish species and training regime, endurance training can lead to an increase in protein metabolism or fatty acid metabolism or glycogen metabolism or a combination of these pathways [41, 52, 91, 184]. Recently, however, Kopp *et al.* [106] showed that swim-training increased the gene expression of *pyruvate dehydrogenase kinase 2*, an inhibitor of pyruvate dehydrogenase, in zebrafish larvae at 15 dpf after 6 days of training (via qRT-PCR). This and the unchanged/enhanced expression of enzymes involved in mitochondrial ATP production suggests that lipid metabolism was stimulated in zebrafish larvae. The expression of this gene and the expression of the gene *succinate dehydrogenase a*, involved in mitochondrial ATP production, was also up-regulated in our micrarray analysis. These findings are in line with the study by Kopp and coworkers and suggests that swim-training stimulated lipid metabolism in zebrafish larvae already at 10 dpf after 5 days of training.

Furthermore, Kopp and coworkers also performed microarray analysis on the effect of swim-training and demonstrated that 26 genes were affected in response to swim-training. Eight of these genes were up-regulated. Two of these genes, *heat shock protein 70kD protein* (*hsp70*) and *heat shock protein 47* (*hsp47*), were also identified within our study. The gene *hsp70* was also up-regulated in our study but *hsp47* was down-regulated. Of the 19 genes which were down-regulated in the study by Kopp, six were also identified in our microarray analysis. The expression of these genes was, however, up-regulated in our study. These differences in gene expression could be due to a difference in density of fish in a tube, due to a different feeding and training regime or due to the different stages when fish were subjected to swim-training.

5.4.3 Swim-training induces molecular changes in muscle growth and structure

In adult vertebrates, endurance training stimulates the switch to slow twitch muscle fibers (from fast twitch muscle fibers) and increases muscle fiber size via hypertrophy [35, 39, 128, 130]. Furthermore, it also improves aerobic capacity of muscle fibers by increasing the capillarity, mitochondrial content and synthesis and activity of aerobic enzymes [2, 17, 29, 52, 67, 91, 177, 218]. In adult zebrafish, the expression of the slow fiber markers *smyhc1* and *stnnC1b* was increased in response to swim-training [155]. Consistent with this, in juvenile zebrafish, swim-training increased the expression of *myoglobin* and the slow fiber markers *smyhc1* and *stnnC1a*. Myoglobin serves as an extra oxygen supply for muscle tissue [130]. This suggested that axial muscle shifted towards a slow aerobic phenotype in response to the training [133]. In the present study, we demonstrated that swim-training increased the expression of the muscle growth promotor myogenin at 5 and 14 dpf. At 5 dpf, however, fish adhered frequently to the wall of the tube, intermitted with short swimming bouts. Thus, at this stage, the fish did not experience an endurance training but did show an increased swimming activity [54]. Consistent with this, we observed the increased expression of the fast muscle fiber marker *tnni2a.4*. On the other hand, at 14 dpf, swim-training increased the expression of the slow fiber markers *stnnC1b* and *smyhc1* which suggest that muscle shifted finally to a slow fiber phenotype and that fish were subjected to endurance training. Pelster and coworkers showed that swim-training led to an increased mitochondrial content in the red fibers of larval zebrafish [163]. Thus, taken together with the present study, this indicates that muscle can already shift due to the training towards a slow aerobic phenotype during early larval development in zebrafish.

This study provides a whole genome microarray analysis of the effect of swim-training during early development in zebrafish on a quantitative and spatial gene expression level. It shows that already during early vertebrate development molecular changes take place that are likely to improve endurance performance. Our work provides a framework for identifying genes that are relevant on the physiological and structural level during early vertebrate development in response to endurance training.

Acknowledgements

We are indebted to Henk Schipper for his advice and support with image acquisition and analysis with the Analysis^{D} software. We would also like to thank Paul Oomen for preliminary experiments with the in situ hybridisations on sections. We are especially grateful to the members of the Zebrafish Facility at Wageningen University for providing help and taking care of the zebrafish.

5.A Supplemental data

Table 5.A.1. Overview of the average flow velocities (absolute and relative velocities) during the swim-training experiments. Data is shown from the swim-training experiments performed for the micro array analysis and muscle marker expression analysis. Values (length and flow velocities) are average values±standard deviation.

Swim-training experiments for Micro array analysis						
Age (dpf)	Length (cm)		Flow Velocity (cm/s)	SD	Flow velocity (BL/s)	SD
5			1,46	0,02		
6			1,56	0,02		
7			1,86	0,03		
8			2,20	0,04		
9			2,46	0,03		
10	0,52		2,89	0,04	5,51	0,08

Swim-training experiments for muscle marker gene expression analysis											
Age (dpf)	Length (cm)	Length (cm)	exp 1		exp2		exp 1		exp2		
	exp 1	exp2	Flow Velocity (cm/s)	SD	Flow Velocity (cm/s)	SD	Flow velocity (BL/s)	SD	Flow velocity (BL/s)	SD	
5	0,41	0,41	1,45	0,03	1,45	0,02	3,50	0,06	3,50	0,06	
6	0,44	0,43	1,56	0,02	1,55	0,02	3,54	0,05	3,58	0,05	
7	0,44	0,43	1,90	0,10	1,87	0,03	4,30	0,22	4,30	0,06	
8	0,48	0,46	2,19	0,03	2,16	0,03	4,57	0,07	4,67	0,07	
9	0,49	0,49	2,44	0,02	2,44	0,04	4,94	0,05	4,97	0,09	
10	0,49	0,49	2,86	0,05	2,86	0,05	5,78	0,10	5,80	0,11	
11	0,53	0,54	3,28	0,06	3,26	0,03	6,23	0,11	6,08	0,06	
12	0,56	0,55	3,58	0,03	3,57	0,04	6,38	0,05	6,49	0,07	
13	0,58	0,60	3,78	0,01	3,77	0,02	6,48	0,03	6,33	0,04	
14	0,69	0,62	3,89	0,03	3,91	0,04	5,62	0,04	6,34	0,06	

Table 5.A.2. Overview of the selected genes from whole genome microarray analysis which were selected for further analysis with qRT-PCR (see also material and methods). The top 20 up-regulated genes are indicated in green. The genes indicated in yellow (with a fold change of 1.75 or larger) were, according to literature, mechanosensitive or involved in skeletal development. Genes of which the qRT-PCR results are highlighted in pink were further selected for analysis with in situ hybridization (Figures 5.2 and 5.3, Table 5.1)

Agilent_ProbeID	Gene_ID	GeneSymbol	GeneName	Microarray	rps11
A_15_P402705	TC380297			9.91	2.19
A_15_P208801	NM_001044323	zgc:152753	zgc:152753	8.32	3.55
A_15_P673711	XM_001922488			6.90	4.96
A_15_P159276	NM_001114488	si:ch211-127b11.1	si:ch211-127b11.1	5.67	2.08
A_15_P711086	NM_001110109	zgc:171537	zgc:171537	5.32	1.37
A_15_P497452	XM_001345886			5.29	7.89
A_15_P726206	NM_001005579	nitr6b	novel immune-type receptor 6b	4.82	no results
A_15_P758236	XM_001919784			4.37	2.23
A_15_P590367	BC163046			4.32	2.75
A_15_P657586	BC129341	rnasel2	ribonuclease like 2	4.29	-2.05
A_15_P193756	NM_131553	fzd8b	frizzled homolog 8b	4.15	-1.26
A_15_P111566	NM_200368	slc5a12	solute carrier family 5 (sodium/glucose cotransporter), member 12	4.15	-1.89
A_15_P174831	NM_001037104	dysfip1	dysferlin interacting protein 1	4.11	2.38
A_15_P740212	NM_001111147	hpx	hemopexin	4.10	2.21
A_15_P288196	XR_082662	LOC100006814	hypothetical protein LOC100006814	4.09	-1.83
A_15_P569127	XM_001919715	LOC100007561	hypothetical LOC100007561	4.02	-1.43
A_15_P492387	NM_001110413	zgc:172131	zgc:172131	3.96	1.06
A_15_P572327	XM_694069	LOC570571	abhydrolase domain containing 9-like	3.95	2.75
A_15_P380445	NM_001013315	dpp7	dipeptidyl-peptidase 7	3.81	1.38
A_15_P729336	NM_205569	fos	v-fos FBJ murine osteosarcoma viral oncogene homolog	3.80	1.45
A_15_P227520	NM_131241	bfb	complement component bfb	3.76	2.02
A_15_P712886	NM_001113644	zgc:172101	zgc:172101	3.70	-1.17
A_15_P340675	NM_214773	acp5a	acid phosphatase 5a, tartrate resistant	3.67	1.46
A_15_P187221	NM_212855	nfe2l1	nuclear factor, erythroid derived 2,-like 1	3.47	1.55
A_15_P185211	XM_001343475	pcdh9	protocadherin 9	3.31	-1.22
A_15_P184776	XM_684119	si:dkey-206f10.1	si:dkey-206f10.1	2.99	2.26
A_15_P149006	NM_201172	slc25a10	solute carrier family 25 (mitochondrial carrier; dicarboxylate transporter), member 10	2.90	1.00
A_15_P364340	NM_203484	cacna1da	calcium channel, voltage-dependent, L type, alpha 1D subunit, a	2.87	-1.18
A_15_P160756	NM_001033104	itih3	inter-alpha (globulin) inhibitor H3	2.57	1.89
A_15_P163406	NM_001006063	ank2	ankyrin 2, neuronal	2.56	1.13
A_15_P145881	XM_688690	LOC565410	novel protein similar to vertebrate capping protein (actin filament) gelsolin-like (CAPG)	2.32	-1.56
A_15_P399720	XM_687354	dZ228E24.5	similar to claudin 10	2.28	1.15
A_15_P130521	NM_212941	mafg2	v-maf musculoaponeurotic fibrosarcoma oncogene homolog g (avian), 2	2.24	1.09
A_15_P664566	NM_212622	ahsg	alpha-2-HS-glycoprotein	2.21	2.12
A_15_P120601	NM_001104937	nos2a	nitric oxide synthase 2a, inducible	2.20	2.25
A_15_P668181	NM_001048064	elnb	elastin b	2.16	-1.19
A_15_P615418	NM_001080626	loxl2b	lysyl oxidase-like 2b	2.15	1.06
A_15_P165896	XM_684948	LOC561540	glutamate receptor 5-like	2.12	1.18
A_15_P275566	NM_213031	gadd45ba	growth arrest and DNA-damage-inducible, beta a	2.02	1.63
A_15_P630636	NM_131234	gata1a	GATA binding protein 1a	2.01	1.38
A_15_P190951	XM_682922			2.01	-1.12
A_15_P290171	NM_001040327	chrna2a	cholinergic receptor, nicotinic, alpha polypeptide 2a (neuronal)	2.00	1.13
A_15_P694976	NM_131457	bmpr1ba	bone morphogenetic protein receptor, type 1ba	1.92	1.22
A_15_P100831	NM_212679	bhlhe40	basic helix-loop-helix family, member e40	1.91	2.07
A_15_P100912	NM_001077767	papss2a	3'-phosphoadenosine 5'-phosphosulfate synthase 2a	1.88	1.25
A_15_P119415	NM_199950	socs3a	suppressor of cytokine signaling 3a	1.86	1.74
A_15_P174316	NM_178219	wnt10b	wingless-type MMTV integration site family, member 10b	1.86	1.38
A_15_P725681	NM_001089325	anpep	alanyl (membrane) aminopeptidase	1.84	1.98
A_15_P103334	NM_214759	lgmn	legumain	1.83	1.60
A_15_P726496	NM_001110373	habp2	hyaluronan binding protein 2	1.83	1.56
A_15_P720356	NM_001025504	ptgs2b	prostaglandin-endoperoxide synthase 2b	1.78	1.78
A_15_P265091	XM_688443	adamts1	ADAM metallopeptidase with thrombospondin type 1 motif, 1	1.77	1.19

green =top 20 selected genes
yellow=mechanosensitive and or bone related genes
pink=genes selected for ish analysis

Table 5.A.3. Overview of the qRT-PCR and in situ hybridization primer sequences of the genes selected from the microarray and qRT-PCR analysis (Table 5.A.2) and which showed a specific expression pattern in the in situ hybridization experiments.

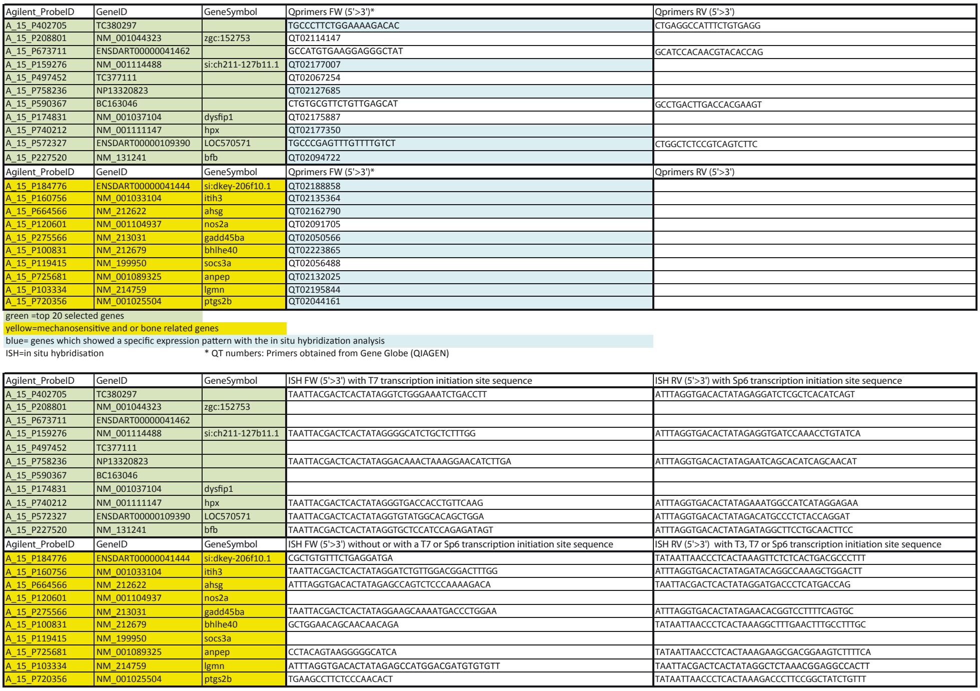

Agilent_ProbeID	GeneID	GeneSymbol	Qprimers FW (5'>3')*	Qprimers RV (5'>3')
A_15_P402705	TC380297		TGCCCTTCTGGAAAAGACAC	CTGAGGCCATTTCTGTGAGG
A_15_P208801	NM_001044323	zgc:152753	QT02114147	
A_15_P673711	ENSDART00000041462		GCCATGTGAAGGAGGGCTAT	GCATCCACAACGTACACCAG
A_15_P159276	NM_001114488	si:ch211-127b11.1	QT02177007	
A_15_P497452	TC377111		QT02067254	
A_15_P758236	NP13320823		QT02127685	
A_15_P590367	BC163046		CTGTGCGTTCTGTTGAGCAT	GCCTGACTTGACCACGAAGT
A_15_P174831	NM_001037104	dysfip1	QT02175887	
A_15_P740212	NM_001111147	hpx	QT02177350	
A_15_P572327	ENSDART00000109390	LOC570571	TGCCCGAGTTTGTTTTGTCT	CTGGCTCTCCGTCAGTCTTC
A_15_P227520	NM_131241	bfb	QT02094722	
Agilent_ProbeID	GeneID	GeneSymbol	Qprimers FW (5'>3')*	Qprimers RV (5'>3')
A_15_P184776	ENSDART00000041444	si:dkey-206f10.1	QT02188858	
A_15_P160756	NM_001033104	itih3	QT02135364	
A_15_P664566	NM_212622	ahsg	QT02162790	
A_15_P120601	NM_001104937	nos2a	QT02091705	
A_15_P275566	NM_213031	gadd45ba	QT02050566	
A_15_P100831	NM_212679	bhlhe40	QT02223865	
A_15_P119415	NM_199950	socs3a	QT02056488	
A_15_P725681	NM_001089325	anpep	QT02132025	
A_15_P103334	NM_214759	lgmn	QT02195844	
A_15_P720356	NM_001025504	ptgs2b	QT02044161	

green =top 20 selected genes

yellow=mechanosensitive and or bone related genes

blue= genes which showed a specific expression pattern with the in situ hybridization analysis

ISH=in situ hybridisation

* QT numbers: Primers obtained from Gene Globe (QIAGEN)

Agilent_ProbeID	GeneID	GeneSymbol	ISH FW (5'>3') with T7 transcription initiation site sequence	ISH RV (5'>3') with Sp6 transcription initiation site sequence
A_15_P402705	TC380297		TAATTACGACTCACTATAGGTCTGGGAAATCTGACCTT	ATTTAGGTGACACTATAGAGGATCTCGCTCACATCAGT
A_15_P208801	NM_001044323	zgc:152753		
A_15_P673711	ENSDART00000041462			
A_15_P159276	NM_001114488	si:ch211-127b11.1	TAATTACGACTCACTATAGGGGCATCTGCTCTTTGG	ATTTAGGTGACACTATAGAGGTGATCCAAACCTGTATCA
A_15_P497452	TC377111			
A_15_P758236	NP13320823		TAATTACGACTCACTATAGGACAAACTAAAGGAACATCTTGA	ATTTAGGTGACACTATAGAATCAGCACATCAGCAACAT
A_15_P590367	BC163046			
A_15_P174831	NM_001037104	dysfip1		
A_15_P740212	NM_001111147	hpx	TAATTACGACTCACTATAGGGTGACCACCTGTTCAAG	ATTTAGGTGACACTATAGAAATGGCCATCATAGGAGAA
A_15_P572327	ENSDART00000109390	LOC570571	TAATTACGACTCACTATAGGTGTATGGCACAGCTGGA	ATTTAGGTGACACTATAGACATGCCCTCTACCAGGAT
A_15_P227520	NM_131241	bfb	TAATTACGACTCACTATAGGTGCTCCATCCAGAGATAGT	ATTTAGGTGACACTATAGATAGGCTTCCTGCAACTTCC
Agilent_ProbeID	GeneID	GeneSymbol	ISH FW (5'>3') without or with a T7 or Sp6 transcription initiation site sequence	ISH RV (5'>3') with T3, T7 or Sp6 transcription initiation site sequence
A_15_P184776	ENSDART00000041444	si:dkey-206f10.1	CGCTGTGTTTCTGAGGATGA	TATAATTAACCCTCACTAAAGTTCTCTCACTGACGCCCTTT
A_15_P160756	NM_001033104	itih3	TAATTACGACTCACTATAGGATCTGTTGGACGGACTTTGG	ATTTAGGTGACACTATAGATACAGGCCAAAGCTGGACTT
A_15_P664566	NM_212622	ahsg	ATTTAGGTGACACTATAGAGCCAGTCTCCCAAAAGACA	TAATTACGACTCACTATAGGATGACCCTCATGACCAG
A_15_P120601	NM_001104937	nos2a		
A_15_P275566	NM_213031	gadd45ba	TAATTACGACTCACTATAGGAAGCAAAATGACCCTGGAA	ATTTAGGTGACACTATAGAACACGGTCCTTTTCAGTGC
A_15_P100831	NM_212679	bhlhe40	GCTGGAACAGCAACAACAGA	TATAATTAACCCTCACTAAAGGCTTTGAACTTTGCCTTTGC
A_15_P119415	NM_199950	socs3a		
A_15_P725681	NM_001089325	anpep	CCTACAGTAAGGGGGCATCA	TATAATTAACCCTCACTAAAGAAGCGACGGAAGTCTTTTCA
A_15_P103334	NM_214759	lgmn	ATTTAGGTGACACTATAGAGCCATGGACGATGTGTGTT	TAATTACGACTCACTATAGGCTCTAAACGGAGGCCACTT
A_15_P720356	NM_001025504	ptgs2b	TGAAGCCTTCTCCCAACACT	TATAATTAACCCTCACTAAAGACCCTTCCGGCTATCTGTTT

”Do not go where the path may lead, go instead where there is no path and leave a trail.”

Ralph Waldo Emerson

Chapter 6

Exploring the molecular link between swim-training and caudal fin development in zebrafish larvae (*Danio rerio*)

Ansa W. Fiaz[1], Karen M. Léon-Kloosterziel[1], Stefan Schulte-Merker[1,2], Johan L. van Leeuwen[1], Sander Kranenbarg[1]

---

[1] Experimental Zoology Group, Department of Animal Sciences, Wageningen University and Research Centre, Wageningen, The Netherlands

[2] Hubrecht Institute-KNAW & UMC Utrecht, Utrecht, The Netherlands

Abstract

In vitro and *in vivo* studies have shown that mechanical forces play an important role during development. The molecular mechanisms via which mechanical forces regulate development have been extensively investigated by *in vitro* studies. However, the knowledge about the molecular pathways that mediate the effect of mechanical forces during development *in vivo* is limited. Previously, we showed that swim-training increased maximum normalized curvatures in the caudal fin (suggesting that the caudal fin experienced increased mechanical loads) and prioritized the development of skeletal structures in the caudal fin. Therefore, we used the zebrafish caudal fin to explore the molecular link between an increased swimming activity and development *in vivo*. Whole genome microarray analysis of caudal fins of zebrafish subjected to swim-training and control fish identified 46 genes which were up-regulated with a fold change of 1.5 or larger at 10 dpf. Fourteen genes were expressed specifically in the following tissues in the caudal fin: the neural tube, the tissue surrounding the hypurals, the finfold, or muscle fibers. Subsequently, we identified two muscle specific genes, *aste1* (*asteroid homolog 1*) and *zgc:65811*, which showed an increased expression specifically in the caudal fin in response to swim-training. This makes these genes interesting candidate genes for further research on the molecular link between mechanical forces and caudal fin development. Our study is the first to investigate the molecular link between swim-training and caudal fin development and offers a system that can provide a deeper understanding of the link between mechanical and molecular signals during development *in vivo*.

Keywords: mechanotransduction, microarray, mechanical load, in situ hybridisation, qRT-PCR

6.1 Introduction

In vitro and *in vivo* studies have shown that mechanical forces play an important role during development (reviewed by [53, 58, 96, 125, 126, 143, 166]). For example, studies have shown that mechanical forces (e.g. shear stress) generated by blood flow have a central role during haematopoiesis and heart valve morphogenesis [1, 213]. Furthermore, mechanical loading imposed by muscle forces plays an important role during chondrogenesis and osteogenesis [32, 68, 111, 178].

The molecular mechanisms via which mechanical forces regulate development are extensively being investigated. For example, studies have shown that transmembrane surface adhesion receptors such as integrins and cadherins, which link the cytoskeleton to the extracellular matrix and neighbouring cells (and vice versa), play an important role in mechanotransduction (reviewed by [58, 86, 96, 125, 126, 143, 166]). These receptors transduce mechanical forces via adhesion complexes to downstream signalling pathways (directly or indirectly) which in turn can induce transcriptional changes in the nucleus.

A diverse range of signalling pathways and transcription factors have been described, which are activated by mechanical forces (reviewed by [58, 96, 125, 126]). For example, it has been demonstrated that mechanical deformation of osteoblasts stimulated the activation of RUNX2, which is a key transcription factor for osteogenesis, via MAPK signaling pathways [92, 105, 140]. Furthermore, mechanical forces activate these MAPK signalling pathways by stimulating focal adhesion kinase via focal adhesions [16, 89]. Many of these signalling pathways have been unravelled by *in vitro* studies [125]. The molecular link between mechanical forces and morphological changes during development *in vivo* is, however, just starting to be revealed. To contribute to a better understanding of the molecular mechanism which translate mechanical forces into morphological changes during development *in vivo*, we explored in this paper the molecular link between increased swimming activity and caudal fin development.

Previously, we demonstrated that increased swimming activity via swim-training accelerated the onset of chondrogenesis and osteogenesis of structures in the caudal fin during larval and juvenile zebrafish development [54, 132]. In addition, we recently showed that increased swimming activity increased maximum normalized curvatures in the caudal fin, suggesting that the caudal fin experiences relatively high mechanical loads during swim-training (Chapter 3). Furthermore, the caudal fin undergoes relatively large morphological changes during zebrafish larval development. Prior to hatching ($\approx$ 3.2 mm Standard Length (SL)), the median finfold consists of a thin double sheet of epidermis and covers the caudal two-thirds of the body [15, 160]. Then, at about 5–6 dpf (days post-fertilization, $\approx$ 4 mm SL), the first cartilaginous structures (hypurals) of the axial skeleton appear in the caudal fin. Eventually, the first finrays develop in the ventral lobe of the caudal fin via direct ossification ($\approx$ 5 mm SL, 10 dpf) [13, 54, 160]. This rapid chain of developmental events and the relatively high mechanical loading makes the caudal fin an interesting model structure to investigate via which molecular pathways mechanical forces influence development *in vivo*.

We subjected zebrafish larvae to swim-training from 5–10 dpf and performed a whole genome microarray analysis on the caudal fins of control and trained zebrafish larvae sampled at 10 dpf (≈ 5 mm SL). we chose this stage because the first ossified structures (hypurals and finrays) appear around 10 dpf in the caudal fin [54, 160]. We identified two genes, *zgc:65811* and *aste1* (*asteroid homolog 1*), which showed a tissue-specific expression pattern and which were up-regulated specifically in the caudal fin. Thus, through combining a training regime with genome-wide micro array analysis, quantitative real time PCR analysis and in situ hybridization experiments, we identified a number of genes that show both a response to training, as well as exhibiting a tissue-specific expression profile. Our study is the first to investigate the effect of swim-training on gene expression during caudal fin development and offers a system that can provide a better understanding of the link between mechanical and molecular signals during development *in vivo*.

6.2 Materials and methods

6.2.1 Husbandry

Wildtype zebrafish were reared at the fish facility of Wageningen University at 27±0.5°C under standard conditions. Eggs were collected by mating two males with three females. Eggs were kept in small containers in a water bath at the breeding facility at 29±0.5°C, and transferred to the fish facility at 3 dpf. The swim-training experiments and the in situ hybridization experiments were approved by the Wageningen University Animal Experiments Committee (protocol nr.2012023g).

6.2.2 Swim-training set-up and regime

The swim-training setup consists of a gravity-fed system, located in a temperature controlled room (for a detailed description see Fiaz *et al.* [54]). Fish were contained in transparent tubes by fine nylon mesh on each end of the tube. Water samples were taken daily from a random tube (control and trained) to measure the water quality (ammonia, nitrite, nitrate, pH and conductivity). Ammonia, nitrite and nitrate were below toxic levels during the swim-training (ammonia$\leq$0.25 mg/ml, nitrite$\leq$0.02 mg/ml, nitrate$\leq$10 mg/ml). Conductivity (891.36±20.77 µS/cm) and pH (7.9±0.17) also remained within the range of standard conditions. Water temperature (28.5±0.2°C) was measured daily.

Fish were subjected to swim-training as described previously in Fiaz *et al.* [54]. Briefly, fish were placed in the swim-training set-up on 4 dpf to acclimate to the conditions. From 5 dpf and onwards, zebrafish larvae were subjected to 3 training sessions of 3 hours per day. Fish were subjected to 50 % of the critical flow velocity (1.44 cm/s±0.04 (5 dpf)–2.81 cm/s±0.08 (10 dpf)) as determined in Fiaz *et al.* [54]. In the tubes with the control fish, there was a continuous water flow of less than 0.1 BL/s but only when the fish in the training tubes were subjected to swim-training. Fish were fed before the first training session and after each training session (during breaks of 30 minutes). Fish were fed *Paramecium* (until 9 dpf), Liquifry no.1 (until 7 dpf, Interpet, Surrey, England) and *Artemia* (from 8–10 dpf, live brine shrimp, Salt Lake Aquafeed, Utah, USA) *ad libitum.* During the swim experiment fish were subjected to a photoperiod regime of 12L:12D.

6.2.3 Whole genome microarray analysis

To analyze the effects of swim-training on caudal fin development on the molecular level, we first subjected the fish to swim-training from 5 until 10 dpf (total length of training: 6 days) as described above. In each of the six tubes (3 control tubes (C1–C3, 3 training tubes (T1–T3)) we placed 30 randomly chosen fish. At 10 dpf, fish (control and trained) were euthanized with 0.1 % tricaine methane sulphonate (TMS, Crescent Research chemicals, USA) buffered with 0.08 % sodium bicarbonate. Each sampled fish was divided in three regions (the head, trunk and tail region; Fig. 6.1) and each region was immediately frozen in liquid nitrogen and stored at −80°C.

To obtain sufficient RNA from the caudal fins for the microarray analysis, we pooled the caudal fins of 15 fish from a tube and subsequently isolated RNA with the Qiagen Rneasy kit according to the manufacturer's protocol (Qiagen, Hilden, Germany). Thus, RNA was isolated from the caudal fins of 15 fish from each control tube (C1–C3) and from each training tube (T1–T3). Micro array experiments were performed according to the manufacturer's protocol (Two-color Microarray-based gene expression analysis, version 6.0, low input quick amp labeling, Agilent Technologies, Palo Alto, USA). Subsequently, 100 ng of pooled RNA of caudal fins of control fish was labeled with Cy5 and Cy3 and 100 ng of pooled RNA of caudal fins of trained fish was labeled with Cy3 and C5. Equal amounts of labeled RNA of the pooled control samples were mixed with equal amounts of labeled RNA of the pooled trained samples (control-Cy3 with trained-Cy5 and control-Cy5 with trained-Cy3 with the following combinations: C1-T1, C2-T2, C3-T3). Samples were subsequently hybridized on two 4×44k Zebrafish Agilent microarray slides (Zebrafish gene expression array V3, Design ID: 026437, Agilent Technologies) and placed in a hybridization chamber at 10 rpm for maximum 17 hours at 65°C. A technical replicate of the C2-T2 combination was also included in the microarray analysis. After washing and mounting, slides were scanned on an Agilent Scanner and data was extracted with Agilent Feature Extraction Software (Version 10.5.1.1). The arrays with the C1-T1 samples did not pass the quality control of Agilent and therefore we did not include these arrays in our further analysis. To select genes for further analysis, we performed the following steps. In the first step we selected the genes which had a red/green (Cy5/Cy3) median signal which was twice as high or more than the red/green background median signal. Subsequently, only genes without a dye bias were used for further analysis. The raw microarray data discussed in this study have been deposited in NCBI's Gene Expression Omnibus [49] and is accessible through GEO Series accession number GSE44395 (http://www.ncbi.nlm.nih.gov/geo/query/acc.cgi?acc=GSE44395).

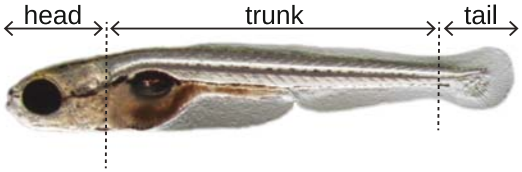

Figure 6.1. Wildtype zebrafish at 10 dpf (total length = 5.4 mm). Dashed line indicates the location of the cuts to divide the fish into head, trunk and tail region.

6.2.4 In situ hybridization

We selected genes which were up-regulated with a fold change of 1.5 or larger from the microarray analysis (Table 6.A.1) for spatial expression analysis with in situ hybridization. We used Primer 3 software to design primers for in situ hybridization ([181], Table 6.A.2) and these primers were extended with a T7, or Sp6 transcription initiation site sequence on the reverse primer. cDNA obtained from fish of 10 dpf was used to perform a PCR with these primers to generate the specific coding sequences of the selected genes (0.4–1.0 kb) to use as template for the DIG labeling reaction. DIG-labeled probes were synthesized according to the manufacturer's instructions (Roche, DIG-labeling) and purified with the Qiagen Rneasy kit (Protocol RNA Cleanup).

Wildtype zebrafish (10 dpf) were euthanized as described above and fixed overnight in 4 % paraformaldehyde (PFA) in phosphate-buffered saline (PBS) at 4°C. After washing with PBS (2×5min), fish were dehydrated in 100 % methanol at RT (room temperature, 2×5 min) and stored at −20°C until further use.

After rehydration (75 %, 50 % and 25 % methanol/PBS, 1×5 min), fish were washed in PBST (PBS+0.1 % Tween®20, 3×5 min). Only the caudal fins of fish were embedded in 1.5 % agar/5 % sucrose and incubated overnight in 30 % sucrose at 4°C. Embedded caudal fins were frozen in liquid nitrogen and stored at −80°C.

Longitudinal sections of 25 µm were made with the cryostat (Leica CM3050S) and transferred onto polysine coated slides (Menzel-Gläser, Thermo scientific). Slides were stored in a box with silica gel at −20°C or if used immediately, dried overnight at RT.

In situ hybridization was performed as described in Smith *et al.*[190] with the following modifications. Probes were diluted in hybridization buffer (50 % formamide, 5×salt [0.75 M NaCl and 0.075 M sodium citrate, pH=7.0], 0.1 % Tween®20, 9.2 µM citric acid, 0.5 mg/ml tRNA yeast (Invitrogen), 90 µl of heparin (5000 U/ml)) to a final concentration of 0.5 ng/µl. Two hundred µl of the probe solution was added to each slide and covered with Nescofilm (Bando Chemical IND., Kobe, Japan). Slides were incubated overnight at 70°C in a humid chamber. Slides were washed in solution A ((50 % formamide, 1×salt, 0.1 % Tween®20), 2×30 min, 70°C) and in 1×TBST (0.14 M NaCl, 2.7 mM KCl, 0.025 M Tris HCl, 0.1 % Tween®20, pH=7.5), 2×30 min, RT). Subsequently, slides were incubated in 400 µl of 2 % blocking buffer (Blocking reagent, Roche, Mannheim, Germany) in 1×TBST for at least 1 h at RT. The blocking buffer was replaced with 200 µl of a 1:2000 dilution of anti-DIG AP FAB fragments (Roche) in 2 % blocking buffer. The slides were covered with Nescofilm and incubated overnight at 4°C. Subsequently, slides were washed with TBST and equilibrated with AP staining buffer ((0.1 M Tris, 0.1 % Tween® 20, 0.1 M NaCl, 0.05 M $MgCl_2$), 2×10min). Slides were incubated in 400 µl of staining solution (1 ml AP staining buffer, 4.5 µl NBT and 3.5 µl BCIP) in the dark. Staining was monitored regularly and stopped by washing in distilled water (2×10 min). After clearing with methanol, washing with PBS and fixation with 4 % PFA/PBS (20 min at RT), slides were mounted in Aquatex® (Merck, Darmstadt, Germany) and incubated overnight at RT to dry. Images were taken with an Olympus DP50 digital camera mounted on a Nikon Microphot-FXA microscope and Analysis^D software (Soft Imaging System GmbH, Germany).

6.2.5 qRT-PCR analysis

Quantitative gene expression analysis of the genes described in Table 6.1 was performed as follows. cDNA was synthesized from the pooled RNA of the caudal fins (control (C2) and trained (T1-T4)) which was also used for the microarray analysis. It was not possible to synthesize cDNA from the pooled caudal fins of the control samples C1 and C3 due to insufficient RNA. To also analyze the expression of selected genes in the head and body region, we isolated RNA and synthesized cDNA from pooled head samples and pooled body samples (control C1–C3 and trained T1–T3) with the Qiagen Rneasy kit according to the manufacturer's protocol (Qiagen). Subsequently, all samples were Dnase treated with DNase I (Invitrogen, California, USA) and reverse transcribed with SuperScript III (Invitrogen) according to the manufacturer's protocol. cDNA was synthesized from 1 µg of RNA of each sample.

Primers for qRT-qPCR (quantitative Real Time PCR) were obtained at Qiagen Gene Globe or designed with Primer 3 ([181]) and obtained at Eurogentec (Liège, Belgium) (Table 6.A.2). cDNA was diluted 1:10 for the qRT-qPCR experiments. The qRT-PCR reactions were performed in a 72-well Rotor-Gene^{TM}Q (Qiagen) according to the protocol described in the Qiagen Quantitect Primer Assay handbook (July 2011). At the end of the run, a melting curve analysis was performed to check for specificity of the product: 35 cycles from 60°C to 95°C (1°C increments every cycle). Samples were run in duplo and fluorescence was measured at the end of every combined annealing and extension step. The C_t values and amplification efficiencies for each sample were obtained upon Comparative Quantitation Analysis from the Rotor-Gene^{TM}Q software (version 1.7). The C_t values of each gene were normalized against the C_t values of the reference genes *40s* and *rps18*. The stability of the reference genes was evaluated with the BestKeeper software tool [165] and this demonstrated that gene expression of the reference genes did not differ between the trained and control samples (average absolute deviation of C_t values of control and trained samples from the mean (of trained and control values) was lower than 1: *rps18*=0.56 *rps11*=0.63). Furthermore, since *rps18* was the most stably expressed (exhibiting the lowest variation), it was chosen for further analysis. The amplification efficiency for each gene was determined by taking the average of the amplification efficiency of all samples. The relative fold change in gene expression between trained and control fish was calculated according to the Pfaffl method [164].

The relative gene expression values (vs *rps18*) were log transformed and used for statistical analysis. Significant differences ($p < 0.05$) between trained and control samples per region (head, trunk or tail) were evaluated with the procedure for linear mixed models followed by contrast analysis in SAS (v9.2).

6.3 Results and Discussion

6.3.1 Swim-training increases expression of muscle specific genes during caudal fin development

To explore the molecular effect of swim-training on caudal fin development, we took an unbiased approach and selected 46 unique genes which were up-regulated with a fold change of 1.5 or larger from the microarray analysis (Table 6.A.1) for further analysis. We investigated the spatial expression pattern of these genes with in situ hybridization on longitudinal sections of caudal fins of wildtype zebrafish at 10 dpf. We were able to define a tissue-specific expression pattern for 14 genes in the caudal fin (Table 6.1). The genes *klf4a* and *LOC563864* were expressed specifically in the neural tube and tissue surrounding the hypurals, whereas the gene *zgc:153154* was expressed specifically in the neural tube (Fig. 6.2A–F). The genes *icn*, *cldne*, *cfdl* and *fat2* were expressed specifically in the finfold (Fig. 6.3A–H). The remaining seven of the 14 selected genes were expressed specifically in muscle fibers (Fig. 6.4A–N; *LOC100331743*, *aste1*, *pvalb1*, *srsf4*, *tnni2a.3*, *zgc:65811*, *zgc:153723*). The expression

Table 6.1. Overview of genes that showed a tissue-specific expression pattern in the caudal fin

Gene ID	Gene Name	Gene Symbol
NM_001113483	*Kruppel-like factor 4a*	*klf4a*
NM_001110521	*novel protein similar to vertebrate EGF-containing fibulin-like extracellular matrix protein 1*	*LOC563864*
NM_001045413	*zgc:153154*	*zgc:153154*
NM_212761	*ictacalcin*	*icn*
NM_131765	*claudin e*	*cldne*
NM_001020532	*complement factor D (adipsin) like*	*cfdl*
XM_001920023	*FAT tumor suppressor homolog 2 (Drosophila)*	*fat2*
XM_002667747	*NAD(P) transhydrogenase mitochondrial-like*	*LOC100331743*
NM_001099430	*asteroid homolog 1 (Drosophila)*	*aste1*
NM_205572	*parvalbumin 1*	*pvalb1*
BC095623	*serine/arginine-rich splicing factor 4*	*srsf4*
NM_205575	*troponin I, skeletal, fast 2a.3*	*tnni2a.3*
NM_200552	*zgc:65811*	*zgc:65811*
NM_001076656	*zgc:153723*	*zgc:153723*

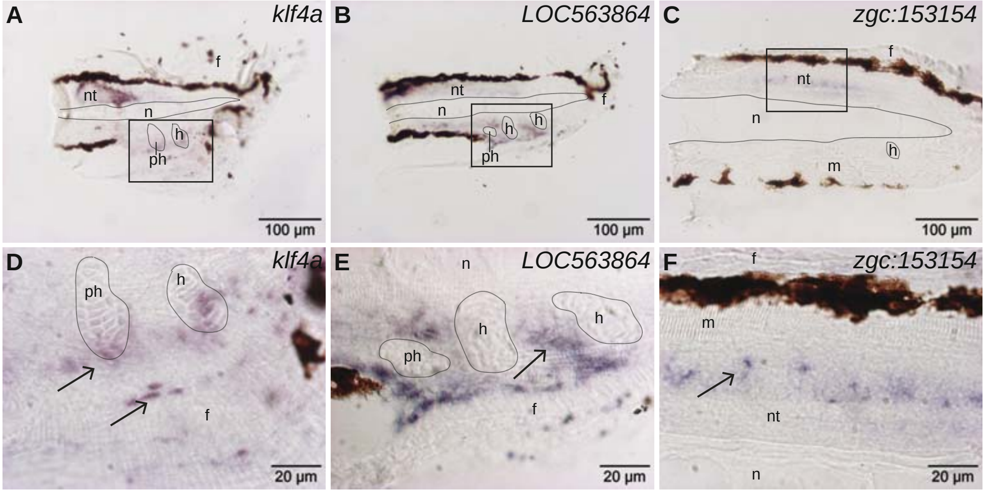

Figure 6.2. Expression analysis of genes that were expressed specifically in the neural tube and tissue surrounding the hypurals. Gene expression is visualized in longitudinal sections of the caudal fin of 10 dpf wildtype zebrafish, anterior is to the left. Representative sections are shown. See Table 6.1 for abbreviations of the gene names. The higher magnification of the area indicated by the black-lined box in A–C is shown in D–F, respectively. **A, D:** The gene *klf4a* is specifically expressed in the neural tube and the arrows in D indicate a high expression in the cells surrounding the hypurals and the finfold. **B, E:** The gene *LOC563864* specifically expressed in the neural tube and the arrow in E indicates a high expression in cells surrounding the hypurals. **C, F:** The gene *zgc:153154* is expressed in a specific subset of cells in the neural tube (arrow in F). f=finfold, h=hypural, m=muscle, n=notochord, nt=neural tube, ph=parhypural.

of these genes was localized throughout the sarcoplasm of muscle fibers.

Subsequently, to analyze if the gene expression of these 14 selected genes was exclusively up-regulated in the caudal fin, we investigated the expression of these genes in the head, trunk and tail region with qRT-PCR (quantitative Real Time PCR) (Figure 6.5). Results following normalization with the reference genes were similar with either *40s* and *rps18* and results normalized for *rps18* are shown (Figure 6.5). The expression of the genes *icn* and *cfdl* was significantly up-regulated in the head and trunk region but not in the tail region (Figure 6.5). However, the expression of the gene *LOC100331743* was significantly up-regulated in the trunk and tail region, whereas the genes *aste1* and *zgc:65811* were significantly and exclusively up-regulated in the tail region. In the following section we will discuss the possible role of the genes *LOC100331743*, *aste1* and *zgc:65811* during caudal fin development in response to swim-training.

The gene *LOC100331743* is predicted to encode the membrane protein NAD(P) transhydrogenase (mitochondrial-like) (Figure 6.4A, D). The enzyme NAD(P) transhydrogenase, present in the inner membrane of animal mitochondria, catalyzes the hydride transfer between NAD(H) and NADP(H), coupled to the translocation of protons across a membrane [90, 185]. During oxidative phosphorylation, this contributes

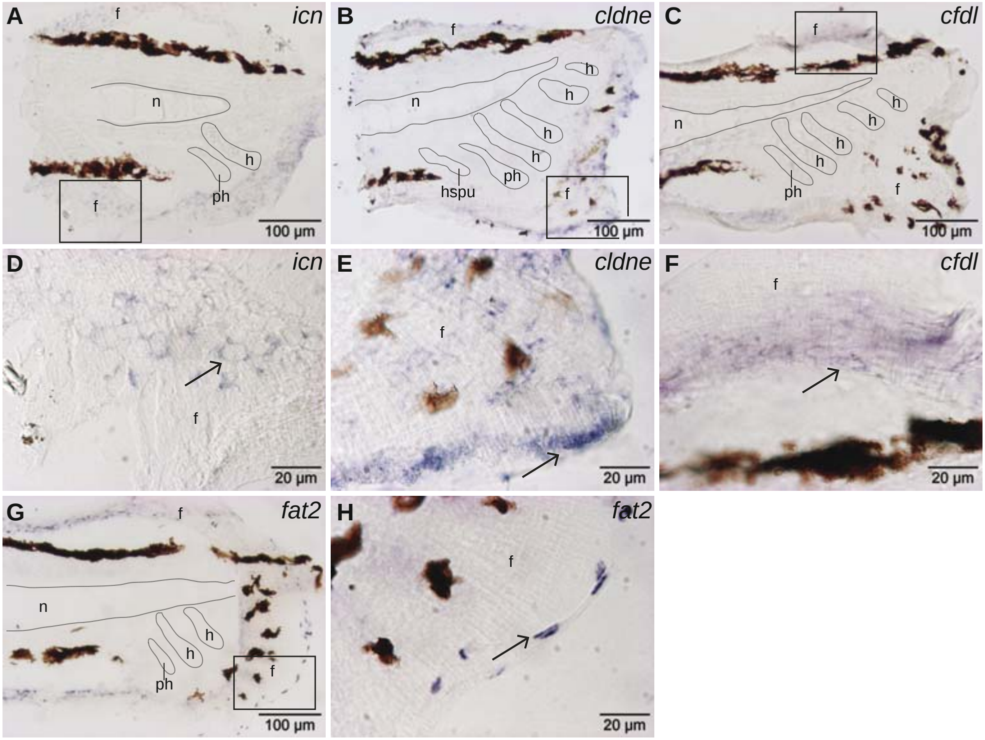

Figure 6.3. Expression analysis of genes that were expressed specifically in the finfold. Gene expression is visualized in longitudinal sections of the caudal fin of 10 dpf wildtype zebrafish, anterior is to the left. Representative sections are shown. See Table 6.1 for abbreviations of the gene names. The higher magnification of the area indicated by the black-lined box in A–C and G is shown in D–F and H, respectively. **A, D**: The gene *icn* shows a clear expression pattern throughout the finfold and the arrow in D indicates that high expression is particularly detected along the peripheral margin of the epithelial cells. **B, E**: The gene *cldne* shows a patchy expression pattern in the finfold and the arrow in E indicates high expression levels along the border of the finfold. **C, F**: The gene *cfdl* shows a diffuse expression pattern in the finfold and the arrow in F indicates high expression levels along the peripheral margin of the epithelial cells. **G, H**: The gene *fat2* shows a distinct expression pattern along the caudal border of the finfold. The arrow in H indicates high expression levels of *fat2* in cells lining the finfold border. f=finfold, h=hypural, hspu=haemal spine of preural vertebra, m=muscle, n=notochord, nt=neural tube, ph=parhypural.

to the synthesis of ATP [201]. In a previous study, we showed that muscle can shift due to the training towards a slow aerobic phenotype during zebrafish larval development (Chapter 5). It could be that this is related with an increase in aerobic metabolism in response to swim-training. However, this remains to be further investigated since the exact biological function of *LOC100331743* is unknown.

The gene *aste1* contains a XPG coding domain (Figure 6.4B, E). The human protein XPG is an endonuclease and plays an important role during DNA repair [31]. This and the increased the expression of *aste1* suggests that swim-training might have

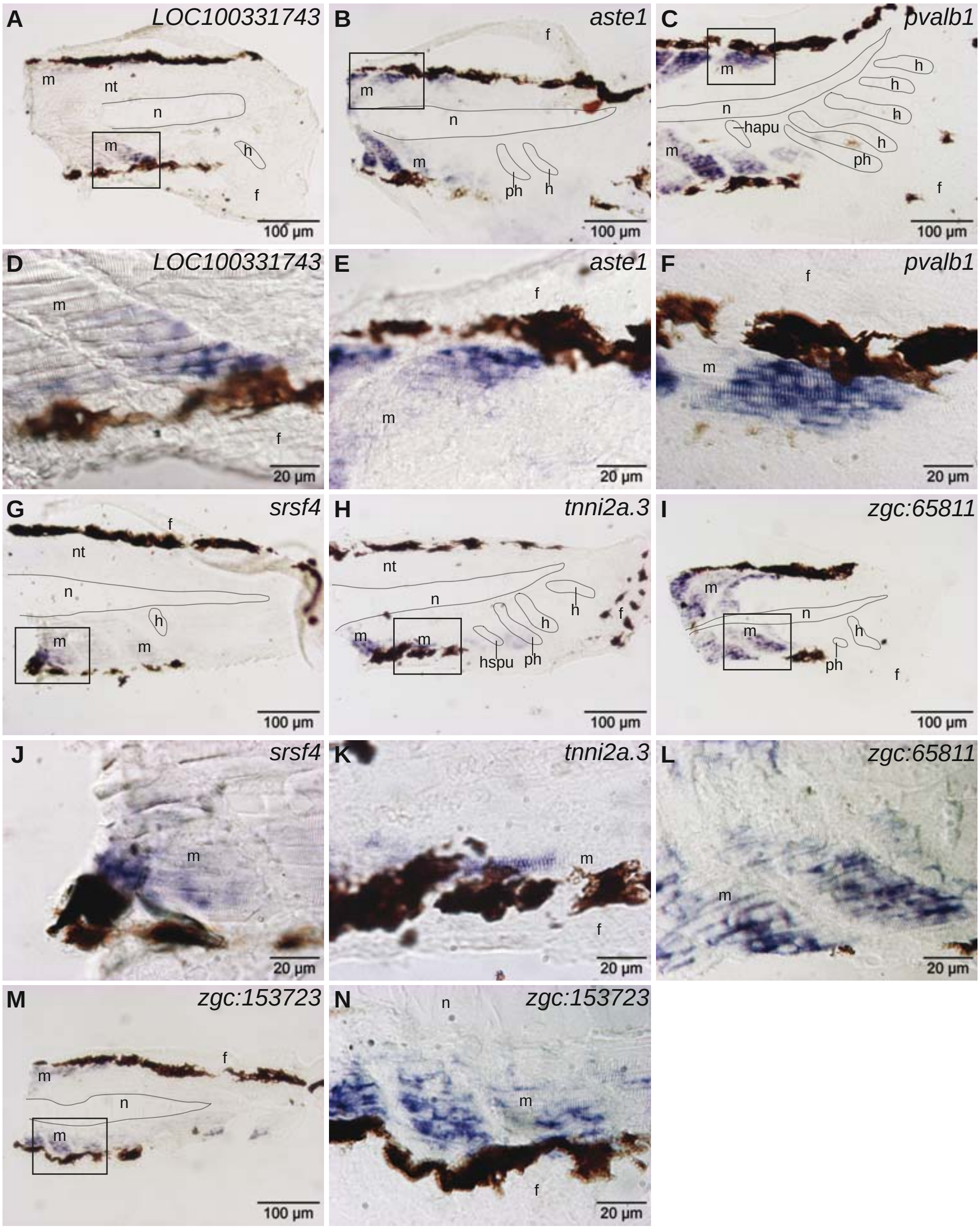
A
LOC100331743
m
nt
n
m
h
f
100 µm
B
aste1
f
m
n
m
ph
h
100 µm
C
pvalb1
m
h
h
n
h
hapu
h
m
ph
f
100 µm
D
LOC100331743
m
f
20 µm
E
aste1
f
m
20 µm
F
pvalb1
f
m
20 µm
G
srsf4
f
nt
n
h
m
m
100 µm
H
tnni2a.3
nt
n
h
f
h
m
m
hspu
ph
100 µm
I
zgc:65811
m
n
m
h
ph
f
100 µm
J
srsf4
m
20 µm
K
tnni2a.3
m
f
20 µm
L
zgc:65811
m
20 µm
M
zgc:153723
f
m
n
m
100 µm
N
n
zgc:153723
m
f
20 µm

Figure 6.4. Expression analysis of genes that were expressed specifically in muscle fibers. Gene expression is visualized in longitudinal sections of the caudal fin of 10 dpf wildtype zebrafish, anterior is to the left. Representative sections are shown. See Table 6.1 for abbreviations of the gene names. **A**–**N**: Gene expression is localized throughout the sarcoplasm of the muscle fibers. **D**–**F, J**–**L, N**: Higher magnification of the area indicated by the black-lined box in A–C, G–I and M, respectively. f=finfold, h=hypural, hapu=haemal arch of preural vertebra, hspu=haemal spine of preural vertebra, m=muscle, n=notochord, nt=neural tube, ph=parhypural.

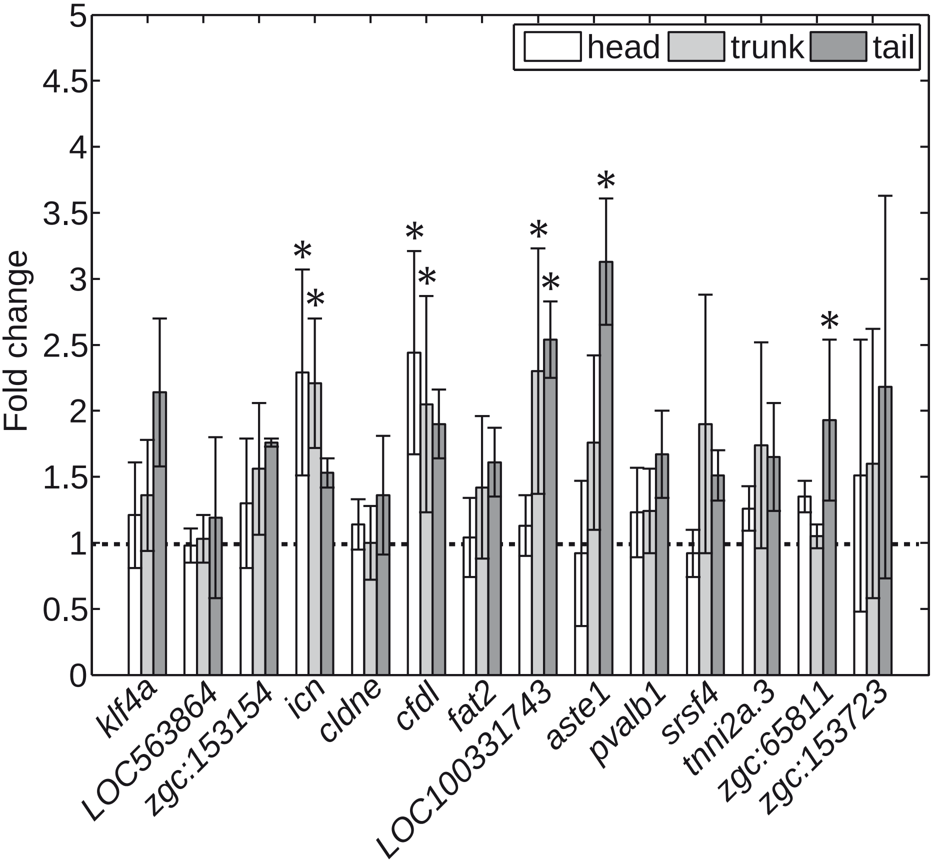

Figure 6.5. Comparison of the quantitative gene expression of the selected genes (Table 6.1) in the head, trunk and tail region. Values represent the fold change in gene expression between trained and control fish and are normalized against the expression of the reference gene *rps18*. The dashed line indicates a fold change of one in gene expression level in trained versus control fish. Values are average ± standard deviation (n=3). Asterisks indicates a significant difference between trained and control fish ($p < 0.05$). See Table 6.1 for abbreviations of the gene names.

stimulated DNA repair in the muscle fibers of the tail region. DNA repair plays an important role during cell division [70]. Previous studies have shown that swim-training increases muscle growth via hyperplasia (increase in muscle fiber number via cell division) in juvenile and adult fish [40, 133, 184]. The gene *proliferating cell nuclear antigen* (*pcna*), which indicates cell division activity, showed an increased expression in axial muscle tissue in response to swim-training in juvenile zebrafish [133]. Future studies are required to investigate if the gene *aste1* is indeed implicated in cell division of muscle fibers and if this is related to muscle growth via hyperplasia.

The gene *zgc:65811* contains a domain which encodes for the CD-9 large extracellular loop region (Figure 6.4I, L). The protein CD-9 belongs to the family of tetraspanin transmembrane proteins. CD-9, via the interaction with other tetraspanins, integrins and signaling enzymes, plays an important role in the regulation of variety of processes such as cell adhesion, proliferation and motility [199, 216]. Furthermore, Tachibana and Hemler [202] showed that the expression of CD9 and of the complex β1 integrin-CD9 was upregulated during murine myoblast differentiation and suggested that CD9 plays a key role during myoblast fusion. This and the increased expression of *zgc:65811* in muscle fibers suggests that swim-training promoted muscle fiber differentiation in the tail region. However, future studies have to performed to reveal the exact biological function of this gene.

6.4 Conclusion and Perspectives

In this report, we used the zebrafish caudal fin to investigate the effect of an increased swimming activity on gene expression during development. We identified two genes, *aste1* and *zgc:65811* which showed a muscle-specific expression pattern and which were up-regulated exclusively in the tail region. This makes these genes interesting candidate genes for further research on the translation of mechanical into molecular signals during caudal fin development. A future analysis of the temporal expression of these genes (e.g. several hours or days after training at different developmental stages) could contribute to the hypothesis on how and when these genes are involved in the translation of mechanical into molecular signals. This might indicate if these genes are a direct response (within several hours) to an increased swimming activity and to what extent these genes are involved in the adaptation of muscle tissue to an increased swimming activity. Moreover, a functional analysis of these genes through knockout-studies will help to clarify the role of these genes during muscle and caudal fin development.

So far, we did not identify any genes related to cartilage or bone development which were up-regulated exclusively in the caudal fin in response to swim-training at 10 dpf, despite our previous findings that swim-training prioritized the development of skeletal structures in the caudal fin [54]. One plausible explanation for this finding could be that changes in expression of genes related to cartilage or bone development were below the detection level of our methods. Possibly, the statistical power of our methods was not large enough to detect these relatively small differences in gene expression. Increasing the power in future studies (e.g. by increasing the number of fish sampled) might indicate if there is a significant difference in expression of genes related to cartilage or bone development in the caudal fin.

In conclusion, our study is the first to explore the molecular pathways via which an increased mechanical load affects caudal fin development in zebrafish and provides a system to unravel the molecular link between mechanical forces and development *in vivo*. Additionally, this could lead to new approaches for tissue engineering and a better understanding of developmental malformations due to abnormal changes in mechanical forces.

Acknowledgments

We thank Henk Schipper for his advice and support with image acquisition and analysis with the Analysis^{D} software. We are especially grateful to the members of the Zebrafish Facility at Wageningen University for providing help and taking care of the zebrafish. We would also like to thank Gerrit Gort for help with the statistical analysis of the gene expression data.

6.A Supplemental data

Table 6.A.1. List of genes from whole genome microarray analysis which were upregulated with a fold change of 1.5 or larger. Values represent fold change of trained versus control fish.

Agilent_ProbeID	GeneID	GeneName	GeneSymbol	array-2a	array-2b	array-3
A_15_P100671	NM_200552	zgc:65811	zgc:65811	2,58	2,50	1,85
A_15_P104819	NM_199272	epithelial splicing regulatory protein 2	esrp2	1,50	1,53	2,55
A_15_P106696	NM_205572	parvalbumin 1	pvalb1	1,81	1,84	2,34
A_15_P108569	NM_199876	zgc:77650	zgc:77650	1,59	1,63	13,67
A_15_P114414	DN900235	death effector domain-containing 1	dedd1	1,67	1,68	5,75
A_15_P117102	NM_212761	ictacalcin	icn	1,58	1,56	1,53
A_15_P119327	NM_001020532	complement factor D (adipsin) like	cfdl	1,60	1,63	2,37
A_15_P130426	AB055669			1,51	1,55	75,06
A_15_P134846	BC095623	serine/arginine-rich splicing factor 4	srsf4	2,00	2,22	3,84
A_15_P138141	ENSDART00000129595			1,85	1,55	5,30
A_15_P142686	NM_001044968	phospholipase C, gamma 2	plcg2	1,53	1,56	1,89
A_15_P152786	NM_205575	troponin I, skeletal, fast 2a.3	tnni2a.3	1,80	1,89	3,27
A_15_P162186	NM_001076656	zgc:153723	zgc:153723	1,58	1,51	1,50
A_15_P168781	NM_131765	claudin e	cldne	1,66	1,53	13,31
A_15_P171111	NM_001009918	transferrin receptor 1b	tfr1b	2,15	1,69	1,55
A_15_P172671	NM_001017913	zgc:113229	zgc:113229	1,56	1,56	1,91
A_15_P174226	NM_001082957	ictacalcin 2	icn2	1,60	1,53	1,72
A_15_P175721	NM_001007132	zgc:123068	zgc:123068	1,69	1,71	2,25
A_15_P177301	BC115310	uncharacterized LOC567193	LOC567193	4,73	4,42	3,47
A_15_P182241	NM_001080040	polycystic kidney and hepatic disease 1 (autosomal recessive)-like 1	pkhd1l1	1,67	1,65	2,19
A_15_P194876	NM_001099430	asteroid homolog 1 (Drosophila)	aste1	1,96	2,45	3,10
A_15_P197801	NM_001007133	zgc:152791	zgc:152791	5,64	5,43	2,57
A_15_P208256	NM_001040365	advillin	avil	1,70	1,84	1,64
A_15_P208541	NM_001098252	sc:d0202	sc:d0202	1,67	1,68	4,72
A_15_P263511	BC095830	resistance to inhibitors of cholinesterase 8 homolog B	ric8b	1,51	1,56	3,36
A_15_P273916	CF265668			1,83	1,66	1,81
A_15_P281316	NM_001045413	zgc:153154	zgc:153154	1,58	1,61	1,83
A_15_P296591	XM_001920023	FAT tumor suppressor homolog 2 (Drosophila)	fat2	1,52	1,55	1,99
A_15_P340727	NM_199215	carbonic anhydrase II	ca2	1,72	1,76	3,16
A_15_P365355	NM_001030096	transglutaminase 1 like 4	tgm1l4	1,74	1,76	1,69
A_15_P375020	NM_001128773	alpha(1,3)fucosyltransferase gene 2	ft2	2,67	1,69	2,53
A_15_P384005	NM_001113483	Kruppel-like transcription factor 4a	klf4a	1,61	1,62	4,17
A_15_P392680	NM_001110521	novel protein similar to vertebrate EGF-containing fibulin-like extracellular matrix protein 1	LOC563864	1,55	1,61	1,54
A_15_P410800	CT733915			1,68	1,66	4,39
A_15_P421675	XM_001922077			1,76	1,75	3,20
A_15_P551247	XM_002667747	NAD(P) transhydrogenase mitochondrial-like	LOC100331743	2,08	1,92	2,39
A_15_P565042	NM_213408	solute carrier family 25 (mitochondrial carrier: glutamate), member 22	slc25a22	1,50	1,57	2,07
A_15_P565267	XM_001923440			2,16	2,06	2,52
A_15_P621876	NM_001100081	novel protein containing lectin C-type domains	LOC100002910	1,81	1,76	1,56
A_15_P626096	NM_001114315	zgc:174178	zgc:174178	1,58	1,73	2,12
A_15_P629651	NM_001083108	si:dkey-91f15.1	si:dkey-91f15.1	1,55	1,55	1,65
A_15_P631151	NM_001030096	transglutaminase 1 like 4	tgm1l4	1,59	1,62	1,62
A_15_P656741	NM_199272	epithelial splicing regulatory protein 2	esrp2	1,53	1,60	2,85
A_15_P657426	NM_001007133	zgc:152791	zgc:152791	7,10	5,63	7,38
A_15_P657831	BC152288			1,62	1,58	84,59
A_15_P664046	AF539738	troponin I, skeletal, fast 2a.3	tnni2a.3	1,97	2,02	2,76
A_15_P690708	NM_001114702	zgc:174710	zgc:174710	1,61	1,71	1,67
A_15_P696126	XM_001921619	wu:fa03e10	wu:fa03e10	1,56	1,67	2,59
A_15_P696151	NM_001103131	zgc:174689	zgc:174689	1,67	1,56	1,61
A_15_P746676	NM_212761	ictacalcin	icn	1,53	1,54	1,81
A_15_P749196	NM_205572	parvalbumin 1	pvalb1	1,77	1,82	2,13
A_15_P756031	CT733915			1,70	1,52	5,23
A_15_P759666	NP13320298		NP13320298	3,12	2,13	7,43
A_15_P761566	BC095623	serine/arginine-rich splicing factor 4	srsf4	1,65	1,66	2,76

Table 6.A.2. qRT-PCR primers and in situ hybridisation primer sequences of selected genes (Table 6.1). See also Table 6.A.1 or Table 6.1 for abbreviations of gene names. In situ hybridisation primer sequence are indicated with a Sp6 or T7 transcription initiation site.

			qPCR primers	
Agilent_ProbeID	GeneID	GeneSymbol	Qiagen or fw primer	rv primer
A_15_P100671	NM_200552	zgc:65811	Dr_zgc:65811_1_SG	
A_15_P106696	NM_205572	pvalb1	Dr_pvalb1_1_SG	
A_15_P117102	NM_212761	icn	GGCTATGCTCATTGCAACCT	AAAGATGTCGCCCAACTCTG
A_15_P119327	NM_001020532	cfdl	Dr_cfdl_1_SG	
A_15_P134846	BC095623	srsf4	Dr_srsf4_1_SG	
A_15_P152786	NM_205575	tnni2a.3	Dr_tnni2a.3_1_SG	
A_15_P162186	NM_001076656	zgc:153723	Dr_zgc:153723_1_SG	
A_15_P168781	NM_131765	cldne	Dr_cldne_1_SG	
A_15_P194876	NM_001099430	aste1	Dr_aste1_1_SG	
A_15_P281316	NM_001045413	zgc:153154	Dr_zgc:153154_1_SG	
A_15_P296591	XM_001920023	fat2	Dr_fat2_2_SG	
A_15_P384005	NM_001113483	klf4a	Dr_klf4a_1_SG	
A_15_P392680	NM_001110521	LOC563864	Dr_LOC563864_2_SG	
A_15_P551247	XM_002667747	LOC100331743	AACTCTGGGTCTGACCATCG	ATCATGTACTCGGCCACACA

			ISH primers			
Agilent_ProbeID	GeneID	GeneSymbol	fw		rv	
A_15_P100671	NM_200552	zgc:65811	ISH-84-T7-fw1	TAATTACGACTCACTATAGGATTCTTCGACATCGACCT	ISH-84-Sp6-rv1	ATTTAGGTGACACTATAGACTGTGGGGTCTTCATCAG
A_15_P106696	NM_205572	pvalb1	ISH-85-T7-fw1	TAATTACGACTCACTATAGGCAGCTGATGTTGATGCTG	ISH-85-Sp6-rv1	ATTTAGGTGACACTATAGAAATACAACATCCCCCGAAC
A_15_P117102	NM_212761	icn	ISH-91-T7-fw1	TAATTACGACTCACTATAGGAACCACCATGGCTACGTCA	ISH-91-Sp6-rv1	ATTTAGGTGACACTATAGAACCATCAGCATTTGCATC
A_15_P119327	NM_001020532	cfdl	ISH-104-Sp6-fw1	ATTTAGGTGACACTATAGAGGGCAAGAGGCTAAAGCA	ISH-104-T7-rv1	TAATTACGACTCACTATAGGCTTTCTGGAGGAGCCACAT
A_15_P134846	BC095623	srsf4	ISH-86-T7-fw1	TAATTACGACTCACTATAGGATATGGCTTTGTGGAGTTTG	ISH-86-Sp6-rv1	ATTTAGGTGACACTATAGATCTGCATTTGGTGGTGTTT
A_15_P152786	NM_205575	tnni2a.3	ISH-87-T7-fw1	TAATTACGACTCACTATAGGTGTTGAGCATCACAAAAGG	ISH-87-Sp6-rv1	ATTTAGGTGACACTATAGAGGCACTGAAAGCAGAGAAG
A_15_P162186	NM_001076656	zgc:153723	ISH-107-T7-fw2	TAATTACGACTCACTATAGGAGTAAAGGGGACCCGACTA	ISH-107-Sp6-rv2	ATTTAGGTGACACTATAGATCTCCTTGGGGATGAGGGT
A_15_P168781	NM_131765	cldne	ISH-93-T7-fw1	TAATTACGACTCACTATAGGGTTTGTGGATGAACTGTG	ISH-93-Sp6-rv1	ATTTAGGTGACACTATAGAACAAACGGCAAGCATTATT
A_15_P194876	NM_001099430	aste1	ISH-88-T7-fw1	TAATTACGACTCACTATAGGATGCCTATGACCTGTCTG	ISH-88-Sp6-rv1	ATTTAGGTGACACTATAGACGTTCTCACTGCTTCGTTT
A_15_P281316	NM_001045413	zgc:153154	ISH-116-T7_fw1	TAATTACGACTCACTATAGGACTCTGCCTTGTGAACTGC	ISH-116-Sp6_rv1	ATTTAGGTGACACTATAGAGCTAGCATTGGCACTTATGGT
A_15_P296591	XM_001920023	fat2	ISH-117-Sp6_fw1	ATTTAGGTGACACTATAGAGCTATTCACCCTCGCTGT	ISH-117-T7_rv1	TAATTACGACTCACTATAGGTGAAATGTCCTCTGGTATC
A_15_P384005	NM_001113483	klf4a	ISH-96-T7-fw1	TAATTACGACTCACTATAGGAACGATTTTGCCCTCCAT	ISH-96-Sp6-rv1	ATTTAGGTGACACTATAGACGGCTTTTCTCCTGTGTGT
A_15_P392680	NM_001110521	LOC563864	ISH-97-T7-fw1	TAATTACGACTCACTATAGGCATGAAATGCATCAACC	ISH-97-Sp6-rv1	ATTTAGGTGACACTATAGAGGGTATGGACCCACAACAA
A_15_P551247	XM_002667747	LOC100331743	ISH-81-T7-fw1	TAATTACGACTCACTATAGGTGTGCGGTACAAGGATG	ISH-81-Sp6-rv1	ATTTAGGTGACACTATAGAGCTCGCTTACCAGGAATAAG

”We are now at a time when massive amounts of data exist categorizing all levels of organic structure, but the search for unifying principles of organization continues. ”

Donald E. Ingber and James D. Jamieson

Chapter 7

General discussion

7.1 Introduction

In fish larvae, a fast increase in swimming performance is important to escape from predators, capture prey and to maintain position in varying flow conditions. During larval development energy is invested in growth and development. When subjecting fish larvae to swim-training, which presumably increases mechanical loads, the total amount of energy increases due to increased food intake and/or the allocation of energy is distributed differently, presumably to increase the chance of survival. In the research described in this thesis, we investigated the effect of swim-training on zebrafish larval development on a molecular, morphological and kinematic level. In the following sections, I will relate the findings of this thesis to the results of other studies and will finally offer perspectives for future research.

7.2 Zebrafish as exercise model for vertebrate development

Several studies have shown that exercise increases muscle growth, decreases stress levels and improves the immune system in fish (reviewed by [41, 153, 154, 184]). The understanding of the mechanisms underlying these effects of exercise is still limited. It was shown in this thesis that exercise can increase growth and leads to morphological and molecular changes in zebrafish larvae, which suggests that exercise induces important regulatory effects already during larval stages. In the following subsections, I will discuss the findings of this thesis and how these can, together with results from other studies, contribute to a better understanding of the mechanisms underlying the effects of exercise during larval development.

7.2.1 Swim-training increases swimming activity and intensity during larval development

We investigated - for the first time - the swimming kinematics of zebrafish larvae in varying flow conditions (Chapter 3). We demonstrated that swim-training increased swimming intensity and activity and time spent on swimming. It may seem obvious that swim-training would affect swimming behaviour but previous studies did not examine the changes in swimming-kinematics when fish were subjected to flow. Yet, to understand how swim-training can lead to morphological and molecular changes it is necessary to know how swim-training affects the functional performance of fish. The detailed analysis of the swimming kinematics could help to elucidate, in future studies, how swim-training leads to changes in the distribution of mechanical forces along the body axis of fish during larval development.

We furthermore showed that flow in the tube (in the swim-training set-up and in the high speed recordings set-up) had a Hagan-Poisseuile flow profile which indicates that fish experience different flow velocities depending on their location in the tube.

Thus, fish are subjected to varying levels of swim-training. This is an important factor to take into account when determining the level of swim-training in future studies.

7.2.2 Swim-training affects larval growth and development

Palstra et al. [155] showed that adult zebrafish could swim at very high optimal swimming speeds of 13 BL/s for 20 days which led to an increased body weight of 41.1 % and body length of 5.6 %. The increased growth was comparable to that normally seen in commercially interesting species such as salmon and trout. The fact that such an increase in growth rate can be achieved in a species that normally shows determined growth, makes the zebrafish an interesting species even for aquaculturists. In a previous study from our lab, it was shown that in juvenile zebrafish, swim-training led to a transiently increased growth [133] and we showed that swim-training can increase growth depending on the feeding and training regime and stocking density of fish in a tube ([54] and Chapter 5). This indicates that already during the larval stage, swim-training can affect growth.

It has been shown that in teleosts, swim-training stimulates muscle growth via hypertrophy (cell growth) or hyperplasia (cell division) of red muscle fibers (although cases are known where white muscle fibers are also involved) (reviewed by [41, 154, 184]). Palstra *et al.* [155] showed in adult zebrafish that swim-training increased the gene expression of muscle fiber markers involved in the regulation of muscle growth. Furthermore, Van der Meulen et al. [133] demonstrated that, in juvenile zebrafish, swim-training increased total cross-sectional red muscle fibre area. There were no differences in the cross-sectional area of individual red muscle fibers between trained and control fish suggesting that muscle growth took place via hyperplasia [133]. In the present study with larval zebrafish, we demonstrated that swim-training increased the expression of the muscle growth promotor *myogenin* at 5 and 14 dpf. Future studies are required to investigate if muscle growth took place via hyperplasia, hypertrophy or both in zebrafish larvae.

Several *in vitro* studies have shown that an increased mechanical loading stimulated the chondrogenesis and osteogenesis of mesenchymal stem cells (reviewed by [96]). *In vivo* studies have further shown that mechanical loading by muscle forces have a critical role during osteogenesis and chondrogenesis during embryonic development (reviewed by [53]). These studies were, however, limited to the appendicular skeleton. In Chapter 4, we demonstrated that swim-training prioritized the onset of cartilage and bone structures in the head and median fins. These are the structures which play an important role in (among others) swimming thus increasing the chance of survival in varying flow conditions. These results are in line with previous findings, where swim-training also stimulated the onset of cartilage and bone structures in the median fins [32, 132]. These observations suggest how swim-training can lead to shifts during skeletal development.

In mammals, endurance training stimulates lipid metabolism, however this is not that clear in adult fish. Depending on the fish species and regime, endurance training can lead to an increase in protein metabolism or fatty acid metabolism or glycogen metabolism or a combination of these pathways [41, 52, 91, 184]. There are indications from our study and from Kopp et al. [106] that swim-training stimulated lipid metabolism in larval zebrafish (Chapter 5). In the present study (Chapter 5) swim-training led to molecular changes already after 5 days of swim-training and in a variety of organ systems e.g. the gastrointestinal system. In adult zebrafish, McClelland *et al.* [131] demonstrated that lipid metabolism is also affected by swim-training. They showed that swim-training led to a down-regulation of the gene expression of *ppar-α* and *ppar-$\beta 1$* in muscle, which are transcription factors involved in the regulation of the fatty acid pathway in mammals [72]. However, in a follow-up study, swim-training did not have an effect on the expression of these genes in either white or red muscle fibers [118]. It remains to be investigated, when zebrafish are subjected to swim-training, how this affects their energy metabolism and which resources are allocated in order to fuel swimming activity and growth.

Currently, Palstra et al. [153] are investigating under what conditions swim-training can stimulate growth and development (of skeletal and cardiac muscle), improve the immune system and reduce stress by using the zebrafish as exercise model (by e.g. subjecting to a certain training regime, feeding regime, at a certain stocking density). Our study demonstrates that exercise can cause changes in swimming kinematics and molecular and morphological changes which probably improve swimming and endurance performance. This indicates that fish can be subjected to exercise at an early stage. This is - under the right conditions (such as stocking density) - likely to enhance growth without harmful effects. It would be interesting to examine the possible effects on later life, e.g. health. Taken together, this makes the zebrafish an interesting exercise model already during early development.

7.3 Caudal fin as model structure to examine mechanotransduction during development *in vivo*

Our findings show that the caudal fin could be an interesting model structure to unravel the molecular link between mechanical forces and development *in vivo*. In Chapter 3, we showed that flow not only increased tail beat frequencies and duration of the swimming burst but also increased normalized maximum curvatures during a swimming burst and averaged over the first three half beats. These maximum curvatures were located in the caudal fin (0.93–0.94 BL) around the location where the first hypurals and the finrays (in the ventral lobe) develop (Figure 3.8). We demonstrated furthermore that normalized maximum curvatures were located at the same position along the body when fish larvae swam in stagnant water. The higher curvatures are presumably caused by a higher mechanical load that will also evoke higher stresses and strains within the caudal region. In Chapter 4, we showed that an increased swimming activity prioritized the onset of skeletal elements in the caudal fin and in Chapter 6 we showed that swim-training increased the expression of muscle specific genes exclusively in the caudal fin. Taken together, these findings suggests that the caudal fin experienced a higher loading which could have induced these molecular and morphological changes.

It is known that mechanical loading plays an important role during chondrogenesis, osteogenesis and myogenesis (see also Chapter 1). These loads lead to changes in the extracellular matrix which are sensed by e.g. transmembrane receptors such as integrins. The transduced mechanical signal induces the activation of intracellular signalling pathways or changes in the cytoskeleton tension which regulate transcription in the nucleus leading to the expression of genes involved in e.g. chondrogenesis, osteogenesis or myogenesis (reviewed by [86, 96, 125, 126]). In this project, we identified two muscle specific genes, *zgc:65811* and *aste1* which showed an increased expression exclusively in the caudal fin. The gene *zgc:65811* contains a domain which encodes for the CD-9 large extracellular loop region which is a tetraspanin transmembrane protein. CD-9 interacts with (among others) integrins and plays an important role in the regulation of variety of processes such as cell adhesion, proliferation and motility [199, 216]. This suggests that the gene *zgc:65811* could be involved in the transduction of mechanical forces. Future studies are required to identify the exact biological function of the gene *zgc:65811* and if it is involved in mechanotransduction.

The analysis of skeletal development in Chapter 4 showed that swim-training prioritized the onset of certain cartilage (e.g. hypurals) and bone structures (e.g. hypurals and finrays) in the caudal fin. This shows that the larval zebrafish skeleton is able to respond to swim-training including changes in mechanical loads and adapt accordingly. However, it is unclear how these changes in mechanical loading are sensed. In larval zebrafish osteocytes appear when the bone matrix has reached a certain thickness [84]. In birds and mammals, osteocytes are the main mechanosensors and are interconnected via cell processes and are contained within a canalicular network (reviewed by [53]). Due this connecting syncytial network, the location where the stimulus is sensed does not have to be at the location where the adaptive response takes place. In larval teleosts, a different mechanosensing mechanism may exist where mechanical forces are probably sensed by chondroblasts, bone lining cells or osteoblasts [53]. In this system, detection of the stimulus and response may be co-localized. The availability of transgenic zebrafish which allows to follow cells such as osteoblasts *in vivo* could elucidate which cells are involved in the sensing of mechanical forces and if the signal detection is co-localized with the adaptive response [74, 88, 196, 197].

7.4 Concluding remarks and perspectives

This thesis explored the effect of swim-training on zebrafish larval development on a kinematic, morphological and molecular level. The results from this thesis indicate that the zebrafish provides a framework to investigate the effect of exercise during vertebrate development and to elucidate the molecular mechanisms via which mechanical forces affect development *in vivo*. In the following paragraphs, I will discuss how the results from our study can provide input for future studies.

In this thesis, we demonstrated that externally applied flow led to significant changes in swimming kinematics of larval zebrafish at one developmental stage. However, between 5–14 dpf, relatively large morphological changes take place such as the development of skeletal structures in the axial skeleton (see also Chapter 4) which influence swimming kinematics. Therefore, a question that we are currently addressing is how externally applied flow affects swimming kinematics during zebrafish larval development. Müller and Van Leeuwen [137] demonstrated that with increasing age, the following three parameters increased with body length and swimming speed: the slip (ratio of mean swimming speed to body wave speed), advance ratio (ratio of mean swimming speed to lateral speed of the tail tip) and stride length (distance covered during one tail beat) (2 dpf (days post-fertilization) (3.4±0.1 mm)–21 dpf(9.6±1.0 mm, total body length)). Thus, the swimming performance of the larvae improves with increasing age, and in a future analysis we intend to examine how flow affects the development of this performance. This could provide a better understanding of the link between functional performance and morphological development.

With the new 3D automated fish tracker (used in Chapter 3 and developed by Voesenek and Van Leeuwen, still unpublished) we were able to accurately track the caudal fin. With the tracking used in Chapter 3, the assumption was made that the caudal fin is a flat plate that can only bend in one direction and move laterally through the water (but the fish is still tracked in 3D space). However, several studies have shown that the caudal fin is flexible structure which undergoes more complex deformations during swimming. In adult fish, it has been shown that the dorsal and ventral lobe differ in lateral excursion amplitude, angle of attack and lateral velocity [8, 63, 114]. In our study, we did observe complex deformations of the caudal fin (e.g. differences in lateral excursion between the ventral and dorsal lobe), especially in the fish subjected to flow at 10 dpf. This raises interesting questions for future research. For example, the first finrays develop in the ventral lobe and it is tempting to relate this to a different loading regime on the ventral lobe versus the dorsal lobe. With an update of our newly developed 3D automated fish tracker, we aim to be able to track the caudal fin in 3D by taking multiple angles of view into account. Knowledge of these complex deformations of the caudal fin could provide us with a better understanding of the role of the caudal fin during larval swimming and how varying flow conditions can affect these caudal fin movements.

The kinematic data obtained in this thesis (and of future studies at different developmental stages and of the caudal fin) can be used as input to examine how varying flow conditions can influence the distribution of forces along the body of the fish larvae with computational fluid dynamics analyses [119]. In addition, this kinematic data can also be used to examine how varying flow conditions affect the strain distribution within the body with a biomechanical model that will developed by our group. The biomechanical model predicts the body movements and strain distribution of zebrafish larvae based on the muscle activation and architecture. The predicted swimming performance (swimming kinematics) can be adjusted to accurately match the recorded data (by comparing the kinematic data and the predicted data). From this model which accurately describes the swimming performance in the recorded sequences, one can then predict the internal strain distribution along the body. The analyses with CFD and the biomechanical model could provide us with better insight in how an increased swimming activity and intensity lead to changes in force and strain distributions along the body and the caudal fin.

Our findings (Chapter 3, 4 and 6) indicate that the caudal fin is an interesting structure to further investigate the role of mechanical forces during development and to unravel the molecular link between mechanical forces and morphological changes *in vivo*. In this thesis, we selected genes from the whole genome microarray analysis above a certain level of fold change between trained and control fish (Chapter 5 and 5). This selection of genes based on the level of fold change led to the exclusion of genes which showed a lower level of fold change but could nevertheless have large effects. For example, the transcription factor *runx2* plays an important role in many different signalling pathways [56], thus relatively small changes in the expression level of this gene can have profound effects. In future studies, including the selection of genes not only based on the level of fold change but also on significant differences in fold change between trained and control fish could lead to the identification of such key regulatory genes. In addition, the zebrafish nowadays offers the possibility to generate gene knock-outs (by using the TALEN approach) to investigate the functional role of these genes during development [11]. Furthermore, the ability to generate transgenic fish allows one to track the expression of these genes during development *in vivo* and when subjecting these transgenic fish to swim-training [78, 79]. This could lead to the identification of specific cells which sense changes in the mechanical environment. *In vitro* studies can further provide insight in the mechanosensing and mechanotransduction mechanisms employed by these specific cells.

In conclusion, the combination of *in vivo* and *in vitro* studies provides, together with the ongoing technological developments and the diverse range of tools and analyses that are available for the zebrafish, many exciting opportunities to unravel the molecular mechanisms which translate mechanical forces into morphological changes during development.

"Mind does its fine-tuning hair-splitting, but no craft or art begins or can continue without a master giving wisdom into it."

Rumi

References

1. **Adamo, L., Naveiras, O., Wenzel, P. L., McKinney-Freeman, S., Mack, P. J., Gracia-Sancho, J., Suchy-Dicey, A., Yoshimoto, M., Lensch, M. W., Yoder, M. C. et al.** (2009). Biomechanical forces promote embryonic haematopoiesis. *Nature* **459**, 1131–1135.

2. **Andersen, P. and Henriksson, J.** (1977). Capillary supply of the quadriceps femoris muscle of man: adaptive response to exercise. *J Physiol* **270**, 677–690.

3. **Arnsdorf, E. J., Tummala, P., Kwon, R. Y. and Jacobs, C. R.** (2009). Mechanically induced osteogenic differentiation–the role of RhoA, ROCKII and cytoskeletal dynamics. *J Cell Sci* **122**, 546–553.

4. **Arunachalam, M., Raja, M., Vijayakumar, C., Malaiammal, P. and Mayden, R. L.** (2013). Natural history of zebrafish (*Danio rerio*) in india. *Zebrafish* **10**, 1–14.

5. **Bagatto, B., Pelster, B. and Burggren, W. W.** (2001). Growth and metabolism of larval zebrafish: effects of swim training. *J Exp Biol* **204**, 4335–4343.

6. **Bainbridge, R.** (1958). The speed of swimming of fish as related to size and to the frequency and amplitude of the tail beat. *J Exp Biol* **35**, 109–133.

7. **Bainbridge, R.** (1960). Speed and stamina in three fish. *J Exp Biol* **37**, 129–153.

8. **Bainbridge, R.** (1963). Caudal fin and body movement in the propulsion of some fish. *J Exp Biol* **40**, 23–56.

9. **Ballintijn, C. M.** (1969). Muscle co-ordination of the respiratory pump of the Carp (*Cyprinus carpio* L.). *J Exp Biol* **50**, 569–591.

10. **Batchelor, G.** (1967). *An Introduction to Fluid Dynamics.* Cambridge University Press, London.

11. **Bedell, V. M., Wang, Y., Campbell, J. M., Poshusta, T. L., Starker, C. G., Krug, R. G., 2nd, Tan, W., Penheiter, S. G., Ma, A. C., Leung, A. Y. H. et al.** (2012). In vivo genome editing using a high-efficiency TALEN system. *Nature* **491**, 114–118.

12. **Bensimon-Brito, A., Cancela, L. M., Huysseune, A. and Witten, P. E.** (2010). The zebrafish (*Danio rerio*) caudal complex - a model to study vertebral body fusion. *J Appl Ichtyol* **26**, 235–238.

13. **Bird, N. C. and Mabee, P. M.** (2003). Developmental morphology of the axial skeleton of the zebrafish, *Danio rerio* (Ostariophysi: Cyprinidae). *Dev Dyn* **228**, 337–357.

14. **Bonewald, L. F. and Johnson, M. L.** (2008). Osteocytes, mechanosensing and Wnt signaling. *Bone* **42**, 606–615.

15. **Van den Boogaart, J. G. M., Muller, M. and Osse, J. W. M.** (2012). Structure and function of the median finfold in larval teleosts. *J Exp Biol* **215**, 2359–2368.

16. **Boutahar, N., Guignandon, A., Vico, L. and Lafage-Proust, M.-H.** (2004). Mechanical strain on osteoblasts activates autophosphorylation of focal adhesion kinase and proline-rich tyrosine kinase 2 tyrosine sites involved in ERK activation. *J Biol Chem* **279**, 30588–30599.

17. **Brackenbury, J. H. and Williamson, A. D.** (1989). Treadmill exercise training increases the oxidative capacity of chicken iliotibialis muscle. *Poult Sci* **68**, 577–581.

18. **Brett, J.** (1964). The respiratory metabolism and swimming performance of young sockeye salmon. *J Fish Res Bd Can* **21**, 1183–1226.

19. **Budick, S. A. and O'Malley, D. M.** (2000). Locomotor repertoire of the larval zebrafish: swimming, turning and prey capture. *J Exp Biol* **203**, 2565–2579.

20. **Burger, E. H. and Klein-Nulend, J.** (1999). Mechanotransduction in bone–role of the lacuno-canalicular network. *FASEB J* **13 Suppl**, S101–S112.

21. **Buss, R. R. and Drapeau, P.** (2002). Activation of embryonic red and white muscle fibers during fictive swimming in the developing zebrafish. *J Neurophysiol* **87**, 1244–1251.

22. **Cahu, C., Infante, J. Z. and Takeuchi, T.** (2003). Nutritional components affecting skeletal development in fish larvae. *Aquaculture* **227**, 245–258.

23. **Carter, D. R. and Wong, M.** (2003). Modelling cartilage mechanobiology. *Philos Trans R Soc Lond B Biol Sci* **358**, 1461–1471.

24. **Charvet, B., Malbouyres, M., Pagnon-Minot, A., Ruggiero, F. and Le Guellec, D.** (2011). Development of the zebrafish myoseptum with emphasis on the myotendinous junction. *Cell Tissue Res* **346**, 439–449.

25. **Cheema, U., Brown, R., Mudera, V., Yang, S. Y., McGrouther, G. and Goldspink, G.** (2005). Mechanical signals and IGF-I gene splicing in vitro in relation to development of skeletal muscle. *J Cell Physiol* **202**, 67–75.

26. **Chen, J. M., Dando, P. M., Rawlings, N. D., Brown, M. A., Young, N. E., Stevens, R. A., Hewitt, E., Watts, C. and Barrett, A. J.** (1997). Cloning, isolation, and characterization of mammalian legumain, an asparaginyl endopeptidase. *J Biol Chem* **272**, 8090–8098.

27. **Cheng, W., Guo, L., Zhang, Z., Soo, H. M., Wen, C., Wu, W. and Peng, J.** (2006). HNF factors form a network to regulate liver-enriched genes in zebrafish. *Dev Biol* **294**, 482–496.

28. **Chow, J. W. and Chambers, T. J.** (1994). Indomethacin has distinct early and late actions on bone formation induced by mechanical stimulation. *Am J Physiol* **267**, E287–E292.

29. **Chow, L. S., Greenlund, L. J., Asmann, Y. W., Short, K. R., McCrady, S. K., Levine, J. A. and Nair, K. S.** (2007). Impact of endurance training on murine spontaneous activity, muscle mitochondrial DNA abundance, gene transcripts, and function. *J Appl Physiol* **102**, 1078–1089.

30. **Chung, A.-Y., Kim, S., Kim, H., Bae, Y.-K. and Park, H.-C.** (2011). Microarray screening for genes involved in oligodendrocyte differentiation in the zebrafish CNS. *Exp Neurobiol* **20**, 85–91.

31. **Cloud, K. G., Shen, B., Strniste, G. F. and Park, M. S.** (1995). XPG protein has a structure-specific endonuclease activity. *Mutation Research* **347**, 55–60.

32. **Cloutier, R., Caron, A., Grunbaum, T. and Le François, N. R.** (2010). Effect of water velocity on the timing of skeletogenesis in the Arctic Charr, *Salvelinus alpinus* (Salmoniformes: Teleostei): An empirical case of developmental plasticity. *Int J Zool* **2010**, 1–15.

33. **Cotman, C. W. and Berchtold, N. C.** (2002). Exercise: a behavioral intervention to enhance brain health and plasticity. *Trends Neurosci* **25**, 295–301.

34. **Cowin, S. C., Moss-Salentijn, L. and Moss, M. L.** (1991). Candidates for the mechanosensory system in bone. *J Biomech Eng* **113**, 191–197.

35. **Cowin, S.** (2001). *Bone mechanics handbook.* CRC Press LLC, Florida, 2nd edition.

36. **Cubbage, C. and Mabee, P. M.** (1996). Development of the cranium and paired fins in the zebrafish *Danio rerio* (Ostariophysi, Cyprinidae). *J Morphol* **229**, 121–160.

37. **Currey, J. D.** (2002). *Bones: structure and mechanics*. Princeton University Press, Oxfordshire.

38. **Danos, N. and Staab, K.** (2010). Can mechanical forces be responsible for novel bone development and evolution in fishes? *J Appl Ichthyol* **26**, 156–161.

39. **Davison, W.** (1989). Training and its effect on teleost fish. *Comp Biochem Physiol Part A: Physiol* **94**, 1–10.

40. **Davison, W.** (1997). The effects of exercise training on teleost fish, a review of recent literature. *Comp Biochem Physiol Part A: Physiol* **117**, 67–75.

41. **Davison, W. and Herbert, N. A.** (2013). Swimming-enhanced growth. In *Swimming Physiology of Fish: Towards Using Exercise to Farm a Fit Fish in Sustainable Aquaculture* (eds. A. Palstra and J. V. Planas), pp. 177–202. Springer-Verlag, Berlin Heidelberg.

42. **Devoto, S. H., Melançon, E., Eisen, J. S. and Westerfield, M.** (1996). Identification of separate slow and fast muscle precursor cells in vivo, prior to somite formation. *Development* **122**, 3371–3380.

43. **Dix, D. J. and Eisenberg, B. R.** (1990). Myosin mRNA accumulation and myofibrillogenesis at the myotendinous junction of stretched muscle fibers. *J Cell Biol* **111**, 1885–1894.

44. **Doty, S. B.** (1981). Morphological evidence of gap junctions between bone cells. *Calcif Tissue Int* **33**, 509–512.

45. **Du, S. J., Gao, J. and Anyangwe, V.** (2003). Muscle-specific expression of myogenin in zebrafish embryos is controlled by multiple regulatory elements in the promoter. *Comp Biochem Physiol B Biochem Mol Biol* **134**, 123–134.

46. **Du, S. J., Li, H., Bian, Y. and Zhong, Y.** (2008). Heat-shock protein 90α1 is required for organized myofibril assembly in skeletal muscles of zebrafish embryos. *Proc Natl Acad Sci USA* **105**, 554–559.

47. **Dudley, H. R. and Spiro, D.** (1961). The fine structure of bone cells. *J Biophys Biochem Cytol* **11**, 627–649.

48. **Dyck, D. J., Miskovic, D., Code, L., Luiken, J. J. and Bonen, A.** (2000). Endurance training increases FFA oxidation and reduces triacylglycerol utilization in contracting rat soleus. *Am J Physiol Endocrinol Metab* **278**, E778–E785.

49. **Edgar, R., Domrachev, M. and Lash, A. E.** (2002). Gene Expression Omnibus: NCBI gene expression and hybridization array data repository. *Nucleic Acids Res* **30**, 207–210.

50. **Egg, M., Tischler, A., Schwerte, T., Sandbichler, A., Folterbauer, C. and Pelster, B.** (2012). Endurance exercise modifies the circadian clock in zebrafish (*Danio rerio*) temperature independently. *Acta Physiol (Oxf)* **205**, 167–176.

51. **Engeszer, R. E., Patterson, L. B., Rao, A. A. and Parichy, D. M.** (2007). Zebrafish in the wild: a review of natural history and new notes from the field. *Zebrafish* **4**, 21–40.

52. **Farrell, A., Johansen, J. and Suarez, R.** (1991). Effects of exercise-training on cardiac performance and muscle enzymes in rainbow trout, *Oncorhynchus mykiss*. *Fish Physiol Biochem* **9(4)**, 303–312.

53. **Fiaz, A. W., Van Leeuwen, J. L. and Kranenbarg, S.** (2010). Phenotypic plasticity and mechano-transduction in the teleost skeleton. *J Appl Ichtyol* **26**, 289–293.

54. **Fiaz, A. W., Léon-Kloosterziel, K. M., Gort, G., Schulte-Merker, S., Van Leeuwen, J. L. and Kranenbarg, S.** (2012). Swim-training changes the spatio-temporal dynamics of skeletogenesis in zebrafish larvae (*Danio rerio*). *PLoS One* **7**, e34072.

55. **Fontaine, E., Lentink, D., Kranenbarg, S., Müller, U. K., Van Leeuwen, J. L., Barr, A. H. and Burdick, J. W.** (2008). Automated visual tracking for studying the ontogeny of zebrafish swimming. *J Exp Biol* **211**, 1305–1316.

56. **Franceschi, R. T. and Xiao, G.** (2003). Regulation of the osteoblast-specific transcription factor, Runx2: responsiveness to multiple signal transduction pathways. *J Cell Biochem* **88**, 446–454.

57. **Franz-Odendaal, T. A., Hall, B. K. and Witten, P. E.** (2006). Buried alive: how osteoblasts become osteocytes. *Dev Dyn* **235**, 176–190.

58. **Freund, J. B., Goetz, J. G., Hill, K. L. and Vermot, J.** (2012). Fluid flows and forces in development: functions, features and biophysical principles. *Development* **139**, 1229–1245.

59. **Fuiman, L. and Webb, P. W.** (1988). Ontogeny of routine swimming activity and performance in zebra danios (Teleostei: Cyprinidae). *Anim Behav* **36**, 250–261.

60. **Fuiman, L.** (1983). Growth gradients in fish larvae. *J Fish Biol* **23**, 117–123.

61. **Gazzola, M., Rees, W. M. V. and Koumoutsakos, P.** (2012). C-start: optimal start of larval fish. *J Fluid Mech* **698**, 5–18.

62. **Germiller, J. A. and Goldstein, S. A.** (1997). Structure and function of embryonic growth plate in the absence of functioning skeletal muscle. *J Orthop Res* **15**, 362–370.

63. **Gibb, A. C., Dickson, K. A. and Lauder, G. V.** (1999). Tail kinematics of the chub mackerel *Scomber japonicus*: testing the homocercal tail model of fish propulsion. *J Exp Biol* **202**, 2433–2447.

64. **Gibb, A. C., Swanson, B. O., Wesp, H., Landels, C. and Liu, C.** (2006). Development of the escape response in teleost fishes: do ontogenetic changes enable improved performance? *Physiol Biochem Zool* **79**, 7–19.

65. **Gilbert, S.** (2000). *Developmental biology.* Sinauer Associates, inc., Massachusetts, 6th edition.

66. **Glucksman, A.** (1941). The role of mechanical stresses in bone formation *in vitro*. *J Anat* **76**, 231–239.

67. **Gollnick, P. D., Armstrong, R. B., Saltin, B., Saubert, C. W., Sembrowich, W. L. and Shepherd, R. E.** (1973). Effect of training on enzyme activity and fiber composition of human skeletal muscle. *J Appl Physiol* **34**, 107–111.

68. **Gomez, C., David, V., Peet, N. M., Vico, L., Chenu, C., Malaval, L. and Skerry, T. M.** (2007). Absence of mechanical loading *in utero* influences bone mass and architecture but not innervation in Myod-Myf5-deficient mice. *J Anat* **210**, 259–271.

69. **Grande, T. and Young, B.** (2004). The ontogeny and homology of the Weberian apparatus in the zebrafish *Danio rerio* (Ostariophysi: Cypriniformes). *Zool J Linn Soc* **140**, 241–254.

70. **Griffiths, A., Miller, J., Suzuki, D. T., Lewontin, R. and Gelbart, W. M.** (1996). *An introduction to genetic analysis.* W.H. Freeman and Company, New York, 6th edition.

71. **Grotmol, S., Kryvi, H., Nordvik, K. and Totland, G. K.** (2003). Notochord segmentation may lay down the pathway for the development of the vertebral bodies in the Atlantic salmon. *Anat Embryol (Berl)* **207**, 263–272.

72. **Gulick, T., Cresci, S., Caira, T., Moore, D. D. and Kelly, D. P.** (1994). The peroxisome proliferator-activated receptor regulates mitochondrial fatty acid oxidative enzyme gene expression. *Proc Natl Acad Sci U S A* **91**, 11012–11016.

73. **Hammond, C. L., Simbi, B. H. and Stickland, N. C.** (2007). *In ovo* temperature manipulation influences embryonic motility and growth of limb tissues in the chick (*Gallus gallus*). *J Exp Biol* **210**, 2667–2675.

74. **Hammond, C. L. and Schulte-Merker, S.** (2009). Two populations of endochondral osteoblasts with differential sensitivity to Hedgehog signalling. *Development* **136**, 3991–4000.

75. **Herbing, I. H. V., Miyake, T., Hall, B. K. and Boutilier, R. G.** (1996). Ontogeny of feeding and respiration in larval Atlantic cod *Gadus morhua* (Teleostei, Gadiformes): I. Morphology. *J Morphol* **227**, 15–35.

76. **Hernández, L. P., Barresi, M. J. F. and Devoto, S. H.** (2002). Functional morphology and developmental biology of zebrafish: reciprocal illumination from an unlikely couple. *Integ and Comp Biol* **42**, 222–231.

77. **Heywood, J. L., McEntee, G. M. and Stickland, N. C.** (2005). *In ovo* neuromuscular stimulation alters the skeletal muscle phenotype of the chick. *J Muscle Res Cell Motil* **26**, 49–56.

78. **Higashijima, S., Okamoto, H., Ueno, N., Hotta, Y. and Eguchi, G.** (1997). High-frequency generation of transgenic zebrafish which reliably express GFP in whole muscles or the whole body by using promoters of zebrafish origin. *Dev Biol* **192**, 289–299.

79. **Higashijima, S.-i.** (2008). Transgenic zebrafish expressing fluorescent proteins in central nervous system neurons. *Dev Growth Differ* **50**, 407–413.

80. **Holloszy, J. O. and Coyle, E. F.** (1984). Adaptations of skeletal muscle to endurance exercise and their metabolic consequences. *J Appl Physiol* **56**, 831–838.

81. **Hosseini, A. and Hogg, D. A.** (1991). The effects of paralysis on skeletal development in the chick embryo. I. general effects. *J Anat* **177**, 159–168.

82. **Hove, J. R., Köster, R. W., Forouhar, A. S., Acevedo-Bolton, G., Fraser, S. E. and Gharib, M.** (2003). Intracardiac fluid forces are an essential epigenetic factor for embryonic cardiogenesis. *Nature* **421**, 172–177.

83. **Howe, K., Clark, M. D., Torroja, C. F., Torrance, J., Berthelot, C., Muffato, M., Collins, J. E., Humphray, S., McLaren, K., Matthews, L. et al.** (2013). The zebrafish reference genome sequence and its relationship to the human genome. *Nature* **496**, 498–503.

84. **Huysseune, A.** (2000). Skeletal system. In *The laboratory fish* (ed. G. Ostrander), pp. 307–317. Academic press, London.

85. **Inaoka, T., Lean, J. M., Bessho, T., Chow, J. W., Mackay, A., Kokubo, T. and Chambers, T. J.** (1995). Sequential analysis of gene expression after an osteogenic stimulus: c-fos expression is induced in osteocytes. *Biochem Biophys Res Commun* **217**, 264–270.

86. **Ingber, D. E.** (2006). Mechanical control of tissue morphogenesis during embryological development. *Int J Dev Biol* **50**, 255–266.

87. **Ingber, D. E. and Jamieson, J. D.** (1985). Cells as tensegrity structures: architectural regulation of histodifferentiation by physical forces transduced over basement membrane. In *Gene expression during normal and malignant differentiation* (eds. L. Andersson, C. Gahmberg and P. Ekblom), pp. 13–32. Academic Press, Florida.

88. **Inohaya, K., Takano, Y. and Kudo, A.** (2007). The teleost intervertebral region acts as a growth center of the centrum: in vivo visualization of osteoblasts and their progenitors in transgenic fish. *Dev Dyn* **236**, 3031–3046.

89. **Ishida, T., Peterson, T. E., Kovach, N. L. and Berk, B. C.** (1996). MAP kinase activation by flow in endothelial cells. role of beta 1 integrins and tyrosine kinases. *Circ Res* **79**, 310–316.

90. **Jackson, J. B.** (2003). Proton translocation by transhydrogenase. *FEBS Lett* **545**, 18–24.

91. **Johnston, I. and Moon, T.** (1980). Endurance exercise training in the fast and slow muscles of a teleost fish (*Pollachius virens*). *J Comp Physiol B* **13**, 147–156.

92. **Kanno, T., Takahashi, T., Tsujisawa, T., Ariyoshi, W. and Nishihara, T.** (2007). Mechanical stress-mediated Runx2 activation is dependent on Ras/ERK1/2 MAPK signaling in osteoblasts. *J Cell Biochem* **101**, 1266–1277.

93. **Kardong, K. V.** (2002). *Vertebrates: comparative anatomy, function, evolution.* McGraw-Hill, New York, 3rd edition.

94. **Karsenty, G. and Wagner, E. F.** (2002). Reaching a genetic and molecular understanding of skeletal development. *Dev Cell* **2**, 389–406.

95. **Kawahara, A., Che, Y.-S., Hanaoka, R., Takeda, H. and Dawid, I. B.** (2005). Zebrafish *GADD45β* genes are involved in somite segmentation. *Proc Natl Acad Sci USA* **102**, 361–366.

96. **Kelly, D. J. and Jacobs, C. R.** (2010). The role of mechanical signals in regulating chondrogenesis and osteogenesis of mesenchymal stem cells. *Birth Defects Res C Embryo Today* **90**, 75–85.

97. **Kihara, M., Ogata, S., Kawano, N., Kubota, I. and Yamaguchi, R.** (2002). Lordosis induction in juvenile red sea bream, *Pagrus major*, by high swimming activity. *Aquaculture* **212**, 149–158.

98. **Kimmel, C. B., Ballard, W. W., Kimmel, S. R., Ullmann, B. and Schilling, T. F.** (1995). Stages of embryonic development of the zebrafish. *Dev Dyn* **203**, 253–310.

99. **Klein-Nulend, J., Semeins, C. M., Ajubi, N. E., Nijweide, P. J. and Burger, E. H.** (1995). Pulsating fluid flow increases nitric oxide (NO) synthesis by osteocytes but not periosteal fibroblasts–correlation with prostaglandin upregulation. *Biochem Biophys Res Commun* **217**, 640–648.

100. **Klein-Nulend, J., Veldhuijzen, J. P. and Burger, E. H.** (1986). Increased calcification of growth plate cartilage as a result of compressive force *in vitro*. *Arthritis Rheum* **29**, 1002–1009.

101. **Knight, J.** (2012). http://www.neuro.uoregon.edu/k12/george_streisinger.html.

102. **Knothe Tate, M. L., Adamson, J. R., Tami, A. E. and Bauer, T. W.** (2004). The osteocyte. *Int J Biochem Cell Biol* **36**, 1–8.

103. **Kobayashi, T. and Kronenberg, H.** (2005). Minireview: transcriptional regulation in development of bone. *Endocrinology* **146**, 1012–1017.

104. **Kogianni, G. and Noble, B. S.** (2007). The biology of osteocytes. *Curr Osteoporos Rep* **5**, 81–86.

105. **Komori, T.** (2000). A fundamental transcription factor for bone and cartilage. *Biochem Biophys Res Commun* **276**, 813–816.

106. **Kopp, R., Köblitz, L., Egg, M. and Pelster, B.** (2011). HIF signaling and overall gene expression changes during hypoxia and prolonged exercise differ considerably. *Physiol Genomics* **43**, 506–516.

107. **Kranenbarg, S., Van Cleynenbreugel, T., Schipper, H. and Van Leeuwen, J.** (2005). Adaptive bone formation in acellular vertebrae of sea bass (*Dicentrarchus labrax* L.). *J Exp Biol* **208**, 3493–3502.

108. **Kranenbarg, S., Waarsing, J. H., Muller, M., Weinans, H. and Van Leeuwen, J. L.** (2005b). Lordotic vertebrae in sea bass (*Dcentrarchus labrax* L.) are adapted to increased loads. *J Biomech* **38**, 1239–1246.

109. **Kumar, A., Murphy, R., Robinson, P., Wei, L. and Boriek, A. M.** (2004). Cyclic mechanical strain inhibits skeletal myogenesis through activation of focal adhesion kinase, Rac-1 GTPase, and NF-kappaB transcription factor. *FASEB J* **18**, 1524–1535.

110. **Laale, H. W.** (1977). The biology and use of zebrafish, *Brachydanio rerio*, in fisheries research. A literature review. *Journal of Fish Biology* **10**, 121–173.

111. **Lamb, K. J., Lewthwaite, J. C., Lin, J.-P., Simon, D., Kavanagh, E., Wheeler-Jones, C. P. D. and Pitsillides, A. A.** (2003). Diverse range of fixed positional deformities and bone growth restraint provoked by flaccid paralysis in embryonic chicks. *Int J Exp Pathol* **84**, 191–199.

112. **Lansman, J. B., Hallam, T. J. and Rink, T. J.** (1987). Single stretch-activated ion channels in vascular endothelial cells as mechanotransducers? *Nature* **325**, 811–813.

113. **Lanyon, L. E.** (1993). Osteocytes, strain detection, bone modeling and remodeling. *Calcif Tissue Int* **53 Suppl 1**, S102–6; discussion S106–7.

114. **Lauder, G. V.** (2000). Function of the caudal fin during locomotion in fishes: kinematics, flow visualization, and evolutionary patterns. *Amer Zool* **40**, 101–122.

115. **Laue, K., Jnicke, M., Plaster, N., Sonntag, C. and Hammerschmidt, M.** (2008). Restriction of retinoic acid activity by Cyp26b1 is required for proper timing and patterning of osteogenesis during zebrafish development. *Development* **135**, 3775–3787.

116. **Lean, J. M., Mackay, A. G., Chow, J. W. and Chambers, T. J.** (1996). Osteocytic expression of mRNA for c-fos and IGF-I: an immediate early gene response to an osteogenic stimulus. *Am J Physiol* **270**, E937–E945.

117. **LeBlanc, A. D., Spector, E. R., Evans, H. J. and Sibonga, J. D.** (2007). Skeletal responses to space flight and the bed rest analog: a review. *J Musculoskelet Neuronal Interact* **7**, 33–47.

118. **LeMoine, C. M. R., Craig, P. M., Dhekney, K., Kim, J. J. and McClelland, G. B.** (2010). Temporal and spatial patterns of gene expression in skeletal muscles in response to swim training in adult zebrafish (*Danio rerio*). *J Comp Physiol B* **180**, 151–160.

119. **Li, G., Müller, U. K., Van Leeuwen, J. L. and Liu, H.** (2012). Body dynamics and hydrodynamics of swimming fish larvae: a computational study. *J Exp Biol* **215**, 4015–4033.

120. **Li, N., Felber, K., Elks, P., Croucher, P. and Roehl, H. H.** (2009). Tracking gene expression during zebrafish osteoblast differentiation. *Dev Dyn* **238**, 459–466.

121. **Lieschke, G. J. and Currie, P. D.** (2007). Animal models of human disease: zebrafish swim into view. *Nat Rev Genet* **8**, 353–367.

122. **Lundgren, J.** (2013). http://www.mathworks.nl/matlabcentral/fileexchange/authors/27012.

123. **Ma, D. K., Jang, M.-H., Guo, J. U., Kitabatake, Y., Chang, M.-L., Pow-Anpongkul, N., Flavell, R. A., Lu, B., Ming, G.-L. and Song, H.** (2009). Neuronal activity-induced Gadd45β promotes epigenetic DNA demethylation and adult neurogenesis. *Science* **323**, 1074–1077.

124. **Mammoto, A., Mammoto, T. and Ingber, D. E.** (2008). Rho signaling and mechanical control of vascular development. *Curr Opin Hematol* **15**, 228–234.

125. **Mammoto, A., Mammoto, T. and Ingber, D. E.** (2012). Mechanosensitive mechanisms in transcriptional regulation. *J Cell Sci* **125**, 3061–3073.

126. **Mammoto, T. and Ingber, D. E.** (2010). Mechanical control of tissue and organ development. *Development* **137**, 1407–1420.

127. **Manoury, B., Hewitt, E. W., Morrice, N., Dando, P. M., Barrett, A. J. and Watts, C.** (1998). An asparaginyl endopeptidase processes a microbial antigen for class II MHC presentation. *Nature* **396**, 695–699.

128. **Marini, M. and Veicsteinas, A.** (2010). The exercised skeletal muscle: a review. *Eur J Transl Myol - Myol Rev* **20**, 105–120.

129. **Matthews, B. D., Overby, D. R., Mannix, R. and Ingber, D. E.** (2006). Cellular adaptation to mechanical stress: role of integrins, Rho, cytoskeletal tension and mechanosensitive ion channels. *J Cell Sci* **119**, 508–518.

130. **McArdle, W. D., Katch, F. I. and Katch, V. L.** (2001). *Exercise physiology: energy, nutrition and human performance.* Lippencott Williams & Wilkins, 5th edition.

131. **McClelland, G. B., Craig, P. M., Dhekney, K. and Dipardo, S.** (2006). Temperature- and exercise-induced gene expression and metabolic enzyme changes in skeletal muscle of adult zebrafish (*Danio rerio*). *J Physiol* **577**, 739–751.

132. **Van der Meulen, T.** (2005). *Epigenetics of the locomotory system in zebrafish.* Ph.D. thesis, Wageningen University, Departement of Animal Sciences, Experimental Zoology, PO Box 338, 6700 AH, Wageningen, the Netherlands.

133. **Van der Meulen, T., Schipper, H., Van den Boogaart, J. G. M., Huising, M. O., Kranenbarg, S. and Van Leeuwen, J. L.** (2006). Endurance exercise differentially stimulates heart and axial muscle development in zebrafish (*Danio rerio*). *Am J Physiol Regul Integr Comp Physiol* **291**, R1040–R1048.

134. **Meyer, A. and Schartl, M.** (1999). Gene and genome duplications in vertebrates: the one-to-four (-to-eight in fish) rule and the evolution of novel gene functions. *Curr Opin Cell Biol* **11**, 699–704.

135. **Mikic, B., Isenstein, A. L. and Chhabra, A.** (2004). Mechanical modulation of cartilage structure and function during embryogenesis in the chick. *Ann of Biom Eng* **32**, 18–25.

136. **Miles, R. R., Turner, C. H., Santerre, R., Tu, Y., McClelland, P., Argot, J., DeHoff, B. S., Mundy, C. W., Rosteck, P., Jr, Bidwell, J. et al.** (1998). Analysis of differential gene expression in rat tibia after an osteogenic stimulus in vivo: mechanical loading regulates osteopontin and myeloperoxidase. *J Cell Biochem* **68**, 355–365.

137. **Müller, U. K. and Van Leeuwen, J. L.** (2004). Swimming of larval zebrafish: ontogeny of body waves and implications for locomotory development. *J Exp Biol* **207**, 853–868.

138. **Müller, U. K., Van Leeuwen, J. L., Van Duin, S. and Liu, H.** (2009). An un-momentous start to life: can hydrodynamics explain why fish larvae change swimming style. *J Biomech Sci Eng* **4**, 37–53.

139. **Murray, P. D. and Drachman, D. B.** (1969). The role of movement in the development of joints and related structures: the head and neck in the chick embryo. *J Embryol Exp Morphol* **22**, 349–371.

140. **Nakashima, K., Zhou, X., Kunkel, G., Zhang, Z., Deng, J. M., Behringer, R. R. and de Crombrugghe, B.** (2002). The novel zinc finger-containing transcription factor osterix is required for osteoblast differentiation and bone formation. *Cell* **108**, 17–29.

141. **Nauli, S. M., Alenghat, F. J., Luo, Y., Williams, E., Vassilev, P., Li, X., Elia, A. E. H., Lu, W., Brown, E. M., Quinn, S. J. et al.** (2003). Polycystins 1 and 2 mediate mechanosensation in the primary cilium of kidney cells. *Nat Genet* **33**, 129–137.

142. **Nefussi, J. R., Sautier, J. M., Nicolas, V. and Forest, N.** (1991). How osteoblasts become osteocytes: a decreasing matrix forming process. *J Biol Buccale* **19**, 75–82.

143. **Nelson, C. M. and Gleghorn, J. P.** (2012). Sculpting organs: mechanical regulation of tissue development. *Annu Rev Biomed Eng* **14**, 129–154.

144. **Nomura, S. and Takano-Yamamoto, T.** (2000). Molecular events caused by mechanical stress in bone. *Matrix Biol* **19**, 91–96.

145. **Nordvik, K., Kryvi, H., Totland, G. K. and Grotmol, S.** (2005). The salmon vertebral body develops through mineralization of two preformed tissues that are encompassed by two layers of bone. *J Anat* **206**, 103–114.

146. **North, T. E., Goessling, W., Peeters, M., Li, P., Ceol, C., Lord, A. M., Weber, G. J., Harris, J., Cutting, C. C., Huang, P. et al.** (2009). Hematopoietic stem cell development is dependent on blood flow. *Cell* **137**, 736–748.

147. **Nowlan, N. C., Murphy, P. and Prendergast, P. J.** (2007). Mechanobiology of embryonic limb development. *Ann N Y Acad Sci* **1101**, 389–411.

148. **Nowlan, N. C., Prendergast, P. J. and Murphy, P.** (2008). Identification of mechanosensitive genes during embryonic bone formation. *PLoS Comput Biol* **4**, e1000250.

149. **Nüsslein-Volhard, C. and Dahm, R.** (2002). *Zebrafish: A Practical Approach.* Oxford University Press, New York.

150. **Nüsslein-Volhard, C.** (2012). The zebrafish issue of development. *Development* **139**, 4099–4103.

151. **Osse, J. W. M. and Van den Boogaart, J. G. M.** (1999). Dynamic morphology of fish larvae, structural implications of friction forces in swimming, feeding and ventilation. *J Fish Biol* **55 (supplement A)**, 156–174.

152. **Pack, M., Solnica-Krezel, L., Malicki, J., Neuhauss, S. C., Schier, A. F., Stemple, D. L., Driever, W. and Fishman, M. C.** (1996). Mutations affecting development of zebrafish digestive organs. *Development* **123**, 321–328.

153. **Palstra, A. P., Schaaf, M. and Planas, J. V.** (2013). Exercise physiology of zebrafish: Swimming effects on skeletal and cardiac muscle growth, on the immune system, and the involvement of the stress axis. In *Swimming Physiology of Fish: Towards Using Exercise to Farm a Fit Fish in Sustainable Aquaculture* (eds. A. P. Palstra and J. V. Planas), pp. 323–342. Springer-Verlag, Berlin Heidelberg.

154. **Palstra, A. P. and Planas, J. V.** (2011). Fish under exercise. *Fish Physiol Biochem* **37**, 259–272.

155. **Palstra, A. P., Tudorache, C., Rovira, M., Brittijn, S. A., Burgerhout, E., van den Thillart, G. E. E. J. M., Spaink, H. P. and Planas, J. V.** (2010). Establishing zebrafish as a novel exercise model: swimming economy, swimming-enhanced growth and muscle growth marker gene expression. *PLoS One* **5**, e14483.

156. **Palumbo, C.** (1986). A three-dimensional ultrastructural study of osteoid-osteocytes in the tibia of chick embryos. *Cell Tissue Res* **246**, 125–131.

157. **Palumbo, C., Palazzini, S. and Marotti, G.** (1990). Morphological study of intercellular junctions during osteocyte differentiation. *Bone* **11**, 401–406.

158. **Palumbo, C., Ferretti, M. and Marotti, G.** (2004). Osteocyte dendrogenesis in static and dynamic bone formation: an ultrastructural study. *Anat Rec A Discov Mol Cell Evol Biol* **278**, 474–480.

159. **Parenti, L. R.** (1986). The phylogenetic significance of bone types in euteleost fishes. *Zool. J. Linn. Soc.* **87**, 37–51.

160. **Parichy, D. M., Elizondo, M. R., Mills, M. G., Gordon, T. N. and Engeszer, R. E.** (2009). Normal table of postembryonic zebrafish development: staging by externally visible anatomy of the living fish. *Dev Dyn* **238**, 2975–3015.

161. **Parsons, S. A., Millay, D. P., Wilkins, B. J., Bueno, O. F., Tsika, G. L., Neilson, J. R., Liberatore, C. M., Yutzey, K. E., Crabtree, G. R., Tsika, R. W. et al.** (2004). Genetic loss of calcineurin blocks mechanical overload-induced skeletal muscle fiber type switching but not hypertrophy. *J Biol Chem* **279**, 26192–26200.

162. **Pavalko, F. M., Chen, N. X., Turner, C. H., Burr, D. B., Atkinson, S., Hsieh, Y. F., Qiu, J. and Duncan, R. L.** (1998). Fluid shear-induced mechanical signaling in MC3T3-E1 osteoblasts requires cytoskeleton-integrin interactions. *Am J Physiol* **275**, C1591–C1601.

163. **Pelster, B., Sänger, A. M., Siegele, M. and Schwerte, T.** (2003). Influence of swim training on cardiac activity, tissue capillarization, and mitochondrial density in muscle tissue of zebrafish larvae. *Am J Physiol Regul Integr Comp Physiol* **285**, R339–R347.

164. **Pfaffl, M. W.** (2001). A new mathematical model for relative quantification in real-time RT-PCR. *Nucleic Acids Res* **29**, e45.

165. **Pfaffl, M. W., Tichopad, A., Prgomet, C. and Neuvians, T. P.** (2004). Determination of stable housekeeping genes, differentially regulated target genes and sample integrity: BestKeeper–Excel-based tool using pair-wise correlations. *Biotechnol Lett* **26**, 509–515.

166. **Planas-Paz, L. and Lammert, E.** (2013). Mechanical forces in lymphatic vascular development and disease. *Cell Mol Life Sci* .

167. **Plaut, I.** (2000). Effects of fin size on swimming performance, swimming behaviour and routine activity of zebrafish *Danio rerio*. *J Exp Biol* **203**, 813–820.

168. **Plaut, I.** (2001). Critical swimming speed: its ecological relevance. *Comp Biochem Physiol Part A Mol Integr Physiol* **131**, 41–50.

169. **Van Praag, H., Kempermann, G. and Gage, F. H.** (1999). Running increases cell proliferation and neurogenesis in the adult mouse dentate gyrus. *Nat Neurosci* **2**, 266–270.

170. **Van Praag, H.** (2008). Neurogenesis and exercise: past and future directions. *Neuromolecular Med* **10**, 128–140.

171. **Praetorius, H. A. and Spring, K. R.** (2001). Bending the MDCK cell primary cilium increases intracellular calcium. *J Membr Biol* **184**, 71–79.

172. **Prendergast, P. J.** (1997). Finite element models in tissue mechanics and orthopaedic implant design. *Clin Biomech (Bristol, Avon)* **12**, 343–366.

173. **Van Raamsdonk, W., Mos, W., Smit-Onel, M. J., Van der Laarse, W. J. and Fehres, R.** (1983). The development of the spinal motor column in relation to the myotomal muscle fibers in the zebrafish (*Brachydanio rerio*). I. Posthatching development. *Anat Embryol (Berl)* **167**, 125–139.

174. **Van Raamsdonk, W., Pool, C. W. and te Kronnie, G.** (1978). Differentiation of muscle fiber types in the teleost *Brachydanio rerio*. *Anat Embryol (Berl)* **153**, 137–155.

175. **Richardson, M. K. and Chipman, A. D.** (2003). Developmental constraints in a comparative framework: a test case using variations in phalanx number during amniote evolution. *J Exp Zool B Mol Dev Evol* **296**, 8–22.

176. **Riemann, D., Kehlen, A. and Langner, J.** (1999). CD13–not just a marker in leukemia typing. *Immunol Today* **20**, 83–88.

177. **Röckl, K. S. C., Hirshman, M. F., Brandauer, J., Fujii, N., Witters, L. A. and Goodyear, L. J.** (2007). Skeletal muscle adaptation to exercise training: AMP-activated protein kinase mediates muscle fiber type shift. *Diabetes* **56**, 2062–2069.

178. **Rodríguez, J. I., García-Alix, A., Palacios, J. and Paniagua, R.** (1988). Changes in the long bones due to fetal immobility caused by neuromuscular disease. a radiographic and histological study. *J Bone Joint Surg* **70**, 1052–1060.

179. **Rodríguez, J. I., Palacios, J., García-Alix, A., Pastor, I. and Paniagua, R.** (1988). Effects of immobilization on fetal bone development. a morphometric study in newborns with congenital neuromuscular diseases with intrauterine onset. *Calcif Tissue Int* **43**, 335–339.

180. **Rombough, P.** (2002). Gills are needed for ionoregulation before they are needed for O_2 uptake in developing zebrafish, *Danio rerio*. *J Exp Biol* **205**, 1787–1794.

181. **Rozen, S. and Skaletsky, H.** (2000). Primer3 on the www for general users and for biologist programmers. In *Bioinformatics methods and protocols: methods in molecular biology* (eds. S. Krawetz and S. Misener), pp. 365–386. Humana Press, New Jersey.

182. **Rudnicki, M. A., Schnegelsberg, P. N., Stead, R. H., Braun, T., Arnold, H.-H. and Jaenisch, R.** (1993). MyoD or Myf-5 is required for the formation of skeletal muscle. *Cell* **75**, 1351 – 1359.

183. **Saint-Amant, L. and Drapeau, P.** (1998). Time course of the development of motor behaviors in the zebrafish embryo. *J Neurobiol* **37**, 622–632.

184. **Sänger, A. M. and Stoiber, W.** (2000). Muscle fiber diversity and plasticity. In *Fish Physiology, Volume 18: Muscle Development and Growth* (ed. I. A. Johnston), pp. 187–250. Academic Press, California.

185. **Sazanov, L. A. and Jackson, J. B.** (1994). Proton-translocating transhydrogenase and NAD- and NADP-linked isocitrate dehydrogenases operate in a substrate cycle which contributes to fine regulation of the tricarboxylic acid cycle activity in mitochondria. *FEBS Lett* **344**, 109–116.

186. **Sfakianakis, D., Leris, I., Laggis, A. and Kentouri, M.** (2011). The effect of rearing temperature on body shape and meristic characters in zebrafish (*Danio rerio*) juveniles. *Environ Biol Fish* **92 (2)**, 197–205.

187. **Shapiro, F.** (1997). Variable conformation of GAP junctions linking bone cells: a transmission electron microscopic study of linear, stacked linear, curvilinear, oval, and annular junctions. *Calcif Tissue Int* **61**, 285–293.

188. **Sire, J.-Y., Huysseune, A. and Meunier, F. J.** (1990). Osteoclasts in teleost fish: light and electron-microscopical observations. *Cell Tissue Res.* **260**, 85–94.

189. **Slack, J. M.** (1995). Developmental biology of the pancreas. *Development* **121**, 1569–1580.

190. **Smith, A., Zhang, D., J.and Guay, Quint, E., Johnson, A. and Akimenko, M.** (2008). Gene expression analysis on sections of zebrafish regenerating fins reveals limitations in the whole-mount in situ hybridization method. *Dev Dyn* **237**, 417–425.

191. **Smith, J. M., Burian, R., Kauffman, S., Alberch, P., Campbell, J., Goodwin, B., Lande, R., Raup, D. and Wolpert, L.** (1985). Developmental constraints and evolution: A perspective from the Mountain Lake conference on development and evolution. *Q Rev Biol* **60**, pp. 265–287.

192. **Sogah, V. M., Serluca, F. C., Fishman, M. C., Yelon, D. L., Macrae, C. A. and Mably, J. D.** (2010). Distinct troponin C isoform requirements in cardiac and skeletal muscle. *Dev Dyn* **239**, 3115–3123.

193. **Sojka, D., Hajdusek, O., Dvorák, J., Sajid, M., Franta, Z., Schneider, E. L., Craik, C. S., Vancová, M., Buresová, V., Bogyo, M. et al.** (2007). IrAE: an asparaginyl endopeptidase (legumain) in the gut of the hard tick *Ixodes ricinus*. *Int J Parasitol* **37**, 713–724.

194. **Spence, R., Gerlach, G., Lawrence, C. and Smith, C.** (2008). The behaviour and ecology of the zebrafish, *Danio rerio*. *Biol Rev Camb Philos Soc* **83**, 13–34.

195. **Spierts, I., Akster, H., Vos, I. and Osse, J.** (1996). Local differences in myotendinous junctions in axial muscle fibres of carp (*Cyprinus carpio* L.). *J Exp Biol* **199**, 825–833.

196. **Spoorendonk, K. M., Hammond, C. L., Huitema, L. F. A., Vanoevelen, J. and Schulte-Merker, S.** (2010). Zebrafish as a unique model system in bone research: the power of genetics and in vivo imaging. *J Appl Ichtyol* **26**, 219–224.

197. **Spoorendonk, K. M., Peterson-Maduro, J., Renn, J., Trowe, T., Kranenbarg, S., Winkler, C. and Schulte-Merker, S.** (2008). Retinoic acid and Cyp26b1 are critical regulators of osteogenesis in the axial skeleton. *Development* **135**, 3765–3774.

198. **Stemple, D.** (2005). Structure and function of the notochord: an essential organ for chordate development. *Development* **132**, 2503–2512.

199. **Stipp, C. S., Kolesnikova, T. V. and Hemler, M. E.** (2003). Functional domains in tetraspanin proteins. *Trends Biochem Sci* **28**, 106–112.

200. **Streisinger, G., Walker, C., Dower, N., Knauber, D. and Singer, F.** (1981). Production of clones of homozygous diploid zebra fish (*Brachydanio rerio*). *Nature* **291**, 293–296.

201. **Stryer, L.** (1995). *Biochemistry.* W.H. Freeman and Company, New York, 4th edition.

202. **Tachibana, I. and Hemler, M. E.** (1999). Role of transmembrane 4 superfamily (TM4SF) proteins CD9 and CD81 in muscle cell fusion and myotube maintenance. *J Cell Biol* **146**, 893–904.

203. **Tatsumi, S., Ishii, K., Amizuka, N., Li, M., Kobayashi, T., Kohno, K., Ito, M., Takeshita, S. and Ikeda, K.** (2007). Targeted ablation of osteocytes induces osteoporosis with defective mechanotransduction. *Cell Metab* **5**, 464–475.

204. **Terai, K., Takano-Yamamoto, T., Ohba, Y., Hiura, K., Sugimoto, M., Sato, M., Kawahata, H., Inaguma, N., Kitamura, Y. and Nomura, S.** (1999). Role of osteopontin in bone remodeling caused by mechanical stress. *J Bone Miner Res* **14**, 839–849.

205. **Thisse, B., Pflumio, S., Frthauer, M., Loppin, B., Heyer, V., Degrave, A., Woehl, R., Lux, A., Steffan, T., Charbonnier, X. et al.** (2001). Expression of the zebrafish genome during embryogenesis (nih r01 rr15402). ZFIN direct data submission (http://www.zfin.org).

206. **Thisse, B. and Thisse, C.** (2004). Fast release clones: a high throughput expression analysis. ZFIN direct data submission (http://www.zfin.org).

207. **Thompson, D. W.** (1992). *On growth and form. The complete revised edition.* Dover Publications, Inc., New York.

208. **Thorarensen, H., Gallaugher, P., Kiessling, A. and Farrell, A.** (1993). Intestinal blood flow in swimming chinook salmon *Oncorhynchus tshawytscha* and the effects of haematocrit on blood flow distribution. *J Exp Biology* **179**, 115–129.

209. **Thorsen, D. H., Cassidy, J. J. and Hale, M. E.** (2004). Swimming of larval zebrafish: fin-axis coordination and implications for function and neural control. *J Exp Biol* **207**, 4175–4183.

210. **Totland, G., Fjelldal, P., Kryvi, H., Løkka, G., Wargelius, A., Sagstad, A., Hansen, T. and Grotmol, S.** (2011). Sustained swimming increases the mineral content and osteocyte density of salmon vertebral bone. *J Anat* **219**, 490–501.

211. **Turner, C. H., Takano, Y., Owan, I. and Murrell, G. A.** (1996). Nitric oxide inhibitor L-NAME suppresses mechanically induced bone formation in rats. *Am J Physiol* **270**, E634–E639.

212. **Vatsa, A., Mizuno, D., Smit, T. H., Schmidt, C. F., MacKintosh, F. C. and Klein-Nulend, J.** (2006). Bio imaging of intracellular NO production in single bone cells after mechanical stimulation. *J Bone Miner Res* **21**, 1722–1728.

213. **Vermot, J., Forouhar, A. S., Liebling, M., Wu, D., Plummer, D., Gharib, M. and Fraser, S. E.** (2009). Reversing blood flows act through *klf2a* to ensure normal valvulogenesis in the developing heart. *PLoS Biol* **7**, e1000246.

214. **Videler, J.** (1993). *Fish swimming.* Chapman and Hall, London.

215. **Wallace, K. N., Akhter, S., Smith, E. M., Lorent, K. and Pack, M.** (2005). Intestinal growth and differentiation in zebrafish. *Mech Dev* **122**, 157–173.

216. **Wang, H.-X., Kolesnikova, T. V., Denison, C., Gygi, S. P. and Hemler, M. E.** (2011). The C-terminal tail of tetraspanin protein CD9 contributes to its function and molecular organization. *J Cell Sci* **124**, 2702–2710.

217. **Wang, Z., Du, J., Lam, S. H., Mathavan, S., Matsudaira, P. and Gong, Z.** (2010). Morphological and molecular evidence for functional organization along the rostrocaudal axis of the adult zebrafish intestine. *BMC Genomics* **11**, 392.

218. **Waters, R., Rotevatn, S., Li, P., Annex, B. H. and Yan, Z.** (2004). Voluntary running induces fiber type-specific angiogenesis in mouse skeletal muscle. *Am J Physiol Cell Physiol* **287**, C1342–C1348.

219. **Webb, P. W.** (1977). Effects of median fin amputation on fast-start performance of rainbow trout (*Salmo gairdneri*). *J Exp Biol* **68**, 123–135.

220. **Weinbaum, S., Cowin, S. C. and Zeng, Y.** (1994). A model for the excitation of osteocytes by mechanical loading-induced bone fluid shear stresses. *J Biomech* **27**, 339–360.

221. **Weisel, G.** (1967). Early ossification in the skeleton of the sucker (*Catostomus macrocheilus*) and the guppy (*Poecilia reticulata*). *J Morphol* **121**, 1–18.

222. **Westerfield, M.** (2000). *The zebrafish book. A guide for the laboratory use of zebrafish (Danio rerio).* University of Oregon Press, Eugene, 4th edition.

223. **Witten, P. E., Hansen, A. and Hall, B. K.** (2001). Features of mono- and multinucleated bone resorbing cells of the zebrafish *Danio rerio* and their contribution to skeletal development, remodeling, and growth. *J Morphol* **250**, 197–207.

224. **Witten, P. E., Gil-Martens, L., Hall, B. K., Huysseune, A. and Obach, A.** (2005). Compressed vertebrae in atlantic salmon *Salmo salar*: evidence for metaplastic chondrogenesis as a skeletogenic response late in ontogeny. *Dis Aquat Organ* **64**, 237–246.

225. **Witten, P. and Huysseune, A.** (2009). A comparative view on mechanisms and functions of skeletal remodelling in teleost fish, with special emphasis on osteoclasts and their function. *Biol Rev Camb Philos Soc* **84**, 315–346.

226. **Wong, M., Siegrist, M. and Goodwin, K.** (2003). Cyclic tensile strain and cyclic hydrostatic pressure differentially regulate expression of hypertrophic markers in primary chondrocytes. *Bone* **33**, 685–693.

227. **Wu, Q., Zhang, Y. and Chen, Q.** (2001). Indian hedgehog is an essential component of mechanotransduction complex to stimulate chondrocyte proliferation. *J Biol Chem* **276**, 35290–35296.

228. **Wu, Q. Q. and Chen, Q.** (2000). Mechanoregulation of chondrocyte proliferation, maturation, and hypertrophy: ion-channel dependent transduction of matrix deformation signals. *Exp Cell Res* **256**, 383–391.

229. **Zebrafish Issue** (1996). *Development* **123**.

230. **Zhao, X., Monson, C., Gao, C., Gouon-Evans, V., Matsumoto, N., Sadler, K. C. and Friedman, S. L.** (2010). Klf6/copeb is required for hepatic outgrowth in zebrafish and for hepatocyte specification in mouse ES cells. *Dev Biol* **344**, 79–93.

Summary

In the last decades, it became clear that not only molecular signals but also mechanical forces are crucial regulators of developmental processes. The molecular mechanism via which mechanical forces mediate their control of developmental processes have been extensively investigated via *in vitro* studies. However, the full range of molecular signals and mechanical forces that regulate development *in vivo* cannot be covered with only *in vitro* studies. *In vivo* studies have just started to reveal the molecular link between mechanical forces and development.

To help fill this gap, we subjected zebrafish larvae to swim-training, which presumably increases mechanical load, and investigated the effect thereof on a molecular, morphological and kinematic level during development. The zebrafish is an established model for vertebrate development and has a reproduction cycle of only three months, transparent embryos and starts to swim as early as 2 days post fertilization. A wide range of genetic analyses and tools to investigate developmental processes at various stages (embryo, larval, juvenile, adult) and levels (e.g. molecular, cellular and organ level) are available for the zebrafish.

To investigate what the effect is of the applied flow on the swimming kinematics of larval zebrafish, we performed a detailed analysis of the swimming kinematics of zebrafish larvae in varying flow conditions at 10 days post fertilization (dpf). We used a two camera set-up (obtaining recordings from the lateral and bottom side of the tube) and a new in-house developed 3D tracker program which allowed us to take pitch and roll angles into account and to accurately track the motion of the center of mass, the lateral bending of the body and motion of the tail fin. Furthermore, our study is the first which calculated the actual swimming speed of larval fish subjected to flow by determining the ambient flow velocity near the position of the fish via particle image velocimetry and computational fluid dynamics analysis of the flow in the tube. The analysis of the swimming kinematics showed that fish subjected to flow had a higher tail beat frequency and swam faster and longer. In addition, normalized maximum curvatures during an individual swimming burst (a forward movement consisting of several tail beats) and averaged over the first three half beats were higher in the caudal fin in fish subjected to flow. These data indicate that the applied flow increased the swimming intensity during a swimming burst and time spent on swimming.

Subsequently, we investigated the effect of swim-training on chondrogenesis and osteogenesis of the cranial, axial and appendicular skeleton during early larval development (5–14 dpf). Swim-training prioritized the development of cartilage and bone structures in the head and in the median fins. We furthermore demonstrated that swim-training can increase growth depending on the feeding regime, training regime and stocking density of fish in a tube during zebrafish larval development. Furthermore, swim-training increased burst frequency which indicates that swim-training not only increased swimming intensity but also swimming activity.

To investigate the effect of swim-training on the gene expression during zebrafish larval development, we performed transcriptome analysis of zebrafish larvae subjected to training and control fish at 10 dpf on a quantitative and spatial gene expression level. We chose this stage because the first ossified structures (hypurals and finrays) appear in the caudal fin around 10 dpf. This analysis demonstrated that swim-training led to molecular changes in the brain, muscle and gastrointestinal system during zebrafish larval development. In addition, we investigated if swim-training affected the expression of genes involved in muscle growth and structure with quantitative real-time PCR in trained and control fish at 5 and 14 dpf. The expression of slow fiber markers was increased after ten days of swim-training, indicating that muscle can already shift towards a more slow aerobic phenotype during zebrafish larval development.

Furthermore, since swim-training prioritized the onset of skeletal elements in (among others) the caudal fin and fish subjected to flow had higher normalized maximum curvatures in the caudal fin, we explored the molecular link between an increased swimming activity and caudal fin development. Fish were subjected to swim-training from 5–10 dpf and we performed a whole genome microarray analysis on the caudal fins of fish at 10 dpf. From this analysis, we identified two muscle specific genes, *aste1* (*asteroid homolog 1*) and *zgc:65811*, which showed an increased expression exclusively in the caudal fin. The gene *aste1* contains an XPG coding domain and might be involved in DNA repair in muscle fibers. Since DNA repair plays an important role during cell division, this suggests that this gene might be implicated in cell division in muscle fibers. The gene *zgc:65811* contains a domain which encodes for the CD-9 large extracellular loop region. The protein CD-9 belongs to the family of tetraspanin transmembrane proteins and is possibly involved in muscle fiber differentiation.

Our study demonstrated that swim-training can increase growth and lead to morphological and molecular changes during zebrafish larval development. We furthermore showed that the applied flow generated larger peak curvatures in the caudal fin and that swim-training led to specific morphological and molecular changes in the caudal fin. Our work suggests that the zebrafish is an interesting model species to elucidate the *in vivo* molecular link between functional performance and morphological development.

Samenvatting

In de afgelopen decennia is het duidelijk geworden dat niet alleen moleculaire signalen maar ook mechanische krachten belangrijke regulatoren zijn van ontwikkelingsprocessen. De moleculaire mechanisms betrokken bij de regulatie van ontwikkelingsprocessen door mechanische krachten zijn uitgebreid onderzocht door *in vitro* studies. Echter, een volledig overzicht van de moleculaire signalen en mechanische krachten die *in vivo* ontwikkeling reguleren kan niet alleen door *in vitro* studies worden beschreven. Diverse *in vivo* studies hebben al de eerste stappen gezet om de moleculaire link tussen mechanische krachten en ontwikkeling te ontrafelen.

Om deze link verder te ontrafelen, onderwierpen we zebravissen aan zwem-training (wat hoogstwaarschijnlijk de mechanische belasting verhoogde) en onderzochten het effect hiervan op een moleculaire, morfologische en kinematische niveau tijdens de larvale zebravisontwikkeling. De zebravis is een geaccepteerd modeldier voor de ontwikkeling van vertebraten en heeft een reproductiecyclus van slechts drie maanden, transparante embryo's en begint al vanaf 2 dagen na bevruchting (dnb) te zwemmen. Verder zijn er een scala aan genetische analyses en technieken beschikbaar om ontwikkelingsprocessen te onderzoeken tijdens verschillende stadia (embryo, larvaal, juveniel, adult) en op verschillende niveaus (bijvoorbeeld moleculair, cellulair en orgaan niveau) in de zebravis.

Om het effect van stroming te onderzoeken op de zwemkinematica van larvale zebravissen, hebben we een gedetailleerde analyse uitgevoerd van de zwemkinematica van larvale zebravissen in variërende stroom omstandigheden op 10 dnb. Door het gebruik van een opstelling met twee camera's (waarbij we opnames maakten van de laterale zijde van de buis en van de onderkant van de buis) en een nieuw in-house ontwikkelde 3D tracker programma konden we rekening houden met de helling- en rolhoeken en nauwkeuring de beweging van het massamiddelpunt, de laterale buiging van het lichaam en beweging van de staartvin volgen. Bovendien is onze studie de eerste die de werkelijke zwemsnelheid van larvale vissen onderworpen aan een stroming heeft berekend. Dit hebben we berekend met behulp van *particle image velocimetry* en *computational fluid dynamics* van de stroming in de buis en de omringende stroomsnelheid in de buurt van de positie van de vis. Analyse van de zwemkinematica toonde aan dat vissen onderworpen aan een stroming een hogere staartslagfrequentie hadden en sneller en langer zwommen. Verder waren de genormaliseerde maximale krommingen van een individuele *burst* (een voorwaartse beweging van enkele staartslagen) en het gemiddelde van de genormaliseerde maximale krommingen van drie halve staart slagen hoger in de staartvin van vissen onderworpen aan stroming. Deze resultaten tonen aan dat stroming niet alleen de zwem-intensiteit verhoogde maar ook de tijd besteed aan zwemmen.

Vervolgens hebben we het effect van zwem-training op de chondrogenese en osteogenese van de schedel en het axiale en appendiculaire skelet onderzocht tijdens larvale zebravisontwikkeling (5–14 dnb). Zwem-training prioritiseerde de ontwikkeling van kraakbeen- en botstructuren in de schedel en mediane vinnen. Verder toonden we aan dat zwem-training de groei kan stimuleren afhankelijk van het voer- en trainingregime en dichtheid van vissen in een buis tijdens de larvale ontwikkeling. Zwem-training verhoogde ook de *burst* frequentie wat aantoont dat zwem-training niet alleen de zwem-intensiteit maar ook de zwem-activiteit verhoogde.

Om het effect van zwem-training op de genexpressie tijdens larvale zebravisontwikkeling te onderzoeken, hebben we een transcriptome analyse uitgevoerd op zebravis larven onderworpen aan training en controle vissen van 10 dnb op een kwantitatieve en ruimtelijke genexpressie niveau. We hebben dit stadium gekozen omdat de eerste verbeende structuren (de vinstralen en hypuralen) in de staartvin zich rond 10 dnb ontwikkelen. De transcriptome analyse toonde aan dat zwem-training leidde tot moleculaire veranderingen in de hersenen, spieren en verteringsstelsel. Daarnaast hebben we onderzocht of zwem-training invloed had op de genexpressie van genen betrokken bij spiergroei en -structuur met kwantitatieve real-time PCR in getrainde en controle vissen op 5 en 14 dnb. De genexpressie van langzame spiervezels markers was toegenomen na tien dagen zwem-training, wat erop wijst dat spieren al naar een langzame aërobe fenotype kunnen transformeren tijdens larvale zebravisontwikkeling.

Verder hebben we, aangezien zwem-training de ontwikkeling van botstructuren in (onder andere) de staartvin prioritiseerde en omdat de genormaliseerde maximale krommingen hoger waren in de staartvin van vissen onderworpen aan stroming, de moleculaire link tussen een verhoogde zwem-activiteit en staartvin ontwikkeling onderzocht. Vissen werden aan zwem-training onderworpen van 5 tot 10 dnb en vervolgens hebben we een whole-genome microarray analyse uitgevoerd op de staartvinnen van vissen van 10 dnb. Uit deze analyse kwam naar voren dat twee genen, *aste1* (*asteroid homolog 1*) en *zgc:65811*, exclusief in de staartvin een verhoogde genexpressie vertoonden. Het gen *aste1* heeft een XPG coderende domein en is mogelijk betrokken bij DNA reparatie in spiervezels. Aangezien DNA reparatie een belangrijke rol speelt bij celdeling, kan *aste1* mogelijk betrokken zijn bij celdeling in spiervezels. Het gen *zgc:65811* bevat een domein dat codeert voor CD-9 grote extracellulaire loop regio. Het eiwit CD-9 behoort tot de familie van tetraspanin transmembrane eiwitten en is mogelijk betrokken bij differentiatie van spiervezels.

Onze studie heeft aangetoond dat zwem-training groei kan stimuleren en dat het kan leiden tot moleculaire en morfologische veranderingen tijdens larvale zebravisontwikkeling. Verder hebben we aangetoond dat variërende stroomomstandigheden leidden tot hogere piek krommingen in de staartvin en dat zwem-training leidde tot specifieke moleculaire en morfologische veranderingen in de staartvin. Ons werk wijst erop dat de zebravis een interessant modeldier is om de *in vivo* moleculaire link tussen functionele performance en morfologische ontwikkeling te ontrafelen.

".....De "F" is van vrienden, dat zijn wij, wij allemaal...."

Najib Amhali

Acknowledgements

This project was a challenging journey and here I would like to thank all the people who supported, contributed and encouraged me to reach the finish line.

Lieve Johan, jij bent een van de meest betrokken professoren die ik ken. Ondanks je zeer drukke schema maak je altijd tijd voor je PhD studenten en ben je erg betrokken bij hun onderzoek, van experimentele opzet tot de data analyse (en dat in een groep met zeer diverse onderwerpen), en dat is zeer bewonderingswaardig. Je kritische vragen en je streven naar perfectie daagden me altijd uit om net iets verder te gaan en het tot in de puntjes uit te zoeken. Bedankt voor de vele (wetenschappelijke) discussies waar ik erg veel van heb geleerd! Bedankt voor de kleine duwtjes in de rug op de momenten dat ik het hard nodig had en voor je aanstekelijke passie voor het onderzoek (en het fietsen! Wist je dat mede door jou ik binnenkort mijn eerste fietstocht ga maken (wel 50 km!)).

Dear Stefan, I already had learned a lot from you during my Master thesis in your lab and even more as your PhD student. Despite your incredible busy schedule, you were always quick to reply my emails and help me out in whatever way you could. Thank you for sharing your enthousiasm for zebrafish research, the endless possibilites of the zebrafish as model organism and in general developmental biology! Thanks for all the support, suggestions, ideas and great sense of humor!

Jaren geleden, begon het allemaal met een plan B waarbij ik samen met jou, Sander, had over een eventuele Master thesis bij Experimentel Zoölogie mocht ik geen Master thesis kunnen doen bij het Hubrecht Instituut. Uiteindelijk werd dit een samenwerking tussen EZO en het Hubrecht Instituut, ook tijdens mijn promotie project. Ik vond het toen al erg fijn om jou als mijn begeleider te hebben mede vanwege je kritische kijk/vragen, creatieve oplossingen en constructieve feedback. Bedankt dat ik altijd binnen kon lopen met al mijn vragen, onze eindeloze discussies over de statistische analyse van mijn data en hulp met het programmeren in Matlab (en het eindeloos lenen van de zebravis bijbel!).

Lieve Karen (mijn eerste kamergenoot!), wat ben ik blij dat ik heb mogen samen werken met jou! Al die uren in ons tropische paradijsje (van ’s ochtends vroeg tot ’s avonds laat, gelukkig ook met muziek alhoewel niet altijd met goed bereik), al die pcr’s en in situ’s die je voor mij hebt uitgevoerd, samen samplen van staartvinnen voor het laatste hoofdstuk tot ’s avonds laat (gelukkig waren er lekkere pannekoeken van je man en kinderen; persoonlijk bezorgd!). Het was erg fijn om met jou te kunnen brainstormen over het opzetten van experimenten tot en met de analyse van data, maar ook over onze tuintjes en lekkere recepten! Bedankt voor de steun, hulp en luisterend oor!

Duizendpoot Henk (ja die naam blijft nu hangen), ondanks al die andere wensen/ taken die jij moest vervullen kon je toch altijd tijd vinden om ook nog mijn wensen te vervullen. Ik kon altijd bij je terecht met al mijn vragen en deze werden dan ook vaak direct beantwoord of problemen werden direct opgelost. Bedankt voor alle hulp met Analysis, omzetten van filmpjes, leveren van harde schijven, maken van back-ups en nog zoveel meer! Het was een eer voor mij om samen met jou een paranimf te mogen zijn (ook omdat we in een situatie kwamen waar jij het beste mee kon omgaan (naast dat we onze kandidaat waren vergeten mee te nemen naar de aula)). Bedankt voor het laten lachen op de moeilijkste momenten!

De gecompliceerde statistische analyses had ik niet kunnen doen zonder de hulp van jou, Gerrit. Gedurende mijn promotie tijd hebben we veelvuldig contact gehad en soms was het uitdaging om precies te begrijpen wat het probleem was, maar gelukkig kwamen we er wel altijd uit. Dankzij jou ben ik zeker kritischer geworden over de statistische analyses, niet alleen in mijn eigen onderzoek. Bedankt voor je hulp en steun!

De uitstekende verzorging van de zebravissen en onderteuning voor de zwemtraining experimenten heb ik allemaal te danken aan de geweldige dierverzorgers van De Haar faciliteiten: Truus, Wian, Sander, Sietze, Aart, Aad, Jasper en Menno. Jullie stonden altijd klaar op mij te helpen met allerlei soorten vragen en mijn wensen. Bedankt dat ik tijdens mijn laatste experimenten bij jullie in het kantoor mocht werken en voor de gezellige koffie pauzes (dus mocht er een vacature komen.. ;)! Rob Steenmans, bedankt voor de ondersteuning en begrip met mijn onmogelijke en soms ellenlange (met verschillende scenario's) dierproef aanvragen. Hierdoor was het niet altijd even duidelijk voor de commissie maar dankzij jou leerde ik duidelijker mijn dierproef aanvragen te schrijven en kritischer te beoordelen.

Voor mijn experimenten op het Hubrecht Instituut werd ik opgevangen door twee hele leuke enthousiaste collega's, Leonie en Ive. Bedankt voor het helpen met het uitvoeren van de micro array experimenten en analyse. Leonie, jouw enthousiasme voor onderzoek en je lach zijn zeer aanstekelijk en ik heb ook erg genoten van onze discussies en van onze gezamenlijke reisje in Portugal (ondanks dat we drie uur vast zaten in een trein in the middle of nowhere...waarvan ik eerder had gezegd dat treinen in Portugal netjes op tijd reden!).

Mijn studenten, Ramona, Paul, Björn, Britt, Twan en Walinka, bedankt dat ik jullie mocht begeleiden. Jullie hebben een groot deel bijgedragen aan verschillende hoofdstukken, ik heb erg veel van jullie geleerd en ook erg genoten van onze tijd samen.

A BIG thank you for my collagues at EZO for the lively discussions, the Famous After EZO Lectures-drinks, great lunch and coffee breaks and the endless UNO-games. Thank you Jos, for helping with the swim-training/high speed recording set-ups (and that I shouldn't be afraid to fix things myself). Thank you, Remco, for helping me with building the high speed recordings set-up, the experiments and the analysis. Thank you, Kees, I am very grateful that you helped me out with the fish tracker and explain, with much patience, this simple biologist the complicated Matlab programming and fish tracker analysis. Mark, thanks for the great music, which made

me forget we live in a very cold cold country and it was great to be your paranimf! Patricia, it was great to work with you in the Academische Jaarprijs competition and the Flight artists team, I learnt a lot from you! It was wonderful, Elsa, that you joined the EZO Group. It was/is at times challenging for us ladies but we will survive! Thanks for all the chit chat, the support, the understanding and LOADS and LOADS of chocolate, muito beijos e abraços! Thank you also, Jan-Wouter, Maurijn, Sebastian and Mike, for your crazy talks and funny YouTube movies! Dear Marcel, your positive attitude is admirable, thank you for all the chit-chat and motivating talks (not only about food)! Annemarie, with your cheerful 'good morning', my day always started great! Thank you for the great help throughout the PhD until the last end! Dear Mees, thank you for the cultural lessons about Bulgaria, looking forward to visit you! Thanks also my collagues at HMI and CBI for the great coffee and lunch breaks. In particular, Maria for the support and help with the qRT-PCR analysis (it is not as straightforward as one thinks) and the ones who travelled with me during this PhD journey, Marjolein, Linda, Danilo, Natalie en Gerco!

Deelname aan de Academische Jaarprijs en het Vliegkunstenaars project waren een zeer welkome afleiding en net wat ik zocht om naast mijn promotie te doen. Bedankt Sander G. en David, dat jullie me hadden gevraagd om hieraan deel te nemen. Het was een zeer leerzame en geweldige ervaring om ons onderzoek te communiceren naar het algemene publiek en ook hun erbij te betrekken. Het Vliegkunstenaarsproject samen met jou, David, nog twee jaartjes te mogen draaien was een grote uitdaging vanwege onze drukke agenda's en jouw verhuizing naar de VS maar het is ons toch gelukt! Bedankt voor de samenwerking en voor de motiverende en inspirerende meetings die ik met je had (zowel in Wageningen also ook later vanuit de VS). Jeffrey, Rinkse en Maarten, hierbij wilde ik ook jullie bedanken voor jullie steun en hulp in die jaren, zonder jullie was het me zeker niet gelukt om dit project te draaien en ook nog aan mijn promotie te werken.

Mijn favoriete fijnmechanicus en mede-Vliegkunstenaar, Eric, bedankt voor het helpen opbouwen van mijn opstellingen. Ik ben je eeuwig dankbaar dat je ondanks je zeer drukke tijdschema toch tijd kon maken om een belangrijk onderdeel, de vierkanten buis, voor mijn high speed experimenten kon maken (zonder dat had ik niet het eerste hoofdstuk kunnen schrijven)! Daarnaast heb ik je beter leren kennen tijdens ons tijd als Vliegkunstenaars. Het tripje naar Duitsland was memorabel, wat een team! Zonder jou was het half niet zo leuk geweest, zeker in aanloop naar de finale.

Alma, bedankt voor alle steun tijdens de laatste jaren, ik had dat erg hard nodig. Onze sessies hebben me zeker verder geholpen om dingen vanuit een ander perspectief te benaderen, om voor mezelf op te komen en mijn wensen te uiten.

My fellow-capoeirista's, thank you for the great games, festival outings, Brazilian parties, music practices, aulas de Português, fantastic new years dinners and many other social get togethers! What better way is there to forget about working life than a game of capoeira and spending time with you? Your performance at my wedding was unforgettable (not only for me but for the whole Turkish community!), love you all e Axé!! Bedankt, Professor Mourão, je kent me al toen ik zooo 'klein' was, bedankt voor de geweldige lessen. Jouw verrassende creatieve combinaties en inzichten in het

spel hebben me erg veel geleerd niet alleen in het spel maar ook daarbuiten.

My Droef 65 Housemates, the Droefkonijnen, the Droevies!, thank you for helping me with the Mozaïk application, great parties and dinners. To come home after a frustrating/exhausting working day with such nice and great people is truly a marvelous gift. I am very happy to have lived with you and that we are still in touch!

Bedankt lieve biologen, Marjon, Kimmetje en Roel, voor de steun, liefde en begrip de afgelopen jaren (al meer dan 10 jaar!). Marjon, het was erg fijn om met jou onze frustraties te delen over het werken in een mannenbolwerk en Matlab! Lieve Kimmetje, mijn huisgenoot, bedankt voor je steun en afleiding, experimenteel eten en leuke film avondjes! Roel, onze uitjes tezamen waren geweldig, heerlijk jouw sarcastisch/cynische humor/commentaar, de kwelder/jouw proefveld tour was super mooi!

Mijn vriendinnetjes Mariëlle, Iris, Marloes, Dieuwertje, het was heerlijk en gezellig om met jullie weer bij te kletsen tijdens een etentje en of theetje. Bedankt voor het luisterend oor en de gezellige uitjes! Thanks Laura, for the visits, mails and phone calls! Although many many many miles away, you were always in my heart supporting me!

Een speciaal BEDANKT voor mijn Paranimfen, Anneke en Yvette, mede huisgenoot, mede bioloog, mede capoeirista's, ik ben zo blij dat jullie mijn paranimfen wilden zijn en me ondersteunen op de DAG! Bedankt voor de discussies over van alles en nog wat, gezellige treinreisjes naar Utrecht, lekkere etentjes, leuke vakanties in Turkije (lekker hygiënisch) en het delen van vele hilarische en of intense momenten in mijn leven.

Mijn lieve schoonfamilie, bedankt voor de zorgen ondanks dat ik altijd in jullie ogen aan het werken, werken en werken was. Ik had geen betere schoonfamilie kunnen wensen! Sevgi ve destekleriniz için çok tesekkür ederim!

My dearest family, mijn lieve familie, heel erg bedankt voor alle leuke uitjes, dineetjes, spelletjes (vooral '30 seconds'!!!) waardoor ik even kon ontspannen en dingen in perspectief kon plaatsen. Mohabbat ke liye shukrya! In het bijzonder wil ik Adeel, Amelia en Zinnie bedanken voor alle knuffels, liefde, geweldige fantasie en onschuldige kijk op het leven!

Liefje, hayatim, kocam, saijna, mera dil, woorden zijn eigenlijk niet genoeg om uit te drukken hoe dankbaar ik ben voor je hulp, steun en liefde (ja zoveeeeel liefde, wel tien vingers!) in de afgelopen jaren. Bedankt voor het luisteren naar al mijn frustraties, zorgen en problemen. Bedankt voor alle koekjes, chocola en snoepjes om de lange dagen en nachten door te komen. Bedankt voor het accepteren dat ik moest werken in het weekend of 's avonds (ellenlange weken achter elkaar), bedankt voor het lichter maken van het leven, bedankt voor alle knuffels, zonder jou had ik die laatste weken en laatste dagen niet gered. Seni sonsuza dek seveceğim!

Personalia

”To be yourself in a world that is constantly trying to make you something else is the greatest accomplishment.”
Ralph Waldo Emerson

Curriculum vitae

Ansa Waseem Fiaz was born on the 8th of February 1981 in Dhera Kanyal in Pakistan. She moved with her mother and siblings to The Netherlands when she was five. Being inspired by her biology teacher at high school, she decided to study biology at Wageningen University. Half way during her studies, she became (for a year) the local committee president of the international student organisation AIESEC in Wageningen and thus supervised a team of 12 members and was responsible for recruitment of sponsors and management of external relations. Via AIESEC she also spent a summer in Brazil to help a local committee with strategic longterm planning and to learn more about the Brazilian culture and language.

After that year, during a student tour visit at the Hubrecht Institute in Utrecht, she became fascinated by the development of organisms and the diverse array of genes and cells involved in the process to form an organism. To strengthen her molecular biology skills, she first investigated the role of endocrine disrupters in the stimulation of aromatase gene expression in human breast cancer cells with quantitative real time PCR (qRT-PCR) at the Departement of Toxicology under the supervision of Dr. Marcel ter Veld. Subsequently, she did a Master project in the lab of Dr. Stefan Schulte-Merker at the Hubrecht Institute in collaboration with the Experimental Zoology group in Wageningen. In this project, she characterized the phenotypes of the *stocksteif* and *no bone* zebrafish bone mutants with cartilage and bone stainings, investigated the spatial expression pattern of bone marker genes with in situ hybridisations in both mutants and performed initial mapping of the stocksteif mutation. At the Experimental Zoology group, she quantified the swim kinematics of the *stocksteif* mutants with high speed videos recordings under the supervision of Dr. Sander Kranenbarg and Dr. Ulrike Müller. For the last project of her Master, to broaden her horizon in science and in cultural aspects, she decided to do her traineeship in Singapore on protein expression. There she investigated the enzyme activity of a mutant prokaryotic phospholipase A_2 (which was expressed and isolated from *E.coli*) in the Protein Science lab of Professor R. Manjunatha Kini and under supervision of Dr. Robin Doley.

After graduating in november 2006, she started to work as junior researcher at the Departement of Agrotechnology and Food Sciences in Wageningen. She participated in the development of an assay to test marine toxins on animal cells to replace animal testing with differential display PCR and qRT-PCR. During this project she also worked on writing a research proposal for a PhD project together with Professor Johan van Leeuwen and Dr. Sander Kranenbarg at the Experimental Zoology group. In 2008, she worked on a project with Professor Johan van Leeuwen to analyse the muscle development during ontogeny in zebrafish larvae with electron microscopy and qRT-PCR in the Experimental Zoology group. Alongside this project, she continued to work on her research proposal (Dr. Stefan Schulte-Merker became involved again at this point) and applied for a Mozaïk grant from the NWO, which was granted in august 2008. In January 2009 she started the PhD project described in this thesis.

In 2009-2010, she was a member of the Wageningen Ecology and Evolution Seminars, which consists of PhD students and post-docs which organizes lectures with young promising scientists from around the world for everybody who is interested. In 2010, she participated in the annual Academic prize competition in the team of Dr. David Lentink with the Flight Artists project. It led to many beautiful high speed movies and demonstrations at among others the Insect Experience in Wageningen, TEDx Amsterdam, the Discovery Festival at NEMO and the first High Speed Film festival.

In her free time, Ansa likes to play capoeira which is an Brazilian fight-dance game combining music, acrobatics and martial arts. She also practices Critical Alignment yoga, and enjoys to cook and to wander around in the beautiful nature of Wageningen and surroundings.

Publications

Fiaz, A. W., Pieters, Remco P.M., Voesenek, Cees J., Van Leeuwen, J. L. Quantification of swimming kinematics of larval zebrafish in varying flow conditions. *To be submitted.*

Fiaz, A. W., Léon-Kloosterziel, K. M., Schulte-Merker, S., Van Leeuwen, J. L. and Kranenbarg, S. Exploring the molecular link between swim-training and caudal fin development in zebrafish larvae (*Danio rerio*). *To be submitted.*

Fiaz, A. W., Léon-Kloosterziel, K. M., Schulte-Merker, S., Van Leeuwen, J. L. and Kranenbarg, S. Exploring the effect of exercise on the transcriptome of zebrafish larvae. *To be submitted.*

Fiaz, A. W., Léon-Kloosterziel, K. M., Gort, G., Schulte-Merker, S., Van Leeuwen, J. L. and Kranenbarg, S. (2012). Swim-training changes the spatio-temporal dynamics of skeletogenesis in zebrafish larvae (*Danio rerio*). *PLoS One* **7**, e34072.

Fiaz, A. W., Van Leeuwen, J. L. and Kranenbarg, S. (2010). Phenotypic plasticity and mechano-transduction in the teleost skeleton. *J Appl Ichtyol* **26**, 289–293.

Müller, U.K., **Wasim, A.**, Fontaine, E., Lentink, D., Kranenbarg, S., Schulte-Merker, S., Leeuwen, J.L. van. (2009). Increased body-axial stiffness reduces escape performance in larval zebrafish. *Integrative and Comparative Biology* **49**, E278 - E278.

Abstracts

Fiaz, A. W., Léon-Kloosterziel, K. M., Gort, G., Schulte-Merker, S., Van Leeuwen, J. L. and Kranenbarg, S. The zebrafish marathon: exploring the effects of swim-training on zebrafish larval development. Abstracts of the 8th European Zebrafish Meeting, Barcelona 9–13 July 2013.

Fiaz, A. W., Léon-Kloosterziel, K. M., Gort, G., Schulte-Merker, S., Van Leeuwen, J. L. and Kranenbarg, S. Swim-training changes the spatio-temporal dynamics of skeletogenesis in zebrafish larvae (*Danio rerio*). Abstracts of the 71st Annual Meeting of the Society for Developmental Biology, Montréal 19–23 July 2012.

Fiaz, A. W., Léon-Kloosterziel, K. M., Gort, G., Schulte-Merker, S., Van Leeuwen, J. L. and Kranenbarg, S. Effect of an increased mechanical loading on chondrogenesis and osteogenesis in the zebrafish (*Danio rerio*) larva. Abstracts of the 2nd Interdisciplinary Approaches in Fish Skeletal Biology meeting, Tavira 26–28 April 2011.

Fiaz, A. W., Léon-Kloosterziel, K. M., Schulte-Merker, S., Van Leeuwen, J. L. and Kranenbarg, S. (2011). Swim training accelerates the onset of chondrogenesis and osteogenesis in the zebrafish (*Danio rerio*) larva. Abstracts of the 7th European Meeting on Zebrafish Genetics and Development, Edinborough 5–9 July 2011.

Fiaz, A. W., Léon-Kloosterziel, K. M., Schulte-Merker, S., Van Leeuwen, J. L. and Kranenbarg, S. (2010) An increased mechanical loading accelerates growth and osteogenesis in zebrafish (*Danio rerio*). Abstracts of the 17th Benelux Congress of Zoology, Gent 22–23 October 2010.

Müller, U., **Wasim, A.**, Fontaine, E., Berg, O., Cao, Y., Lentink, D., Kranenbarg, S., Leeuwen, J.L. van. (2010) Exploring Fluid-structure Interaction during Undulatory Swimming in Fish. IFMBE Proceedings of the 6th World Congress of Biomechanics, Singapore .

WIAS TSP

	ECTS[1]
Basic package	
WIAS Introduction Course	1.5
Course on philosophy of science and or ethics	1.5
Scientific Exposure	
Six international conference, including the Interdisciplinary Approaches in Fish Skeletal Biology (twice), the European Meeting on Zebrafish Genetics and Development, the Society for Developmental Biology Annual Meeting and the Annual Meeting of the Society for Experimental Biology	6.6
WIAS Science day	0.3
Five oral/poster presentations	5.0
In-Depth Studies	
Advanced visualisation, integration and biological interpretation of -omics data	0.9
Four advanced statistics courses, including Statistics Course on generalized linear models and Design of Animal Experiments	3.3
EZO PhD lectures/journal club meetings	2.0
Professional Skills Support Courses	
Course on supervising Msc students	0.6
Techniques for writing and presenting a scientific paper	1.0
Advanced course on guide to scientific artwork	0.6
Several courses on mediatraining, presentation and negotiation skills by NWO	1.1
Research Skills Training	
Writing and obtaining a Mozaïk grant proposal for PhD research by NWO	6.0
Didactic Skills Training	
Two lectures at Hogeschool Utrecht	2.0
Supervision of 4 Msc (1 part-time) and 2 Bsc students	8.0
Management Skills Training	
Flight Artists outreach project	17.0
Annual Academic Prize competition	4.6
Member of Wageningen Evolution and Ecology Seminars	0.3
Total ECTS	**62.3**

Herewith the WIAS Graduate School declares that the PhD candidate has complied with the educational requirements set by the Educational Committee of WIAS.

---

[1] One ECTS (European Credit Transfer and Accumulation System) equals a workload of 28 hours.

This research was supported by the Netherlands Organisation for Scientific Research (NWO) under project number: 017.005.014.

Cover Design: Liezelotte Nagtegaal and Ansa W. Fiaz
Layout: Ansa W. Fiaz

This thesis was printed by GVO printers and designers B.V.|Ponsen & Looijen

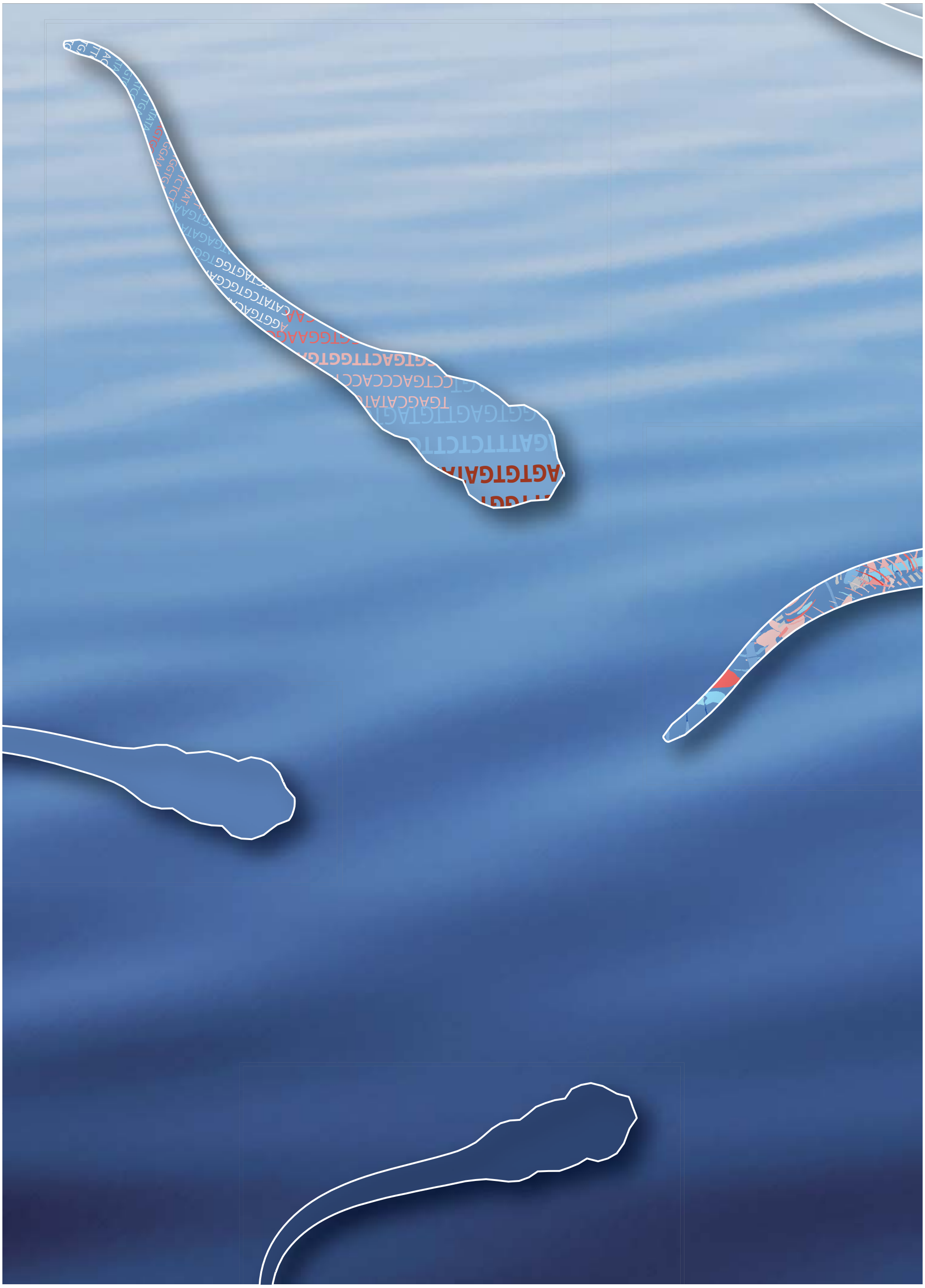Financial support from the Experimental Zoology Group (Wageningen University) for printing this thesis is gratefully acknowledged.